NASA CR-54491

FINAL REPORT

DISPERSION STRENGTHENED CHROMIUM ALLOYS

by
RE ALLEN

prepared for

NATIONAL AERONAUTICS AND SPACE ADMINISTRATION

JUNE 5, 1969

CONTRACT NAS3-7607

NASA LEWIS RESEARCH CENTER
CLEVELAND OHIO
JOHN P MERUTKA PROJECT MANAGER
MATERIALS AND STRUCTURES DIVISION

MATERIAL AND PROCESS
TECHNOLOGY LABORATORIES

AIRCRAFT ENGINE GROUP
GENERAL ELECTRIC
LYNN MASSACHUSETTS/CINCINNATI, OHIO

DISPERSION-STRENGTHENED CHROMIUM ALLOYS

by

R. E. Allen

Prepared for

NATIONAL AERONAUTICS AND SPACE ADMINISTRATION

CONTRACT NAS 3-7607

NASA-Lewis Research Center
Cleveland, Ohio
John P. Merutka, Project Manager
Alan Arias, Project Advisor
Materials and Structures Division

MATERIAL AND PROCESS TECHNOLOGY LABORATORIES

GENERAL ELECTRIC COMPANY

Page Intentionally Left Blank

FOREWARD

The research described herein, which was conducted by the General Electric Aircraft Engine Group, was performed under NASA Contract NAS3-7607. The work was done under the management of the NASA Project Manager, Mr. John P. Merutka, Materials and Structures Division, NASA-Lewis Research Center.

TABLE OF CONTENTS

TABLE OF CONTENTS (CONT'D)

LIST OF TABLES

LIST OF TABLES (CONT'D)

LIST OF ILLUSTRATIONS

LIST OF ILLUSTRATIONS (CONT'D)

LIST OF ILLUSTRATIONS (CONT'D)

LIST OF ILLUSTRATIONS (CONT'D)

LIST OF ILLUSTRATIONS (CONT'D)

1. ABSTRACT

Oxide dispersion strengthening of a Cr-4%Mo alloy was investigated using ball milled blends of either elemental or prealloyed metal powders and MgO, Y_2O_3, or ThO_2 powders. These blends were contaminated by both oxygen and carbon during milling. To reduce the amount of contamination, carbothermic and hydrogen cleaning processes were developed. Program goals of < 1.5 micron interparticle spacing (IPS) and < .1 micron oxide particle size (P. S.) with good thermal stability of densified material could not be achieved in compacts produced from submicron blends. However, hot-rolled compacts produced from coarse flake (50% < 2μ flake thickness) prealloyed Cr powder had a stable dispersion with IPS = 1.0 micron, PS = .07 micron, thereby meeting the goals. Although this material had excellent hot tensile strength, it had a high ductile-to-brittle transition temperature and low creep strength. It is speculated that further thermo-mechanical processing work could lead to improvements in mechanical properties.

2. SUMMARY

Ball milled blends of Cr-Mo alloys with MgO, Y_2O_3 or ThO_2 were used in the investigation of a powder metallurgy process for the production of oxide dispersion strengthened Cr alloys. In an attempt to achieve particle size (PS) and interparticle spacings (IPS) goals of .1 and 1.5 microns, respectively, submicron blends (99% < .5μ) elemental metal/oxide powders were produced by ball milling at -50°F in toluene. When densified this submicron blend yielded a fine dispersion which was highly unstable during subsequent thermal exposures. In addition, the microstructure contained tramp oxides and carbides which resulted from carbon contamination during ball milling and from oxygen impurities in the impure, fine Cr starting powders. A carbothermic cleaning process was developed to reduce these impurities, but the severe (2200°F - 2400°F) exposure associated with carbothermic cleaning caused dispersoid agglomeration thus precluding achievement of PS, IPS goals in the densified product. Further, this agglomeration rendered the alloys from submicron blends unworkable and yielded as-compacted alloys with poor high temperature strength.

In an effort to eliminate the high temperature cleaning step associated with oxygen removal, coarse high purity prealloyed starting powders were ball milled to 99% < 1μ. The resulting blend was then subjected to a low temperature H_2 cleaning processed developed for removal of carbon picked up during ball milling. A detailed kinetic study of this cleaning process indicated that purity goals of < 100 ppm each of carbon, oxygen, and hydrogen were not achievable in such a fine blend.

Further relaxation in blend size to thick flakes (50% < 2μ) was made in order to ease contamination/cleaning problems. Compacts produced from such coarse prealloyed ball milled flakes exhibited the most promising properties of the alloys investigated. Sheet material produced from Cr-4Mo-.15(La+Y)-4$^{v}/_{o}$$ThO_2$ had an oxide PS and IPS of .07 and 1.0μ respectively. This alloy had goal thermal stability and exceptionally high tensile properties (at temperatures as high as 2400°F), a

ductile-to-brittle transition temperature (DBTT) of 900°F and showed a strong strain rate sensitivity. Although the dispersion in this alloy nearly met program goals, complete achievement of these goals (which included a maximum PS of .2μ) was prevented by the presence of large Cr_2O_3 particles.

3. INTRODUCTION

Chromium possesses several valuable high-temperature attributes which make it a promising candidate for applications in advanced turbo-machinery systems, including turbine buckets, vanes, and nozzle partitions in air-breathing engines. The excellent high-temperature strength [1], oxidation resistance and modulus to density ratio of Cr is offset at present by poor low-temperature ductility and by poor nitridation resistance at temperatures above 2000°F. Clark[1] has reported progress in the improvement of nitridation resistance, but in conventionally processed alloys, high ductile-to-brittle transition temperature (DBTT) remains a problem. In those alloys with the best hot strengths, DBTT in the tension test is above 400°F. Further, in work to date, a decrease in DBTT is usually accomplished at the expense of high-temperature properties. It is here that powder metallurgy will hopefully make its contribution, with improved high-temperature strength retention and accompanying depressed DBTT.

Work in Fe-base alloys by Hahn and Rosenfield[3] has shown that the ductile-to-brittle behavior of oxide dispersion-strengthened materials is improved due to the influence of finely dispersed oxides on crack propagation. The influence of such dispersions on both low-temperature strength and retention of the strength to high homologous temperatures is, of course, well documented[3,4]. Although mechanistic studies of these alloy systems have been unable to arrive at a unanimous agreement of the exact strengthening mechanism or mechanisms, the important variables have been delineated. These include, among many, a stable oxide particle size and interparticle spacings which are less than .1μ and 1.5μ, respectively. Grain size in such alloys varies widely, but in all cases has a similar elongated morphology. In both SAP [5] and TD Co[6], the large grained material had the best creep properties and showed a large interlocking grain structure analogous to that found in doped W wire[7]. In all cases, the successful alloys had a strong preferred orientation.

The objective of this program was to investigate powder metallurgy techniques for producing oxide dispersion strengthened Cr-Mo alloys with metallographic parameter goals of 1.5 microns IPS and 0.1 micron PS. The basic approach was to ball mill mixtures of metal and oxide powders for subsequent densification and evaluation. Three different types of blends were used in an effort to achieve the microstructural goals, as follows: 1) an elemental metal/oxide blend in which particle size was 99% < .5μ; 2) a prealloyed metal flake/oxide blend in which the metal flakes were 99% < 1μ in thickness; and 3) a prealloyed metal flake/oxide blend in which the flakes were 50% < 2μ in thickness.

The powder blends were then densified by various procedures including extrusion, hot isostatic pressing, and a hot pressing. Some of the resulting compacts were further worked by hot rolling, swaging, or drop forging. Finally the materials were evaluated microstructurally and some property measurements were made of some of the materials.

4. PRODUCTION OF A MECHANICAL BLEND OF SUBMICRON METAL/OXIDE POWDERS BY BALL MILLING

Dispersion strengthening of alloys by powder metallurgy has been under intensive investigation since the development of SAP type Al-Al_2O_3 alloys in 1946 [8]. More recent work has been aimed at higher temperature materials, e.g., Fansteel TD-Ni. Successful strengthening of these alloys has been associated with particle sizes in the range of 0.01 to 0.1 microns and inter-particle spacings (IPS) in the range of 2.0 microns or less. Hence, in order to produce dispersion strengthening in chromium, target parameters have been established which include: 1) a dispersoid size of less than 0.1 microns, 2) an IPS of less than 1.5 microns. Cremens [9] devised a general relationship from which it may be shown that to attain IPS of 1.5 microns, spherical starting matrix and dispersoid powders must be used that have less than 0.5 microns and 0.1 microns diameters, respectively.

Previous studies in the Material and Process Technology Laboratories (MPTL) indicated that powders in the above particle size range were achievable by low temperature (-50°F) ball milling. Interstitial contamination was to be avoided by use of complete glove box handling throughout the entire process. This process was, therefore, applied to this program.

4.1 STARTING MATERIALS

Elemental Matrix Powders - The chromium and molybdenum powders for the elemental matrix powder approach in this program were obtained from Continental Ore Company.* Both powders contain relatively equiaxed particles with a Fisher sub-sieve size of 1.6 microns. Chemical analysis of the chromium powder is shown in Table 1. The interstitial content of the molybdenum powder, which was 99.92% purity, is shown in Table 2. The reactive element

* Parent company is Aciéries de Gennevilliers, 119, Av Louis Roche Paris, France.

additions of yttrium, thorium, and hafnium were procured in the form of hydrides from Metal Hydrides, Incorporated. These -60 mesh powders were received at a purity level of 98%, with oxygen as the major contaminant.

Prealloyed Powders - The starting powder for production of submicron prealloyed matrix approach was to be obtained from Hoeganaes Sponge Iron Company as argon atomized powders. After three unsuccessful attempts by the vendor, process development at Hoeganaes for the atomization of these powders was terminated. An alternate procedure was initiated at the Material and Process Technology Laboratories (MPTL) of General Electric Company. The alternate procedure consisted of mechanical comminution of induction melted ingots of a Cr-3Mo-0.25 each Y, Th, Hf alloy. These ingots were prepared from Union Carbide electrolytic flake chromium with molybdenum addition obtained from the Lamp Metals and Components Department of General Electric Company and the reactive metal additions in the form of hydrides from Metal Hydrides, Incorporated. Melting was carried out in an yttria stabilized zirconia crucible in a high purity argon atmosphere. Comminution of the as-cast alloy was accomplished in three distinct stages; 1) cold forging, 2) pulverization, 3) ball mill comminution. Initially the ingot was cold forged between two molybdenum plates. Large pieces so obtained were further pulverized in a molybdenum mortar and pestle to -6 mesh material and this material used as charge for the ball mills. A Cr-4Mo-.15 (La+Y) alloy was also produced for a similar purpose. This high purity material was produced by arc melting 80 gram buttons from iodide Cr and high purity Mo (Table 3). These buttons were crushed to ~60 mesh under argon in a mortar and pestle.

Dispersoid Powders - The magnesia used in this program was procured from Matheson, Coleman, and Bell Chemical Company with an 0.04 micron particle size. Chemical analysis of MgO powder is recorded in Table 4. One micron yttria was purchased from American Potash and Chemical Corporation with the

chemical analysis shown in Table 5. High purity (99.9%) thorium oxide powders used with the elemental powder mixtures were obtained from Research Labs, Incorporated, Newtown, Ohio. The ThO_2 used with the prealloyed powders was obtained as a 50 Å - 150 Å diameter sol from Thorium Limited.

4.2 EQUIPMENT AND PROCEDURE

One of the vacuum-tight ball mills used in this program is pictured in Figure 1. The removable cover, which contains a small vacuum valve, makes a vacuum-tight connection with the main body through the use of the large "O" ring seal. Each ball mill was initially leak checked with a helium mass spectrograph leak detector to insure vacuum tightness. In order to minimize powder contamination due to wall and media wear, both were constructed of molybdenum which is an alloying element in the final material, rendering such contamination innocuous. Approximately 1500 grams of 3/8-inch, 5/8-inch, and 7/8-inch diameter Mo-0.5Ti-0.08Zr rondels, with a length-to-diameter ratio approximately one, were used as attritors with the molybdenum-lined mill.

Ball milling was carried out at -50°F in the cold chamber shown in Figure 2. The main features of the chamber are: a) a cascade, Freon-Ethane compressor system capable of cooling the 5 ft^3 chamber to -120°F; b) three cylindrical rolls, with self-adjusting ball bearings lubricated with General Electric F-85 silicone fluid; c) an external 3/4 horse power electric motor connected to the center roller by a 1/2 inch diameter rotating shaft through the chamber wall; and d) a temperature indicator and controller.

All weighing of powders, charging, and unloading of the mills was done in the glove box in the presence of a heated titanium gettering strip. Weighing was done on a torsion balance sensitive to $\pm$ 0.005 grams.

The charged, sealed mill was then removed from the glove box and connected to a valving manifold where it was evacuated to approximately 3 X 10^{-3} torr,

and backfilled with approximately 250 cc of toluene and 15 psi argon. Ball milling was carried out at -50°F at a speed of 86 rpm. Ball mill temperature was measured with a copper-constantan thermocouple positioned at the center of the chamber near the ball mills.

Powder Analysis - The particle size analysis of submicron powders, both the starting dispersoid powders and the milled mixtures employed an electron microscopy technique based on particle diameter (rather than surface area or volume.) Since the mixed powders contain particles which vary widely in both size and density, segregation is a critical problem and careful sampling procedures were used in selecting a random sample for analysis. The sample was prepared for viewing and photographed in the electron microscope. A Zeiss particle size analyzer was used to determine the size distribution of particle diameters from the electron micrograph. From particle size analyses the median particle diameter of the as-received MgO powders was determined to be 0.09 microns (see Figure 3). Size distribution of prealloyed powders was conducted by BET* analysis which is a measure of surface area. Electron microscopy of this powder was impossible because of the extremely large dimension of the flat flake surface. The thickness measurement on the other hand was too small for accurate measurement by optical microscopy. The BET method, therefore, was utilized as the best alternative. Flake thickness was estimated from BET numbers, by assuming the particles were perfectly flat and by neglecting their peripheral area.

4.3 BALL MILLING RESULTS

Particle size distribution of the ball milled elemental powders is illustrated as a function of ball milling time in Figure 4. Since the goals for the submicron blend were stated as 99% less than 0.5 microns,

* Brunauer Emmet Teller

the data from Figure 4 was replotted in Figure 5 as percent of particles smaller than 0.5 microns versus ball milling time. The contract goal of 99% smaller than 0.5 microns is seen to be attained after approximately 450 hours ball milling time. Powders produced by ball milling the elemental mixture at -50°F for 500 hours in toluene are shown in Figure 6. At a magnification of 10,000 times, the powder had a slight flake topology, as may be seen by the transparency of many of the particles. The thickness of one of these flakes was estimated from the extinction fringes pictured in Figure 6B to be 0.05μ.

An attempt to achieve the submicron blend was made using prealloyed (Cr-3Mo-.25 ea (Hf, Th, Y) powders also. Ball milling of -6 mesh prealloyed powders was carried out in the same manner as the elemental powders. The particle size of the prealloyed powder after 300 hours and 540 hours is shown in Figures 7A and 7B respectively. In order to remove the coarse particles seen in Figure 7B, the powders were screened after 500 hours ball milling time and the -325 mesh material recharged for additional ball milling. The powders in Figure 7C have a total of 980 hours milling time, 480 hours of which were logged after the above screening operation. Although it may be seen in Figure 7C that a large percentage of the flakes have thicknesses of less than one micron, the particle size goal of 99% < .5μ could not be achieved in these powders in a reasonable length of time (1000 hrs). Surface area of a Cr-4Mo-.15 (La + Y) alloy as a function of ball milling time is given in Figure 8. The powders shown in this Figure were subsequently used in the flake approach in which the particle size requirements were somewhat relaxed. Two separate particle sizes were; 1) 99% less than 1μ flake thickness, and 2) 50% less than 2μ flake thickness. These sizes were achieved after 740 and 200 hours (respectively) of ball milling time. Average molybdenum contamination rate in oxide-free samples was .004%/hr and after 740 hours Mo pickup amounted to 2.9%. In samples milled with ThO_2, Mo contamination was 2.5% after 800 hours milling (Average Rate =.003% ^{Mo}/hr).

Consideration of comminution mechanisms by metallography and X-ray diffraction indicates the grinding takes place mainly by cleavage in coarse monocrystalline particles (> 20μ) but as particle size decreases, plastic flow becomes increasingly important. Thus, large angular equiaxed particles transform during milling to fine plate-like flakes with large diameter to thickness ratio (D/t) and with a strong deformation texture. X-ray texture analysis indicates that the flat plate-like surface of the flakes corresponds to {100} and that the particles are heavily cold worked. The strongest texturing was observed in samples which contained relatively coarse flakes. As the flakes become thinner, they break up and tend towards an equiaxed morphology. This results in loss of the parallel flake alignment in the samples used for X-ray analysis. This is shown quite clearly in Table 6 which is a comparison of peak intensities from the Cr flakes with ASTM standard (randomly oriented) powders. Diffraction optics associated with the diffractometer are such that if the planes of preferred orientation are parallel to the face of the cold-pressed coin, diffracted intensity from these planes is enhanced. In Table 6 it may be seen that in the as-milled powders, the (200) refelctions are more intense than would be expected from completely random orientations. Texturing is maximum after 207 hours ball milling time where I_{200} is 35.4 times as great as in the randomly oriented ASTM powders. After 600 hours, however, this relative intensity factor has dimished to only 3.6.

That the flake formation is indeed a result of slip rather than cleavage is clearly indicated by extensive peak broadening observed in the back reflection region of the X-ray diffraction spectra. Heavy cold working in the as-milled powders broadened the (211) peak considerably and $K\alpha_1$ and $K\alpha_2$ resolution was impossible. After annealing this sample at 2400°F/24 hrs/VAC, however, the peak sharpened considerably and the $K\alpha_1$ and $K\alpha_2$ lines were clearly distinguishable.

According to the texture analysis of Calnan and Clews [10], deformation textures which arise from compressive loading at low temperatures in BCC metals are the {111}, {112} and {100}. Under compressive stresses large enough to exceed the critical resolved shear stress, each powder particle, therefore, plastically deforms and the accompanying rotation of crystallographic planes tends to create flakes whose large surfaces are parallel to the {111}, {112}, or {100} planes. External surface energy of the individual flakes is also a function of orientation. Work by Bacigalupi and Neustadter [11] has shown that the {110} orientation is the most favorable surface energetically. This is not one of the favored texture planes, however, and is, therefore, not observed experimentally in the flake powders. On the other hand, the two common texture planes, {211} and {111} are energetically less favorable as external surfaces than the {100}. The observed {100} flake texture, therefore, evidently arised from slip on the {112} <111> system and is due to a combined influence of deformation and surface energy effects.

Chemical analyses of as-milled powders consisted mainly of interstitial (C, O, H, H) and molybdenum determinations. Oxygen, hydrogen, and nitrogen concentrations were determined by gas fusion analysis of powders encapsulated in 5 mm diameter tin capsules which were loaded and sealed in the glove box. An empty calibration capsule was exposed to identical procedures and analyzed with each set of specimen to establish the baseline gas concentrations from handling procedures. Carbon content of the loose powders was determined by conductometric analysis of concentrations less than 0.2% carbon. Above this concentration the analysis was carried out gravimetrically. Results of these analyses are plotted as a function of ball milling time in Figure 9. The general trend of this data indicates that carbon contamination is a direct function of powder surface area.

X-ray fluorescent analysis was used to determine molybdenum content of powders. The calibration curve for this procedure was obtained using standards of known molybdenum concentration prepared from the starting powders. Molybdenum contamination from liner and rondel wear is shown in Table 8. As may be seen, pickup was rather unpredictable when viewed in terms of ball milling time.

Powder handling procedures both before and after ball milling were designed to provide an inert environment to the powders at all times. After milling, toluene was removed from the ball mill by evacuation with a mechanical vacuum pump. In order to increase the removal rate, heater tape was wound on the outer diameter and the ball mill heated to 250°-300°F. Toluene removed from the mill was collected in a liquid nitrogen cold trap positioned between the ball mill and the pump. When the ball mill pressure reached 3×10^{-2} torr, it was backfilled with argon and transferred to the welding chamber for cleaning and encapsulation.

5. REMOVAL OF INTERSTITIAL CONTAMINATION FROM THE METAL/OXIDE BLEND

5.1 SOURCES OF CONTAMINATION

As-milled powders were contaminated by interstitial elements varying in amounts from 0.36 to 1.7%. This contamination originates from three main sources: i) powder production; ii) ball milling; and iii) powder handling. Elemental chromium powders purchased for this investigation were produced by magnesiothermic reduction of Cr_2O_3 and contain 0.5% oxygen and 0.08% carbon "as-purchased." The above oxygen contamination includes 0.25% MgO which is residual from the original reduction process.

In addition to the impurities inherited from powder production, additional impurities result from the -50°F ball milling treatment. Adsorption of carbon from ACS grade toluene grinding fluid onto freshly produced powder surfaces results in carbon contents as high as 0.7% after milling. The final carbon content of the powder is a function of ball milling time as was shown in Figure 9. Further oxygen contamination of the purchased powders during powder handling procedures was very small.

5.2 CLEANING OF THE SUBMICRON BLEND

Since the major interstitial contaminants were oxygen and carbon, the various cleaning investigations focused on them. Initially, cleaning was to be carried out with one element at a time. This approach proved to be unsuccessful, however, and the final investigation involved removal of both oxygen and carbon simultaneously.

Carbon contamination of these powders is especially critical since small amounts of carbon are very detrimental to ductility. If present as

carbides, the volume fraction precipitated may approach an amount equal to 18.3 times weight fraction of carbon. Powders with 0.6% carbon and 5 $v/_o$ oxide could therefore conceivably contain 16 $v/_o$ of hard particles after compaction.

Inefficient removal of toluene after ball milling was considered as a cause of contamination, but vacuum evaporation of the toluene in the temperature range from 200° to 300°F does not improve the efficiency of removal over that at room temperature. Replacement of toluene by another organic liquid was also considered and an attempt was made to displace the adsorbed toluene with a volatile liquid which could be more easily removed. The procedure used was as follows: as-milled dry powder was added to a flask of the liquid under investigation, shaken well, and allowed to settle. After decanting the liquid, the powders were dried at room temperature by vacuum evaporation. The effect of this procedure, used in conjunction with several different liquids, was not successful. The results are reported in terms of powder carbon content in Table 9.

Hydrogen Cleaning - Both carbon and O_2 may be eliminated with a H_2 treatment carried out under the proper conditions. The reactions of interest here are:

$$C + 2H_2 \rightarrow CH_4 \qquad \text{(Equation 1)}$$

$$1/6\ Cr_{23}C_6 + 2H_2 \rightarrow 23/6\ Cr + CH_4 \qquad \text{(Equation 2)}$$

$$Cr_2O_3 + H_2 \rightarrow 2Cr + 3H_2O \qquad \text{(Equation 3)}$$

The operating conditions where the free energy of reaction is negative for Equations 1 and 2 are shown schematically in Figure 10. It may be seen that Equation 2 requires very refined experimental procedures in terms of hydrogen purity. In the temperature region of interest (1000°-2000°F), for example, the $P_{CH_4}/P^2_{H_2}$ ratio must be less than 10^{-5} to 10^{-6} respectively in order for the free energy of reaction to be negative. Removal of carbon according to Equation 1, on the other hand, is much less demanding, expecially

in the range from 800° to 1200°F. In this range, the equilibrium $P_{CH_4}/P^2_{H_2} \gg 1$ and the reaction should progress quite readily even in relatively impure hydrogen. The reduction of oxygen according to Equation 3 is well documented [12,13] and may be accomplished in commercially pure cylinder hydrogen over a relatively wide range of temperatures. At 1800°F, for example, the reaction is feasibly if the dew point is less than -40°F.

According to the above analysis, the first step of the cleaning process should be removal of adsorbed carbon at a low enough temperature to avoid carbide formation. The temperature could then be increased in the second step to implement the reduction of Cr_2O_3. The problem here is that the operating conditions which give de-oxidation may cause carburization of the powders if the hydrogen contains appreciable methane concentrations.

The hydrogen cleaning apparatus used in this study is shown schematically in Figure 11A. The powders, which were loaded into the stainless steel cleaning capsule in air, were subjected to alternate hydrogen flow (one hour) and vacuum (1/2 hour) cycles at 1800°F. A vacuum cycle was used in an effort to aid removal of the reaction products from the interstices between powder particles. Carbon content of powders subjected to this cleaning procedure is given in Table 10. As illustrated by the increase in carbon contents during cleaning runs 1, 2, and 3, the P_{CH_4}/P_{H_2} ratio was evidently too high in the hydrogen used. Whether this results from small amounts of impurities in the purchased (99.999% H_2) gas or from contamination in the gas train is not known. In any case, the as-milled powders were actually carburized during cleaning (starting carbon = 0.73%).

Since the elevated temperature exposure was necessary for removal of oxygen, and since no elaborate hydrogen purification apparatus was available for the required removal of carbon-bearing impurities from the cleaning gas, this technique was abandoned.

Carbothermic Cleaning - The second technique investigated utilizes the following reaction for interstitial cleaning:

$$3C + Cr_2O_3 \rightarrow 3CO + 2Cr \qquad \text{(Equation 4)}$$

The equilibrium between carbon, O_2, and chromium at elevated temperature and reduced pressure can be described in more detail through the use of the Pourbaix-Ellingham diagram [14] shown in Figure 12. The operating conditions corresponding to equilibrium between various two-phase combinations are appropriately labeled on the diagram; e.g., if temperature and pressure are regulated such that they lie above the upper line, the equilibrium phases will be Cr_2O_3 and carbon. All carbides are metastable in this region and would tend to decompose to graphite according to the reaction $Cr_xC_y + zO \rightarrow x/2\ Cr_2O_3 + YC$. Likewise, if the operating conditions (P_{CO}, and temperature) are held in the region below the lower line, all Cr_2O_3 should be reduced according to Equation 4. The effective removal of both carbon and O_2 is, therefore, a matter of adjusting the operating conditions and the carbon content so that at the end of an isothermal cleaning treatment, the original chromium, carbon, Cr_2O_3 mixture has traversed the two phase fields from high P_{CO} to low P_{CO} and has arrived at the lower line with only trace amounts of Cr_2O_3 and $Cr_{23}C_6$ remaining.

Cleaning was carried out initially in a 1-1/2 inch ID, tantalum wound resistance furnace which was operated inside a vacuum (10^{-5} tor) glove box. All powder handling was carried out in this chamber. Loose, as-milled powders were spread out in a thin layer on metal trays and placed in the horizontal tube furnace for cleaning. These trays were made of either tantalum, zirconium, or titanium, each of which is an excellent "getter" for interstitials. The experimental variables investigated were temperature, time, powder depth, and tray (getter) material. Evaluation of the cleaning procedure was in terms of gas analysis of the loose powders. The powders were encapsulated under helium in a small tin

capsule which was transported to the vacuum fusion apparatus in a helium filled glass capsule where it was analyzed for oxygen, hydrogen, and nitrogen. Carbon content of the powders was measured using air handling procedures in conjunction with either gravimetric or conductometric analysis.

Starting material for this series of experiments was a Cr-5 $v/_o$ MgO-1.0Mo-0.25 Hf, Th, Y alloy which had been ball milled at -50°F for 500 hours in toluene. In addition to the 2.6% MgO which was added as dispersoid, the powder contained 0.25% MgO which was residual from the powder production process. Total oxygen content prior to cleaning was 1.04% as dispersoid, 0.10% (production MgO) and 0.46% as contamination. The results of this series of powder cleaning runs is given in Table 11 (numbers 10 through 16). Oxygen content in this Table is reported as the contamination portion of the total oxygen concentration and was derived by subtracting either 0.10% or 1.14% from the analyzed total oxygen content. The data tabulated in numbers 10 through 16 of Table 11 is also shown graphically in Figures 13 and 14. Figure 13 demonstrates the effect of cleaning temperature on carbon content with time and "getter" materials as parameters. A comparison of the efficiency of gettering materials in aiding carbon removal made from this graph suggests that zirconium is the most efficient. Since zirconium has very poor high temperature strength,

later experiments were conducted in tantalum boats with strips of zirconium sheet mixed in with the powder. Oxygen content of these same powders expressed as a function of cleaning temperature is given in Figure 14. Experimental difficulties inherent in analyzing a loose powder mixture containing an oxide dispersoid is evidenced by the large amount of scatter in these data. Credibility of the oxygen results was questioned still further when samples analyzed after densification by gas pressure bonding (numbers 11 and 15 in Table 11) exhibited higher oxygen contents than did the loose powders. The higher oxygen content in the compacted alloy could have resulted from powder handling during

densification, but the disagreement could also be the result of dispersoid segregation or poor sampling of the loose powders. In an effort to resolve this difficulty, analytical techniques were unsuccessfully sought which would differentiate between MgO, Y_2O_3, and Cr_2O_3.

The above process was limited by the small furnace size to 5-20 gram samples sizes. In an effort to increase the output of the above furnace, an attempt was made to convert the cleaning from a batch process to a continuous process. Continuous cleaning was to be accomplished through use of a moving tray. Dwell time in the furnace hot zone was regulated by varying the speed of boat travel through the furnace. A line drawing of the apparatus used for the investigation of this continuous cleaning process is shown in Figure 11B. Initially, a fifteen inch long zirconium tray was moved slowly through the furnace hot zone (2200°F) with a dwell time of five minutes. Gas analysis of loose powders from this investigation indicated that neither carbon nor oxygen was being removed. This lack of cleaning was evidently the result of redeposition of both carbon and oxygen in cold portions of the furnace. A compromise between continuous and batch cleaning was then proposed in which several boats could be cleaned without breaking the vacuum. This semi-continuous method is identical to batch cleaning except several short boats were connected so that when one was in the hot zone, the others were completely outside the furnace. When cleaning of one tray was completed, a mechanical feed-through mechanism was actuated to pull it out of the furnace and simultaneously pull the next one into the hot zone. Chemical analysis of the powders cleaned using this procedure showed that while the powder from the second boat was cleaned (200 ppm carbon), powder from the first boat was not (1800 ppm carbon). This indicated that CO which was driven off the second boat was redeposited on the first despite the fact that it was outside the furnace. This phenomenon is further confirmed by consulting the Pourbaix-

Ellingham diagram of Figure 12 where the approximate operating conditions in the hot zone and in the colder portions of the furnace are noted. Equilibrium phases in the hot zone are $Cr_{23}C_6$ and chromium, while those in the cold zone are Cr_2O_3 and carbon. Carbon monoxide, therefore, transports carbon and oxygen from the hot center to the cold portions of the furnace, and only a small amount of cleaning is accomplished. All subsequent cleaning was, therefore, done by a batch process.

One hundred gram quantities of powder which were cleaned in preparation for extrusion were exposed for cleaning in a stack of three 2-inch X 5-inch tantalum boats with a 0.275-inch powder depth.

The foregoing results, obtained from chemical analysis of loose powders, indicate that both carbon and oxygen may be substantially reduced by carbothermic cleaning. Although analysis of loose powders indicated that the oxygen content was quite low, the data contained large amounts of scatter. High oxygen content of these same powders after compaction therefore raised a question as to the efficiency of the process in reducing oxygen. In order to answer this question, carbothermic cleaning was carried out on chromium powders which contained no oxide dispersoids. Analytical errors resulting from poor sampling of oxide dispersoids which were present in the powders were thereby eliminated. This work is also reported in Table 11(1-5). Starting material was the French chromium powder which was ball milled without dispersoid for 465 hours at -50°F in toluene. Carbon content of the as-milled powder was exceptionally low with the result that an insufficient quantity was available for stoichiometric combination with the 0.403% oxygen present as contamination. The analyses indicate that after a very rapid decarburization period, the powder was actually oxidized. The extent of this oxidation increased with increasing temperature. Carbon content of the cleaned powders was very low in those cases where the powder

was cleaned at temperatures greater than 1800°F. Initial oxygen analysis indicated that oxygen was substantially reduced at 1600°F. Carbon analysis of the sample cleaned at 1600°F indicated only a small reduction of carbon, thereby challenging the oxygen analysis. A recheck using powders which had been exposed to air showed only a minor reduction in oxygen which was in close agreement with the corresponding decrease of carbon. Powder cleaning reported in Table 11 as numbers 6 through 9 was conducted using the same starting powders with an addition of high purity graphite. These results are also shown graphically in Figure 14 where they are compared with the results of the previously cleaned Cr + MgO powder. As shown, a 2400°F/50 min exposure of chromium graphite mixtures reduced the oxygen content to 130 ppm. Although the previous work with Cr + MgO indicates complete removal of oxygen at a lower temperature than 2400°F in the same fifty minute exposure period, these results were obtained with powder depths of 0.05 inches as compared to a depth of 0.275 inches for the chromium-graphite mixture. Gas analysis of powders cleaned at 2400°F and subsequently exposed to air indicate that the product has sintered sufficiently that oxygen contamination from air handling was no longer a critical problem.

5.3 CLEANING OF FLAKE SHAPED PREALLOYED POWDERS

In the submicron blend discussed previously[5.2], interstitial contamination originated from two sources: 1) oxygen from the purchased powders; and 2) carbon from the ball milling step. A cleaning process was developed which was capable of the simultaneous removal of both, but the high reaction temperatures required caused dispersoid agglomeration. The cleaning technique discussed in this section was designed to be used with a coarse ultrapure prealloyed powder. Ball milling of a coarse starting product to submicron powders is more difficult than with the previous fine starting powders but oxygen contamination should be minimized since the major source of oxygen has been removed. If further oxygen contamination of this powder can be avoided, cleaning may be aimed at removal of carbon alone.

In the design of the experimental equipment for removing carbon from the as-milled powders, several thermodynamic, diffusion, and practical factors were taken into consideration and will now be discussed.

Thermodynamic Considerations

The form in which the carbon contaminant is present in the powders is not known. It may be present as adsorbed carbon, an adsorbed carbon-hydrogen complex or as carbides. It seems unlikely that Cr carbides are present in the as-milled powders since milling was done at -50°F. It will be shown using thermodynamic arguments that if the carbon is present as adsorbed multilayers, removal by the methane reaction in a high-pressure hydrogen cleaning system is quite feasible. If on the other hand, the carbon is present initially as a Cr carbide, or if carbides form during cleaning, purity requirements of the hydrogen cleaning environment are much more demanding and probability of successful cleaning is greatly diminished. In order to avoid carbide formation, cleaning conditions were sought which would suppress the carbide reaction while enhancing the CH_4 reaction. Several reactions can occur upon heating carbon-contaminated Cr powders in a H_2 environment. The various carbothermic reactions considered here are shown in Table 12 together with the free energy of reaction for each as a function of temperature. As can be seen in the Table, the free energies of the various reactions involving chromium increase negatively with increasing temperature. In contrast, the reaction between carbon and hydrogen to form methane is favored by decreasing temperature. Since the objective is to remove carbon, hydrogen cleaning then should be done at as low a temperature as practical.

From inspection of the equations shown in Table 12, and consideration of LeChatelier's principle, it can be seen that an increase in the hydrogen pressure will tend to make reaction I proceed to the right and reactions

III, V, and VII, which involve chromium and methane, proceed to the left. However, changes in pressure will have no effect on the direct reaction between carbon and chromium (reactions II, IV, and VI).

Since the reactions involving gases (I, III, V, and VII) are the reactions necessary to achieve cleaning, a more detailed inspection is in order. If the reactions considered proceed under standard conditions, the equilibrium partial pressure of P_{CH_4} and P_{H_2} may be obtained from knowledge of the standard free energies of reaction according to,

$$\Delta F^\circ = -RT \ln K$$

$$\text{where } K = \frac{P_{CH_4}}{(P_{H_2})^2}$$

If, however, the reaction is forced away from standard conditions by artificially applying a constant high pressure of hydrogen, the applicable equation is,

$$\Delta F_R = \Delta F^\circ + \ln Q$$

$$\text{where } Q = \frac{P'_{CH_4}}{(P'_{H_2})^2}$$

This quantity, Q, is not the equilibrium constant K but is a ratio of the new partial pressures observed as a result of the artificial application of P'_{H_2} to the system. If the reaction proceeds to equilibrium under the application of contant P'_{H_2} pressure,

$$\Delta F_R = 0 = \Delta F^\circ + RT \ln \frac{P'_{CH_4}}{(P'_{H_2})^2}$$

and P'_{CH_4} may be calculated using the known values of P'_{H_2} and ΔF°[13]. Application of this equation to the reactions of interest may be done for varying temperature and P'_{H_2} and the corresponding P'_{CH_4} calculated. This was done for reactions I and III and the resulting P'_{CH_4} values are plotted in Figure 10 as a function of T with P'_{H_2} as a parameter. Values of P_{CH_4} in excess of that shown by the appropriate lines on the diagram quench the cleaning reations and the equations shown proceed to the left recontaminating the powders. If P_{H_2} is maintained constant at the values shown and if the methane pressure formed during cleaning is less than that shown by the appropriate line, the reaction is spontaneous and cleaning is possible. Here it can be seen that there is a strong pressure effect and corroborates the previous statement that an increase in the system pressure (which in the present experimental program can be shown to be almost entirely due to hydrogen) increases the equilibrium methane pressure and favors the formation of methane by all of the reactions involving gases. If carbon is present as an adsorbed layer, the equilibrium partial pressure of CH_4 in 1 atmosphere of hydrogen is 70 atmospheres at 800°F. At 10 atmospheres hydrogen pressure and the same temperature, P_{CH_4} is 2500 atmospheres. Removal of adsorbed carbon is, therefore, favored by low temperatures and elevated hydrogen pressures.

Diffusion Considerations

If the carbon contamination is assumed to consist of an adsorbed layer, then it is exposed both to the hydrogen gas and the chromium metal. Reaction with the former involves gaseous diffusion, whereas reaction with chromium requires solid-state diffusion. At low temperatures, it seems likely that gaseous diffusion will predominate and that the solid-state diffusion reaction would be negligible, thus enhancing carbon removal.

Practical Considerations

There are two general methods which could be used for removing the carbon with hydrogen, a dynamic or flowing system and a static system. The advantages and disadvantages of each as applied to this process were considered and a discussion of the more important factors follows. The important requirements of the task to be performed are:

1) Removal of carbon from loose or cold-pressed Cr powders by gaseous reaction with H_2 (cleaning goal = 100 ppm). Accomplish this in such a way as to avoid carbide formation (low temperature, high hydrogen pressure).

2) Maintain a low oxygen environment which will not oxidize the Cr powders. (goal = 100 ppm O_2 in excess of ThO_2)

3) Avoid mechanical or thermal disturbances which would destroy the initial "blend" of oxide and metal powders.

Thermodynamic considerations of task 1 were discussed previously and indicated that cleaning of adsorbed carbon is favored by high hydrogen pressures and low cleaning temperatures. Such operating conditions are most easily accomplished in a static system. Kinetic consideration of the CH_4 reaction shows that even in the above case of adsorbed carbon for example, removal of reaction products may be a problem in spite of the fact that equilibrium CH_4 pressure is considerably greater than the applied H_2 pressure. Here, it is a case of replenishing the depleted supply of reacted H_2 in the powder voids which may limit the reaction rate. In addition to dust losses and/or flow-connected segregation of the ultrafine ThO_2, another potential problem in a flow system is oxidation of the reactive alloying elements by trace amounts of oxygen present in even high

purity hydrogen. The partial pressure of oxygen in equilibrium with Cr_2O_3 at 1000°F for example is 10^{-40} atmospheres. This is a number which is well beyond even the purest of bottled hydrogen for example, and in a flowing system even trace amounts would be critical because a constant oxygen supply would be maintained by the continuing flow of hydrogen. Stein [15] developed a hydrogen cleaning system for Fe in which he overcame this problem by using a closed loop in which the H_2 was regenerated in a gettering chamber and then recirculated for cleaning. His normal procedure was to circulate hydrogen through the gettering chamber for extended periods of time in order to remove all traces of contamination originating from the equipment itself and the original charge of hydrogen. After this was completed, he heated the sample to temperature for cleaning while continuing the recirculation of gettered hydrogen. A modified version of this technique in which gettering could be accomplished at high pressure was incorporated into the design of the present static system, which is shown schematically in Figure 15. Major components of the closed system are two independently heated, hot-walled pressure vessels and an interconnecting high-pressure gas train. Metal-to-metal seals were used in both vessels to avoid outgassing problems normally associated with "O" ring closures. All connections in the gas train were also metal/metal for the same reason. Sample temperature in the reaction vessel and hydride temperature in the source vessel were both monitored using thermocouples located in a well in the vessel wall. In both cases, the hot junction was adjacent to the center of the sample. Ten grams of the powder to be cleaned were spread in a thin layer on the bottom of a 2-3/4" diameter nichrome can. The metal can was intentionally oxidized prior to cleaning in order to prevent metallic contamination of the powders from the nichrome. This can was placed on a rack which contained similar cans of zirconium Getterloy* powder vertically above and below it. The source furnace was positioned horizontally and contained 100 grams of hydride powders in a trough-shaped boat approximately 4" long.

*64% Zr-36%Ti powder purchased from Penn Nuclear Corp., Penn, Pensylvania, 15675

High pressure hydrogen was generated by heating the hydride into the 1200-1650°F range. Achieving the needed ultra high purity environment necessary to avoid Cr oxidation was accomplished by evacuating to 30μ Hg, back filling with ~15 psig H_2 and gettering with hydride powders which were decomposed and rehydrided several times before heating the Cr powders. Thus, impurities brought into the system during loading were mixed with the high-pressure hydrogen and subsequently reacted with the hydride during rehydriding. After two or three 15-250 psi H_2 cycles to getter the hydrogen, the Cr sample was heated to the desired temperature and pressure. Pressure cycling was accomplished again, by decomposing the recombining the hydride powders.

Results

A cursory investigation of the effect of cleaning temperature (T_C), cleaning time (t_C), hydrogen pressure (P_{H_2}) and number of pressure cycles (N) on the kinetics of carbon removal was conducted. Of the four temperatures investigated (400°, 600°, 800°, and 1000°F), 800°F was the most efficient observed temperature for removal of carbon by reaction with hydrogen and was, therefore, used to investigate t_C, P_{H_2}, and N.

Initially, it was projected that removal of reaction products from the powder voids, particularly during the late stages of cleaning might be essential for the continued removal of C. Pressure cycling in the reaction vessels was designed to accomplish this removal of the CH_4 reaction product and was to be carried out by decomposing and rehydriding the Ti H_2 source powders. Two problems were encountered in cycling experiments as follows:

First, the hydride decomposition does not occur over a wide temperature range and as a result, H_2 pressures were difficult to achieve reproducibly. The kinetics of hydride decomposition/reformation are also dependent upon

their interstitial impurity content. When the hydrides "getter" reaction products from the cleaning process, they become more sluggish during both pressurization and depressurization. This is particularly noticeable during rehydriding and contaminated powders may not reduce the pressure to the desired level. In cleaning Run No. 2 for example, the H_2 pressure was reduced from 300 to 140 psi instead of the desired 50 psi.

The second problem involves the slow heating and cooling rate of the source pressure vessel. Heating the hot-walled vessel from room temperature to 1650°F, for example, requires approximately 4 hours. Cooling may be accelerated by application of cooling air or cooling H_2O coils to the outside of the vessel, but even here cooling may occupy more than an hour. The period of the pressure cycle then is at least 5 hours. During this complete cycle, the Cr powder is maintained at the desired cleaning temperature. In order to determine the importance of pressure cycling, cleaning time is reported in Table 13 as both time at high pressure and as total time at temperature. No systematic trend in the data was found when exposure time was considered to be only that time spent at high H_2 pressures. When the 800°F data is plotted as a function of total time at temperature, the resulting curve shows a rapid initial decrease in carbon content followed by the asymptotic approach to a fixed value of percent carbon at longer times. This carbon plateau was not a function of hydrogen pressure as may be seen in Figure 16. The horizontal region of the 800°F curve contains points which were obtained at 50, 200, 250, and 300 psi H_2 pressures. Since the 50 psi point falls at shorter times but at the same final C percent as the higher pressure points, it is obvious that P_{H_2} was not an important variable in this region. At short times, however, pressure seemed to exert a slight effect, as may be seen by the two 60 minute points on the 800°F curve. Here 60.4% of the C initially present was removed in 500 psi H_2 while only 53.4% C was removed in 250 psi H_2.

All samples cleaned were 10 gram size except samples 10 and 11 of Table 13 which were 100 grams. Data from these tests fall on the same general curve as that obtained from 10 gram samples.

The formation of loosely bound agglomerate groups of Cr particles during ball milling would tend to hinder access of H_2 to surface reaction sites for the formation of CH_4 in subsequent H_2 cleaning. Such groupings might be predicted to occur during ball milling. If this were the case, ball milling cleaned powders for a short time might break up such clumps and, therefore, aid H_2 exposure to new surfaces. In order to check this possibility, Run No. 10 was ball milled for 24 hours and re-exposed in Run No. 11. The results fall on the plateau as would be normally expected without such treatment.

Normally, the procedure for cleaning involved 2 or 3 pressurizing cycles, which were aimed at purifying the initial environment. These were followed by the initial heating of the cleaning vessel. Heating time to 800°F usually occupied from 3 to 3-1/2 hours. Sample number 8 was an exception to this procedure and heating in this case was done in approximately half this time. The results of this test (94.3% C removed or .08% C remaining) are the best obtained to date.

Discussion of Results

The observed optimum in cleaning temperature is not unexpected since the driving force for CH_4 formation increased by decreasing temperature. The actual mechanism of formation of the CH_4 molecule would be expected to be thermally activated and this would favor high temperatures. The most efficient cleaning temperature should then occur at an intermediate temperature as a result of the compromise between these two factors.

Progress of the reaction with time shows behavior which is typical of many chemical and metallurgical reactions. A rapid initial reaction rate decreases with time and approaches zero at long times. This is the behavior shown in Figure 13. A surprising feature of this plot, however, is that the asymptotic value in the figure is not much closer to 100% "C removed" as is normally observed in most kinetic phenomena of this type. This evident plateau at 80 "%C removed" coincides with one monolayer of carbon on the surface of flakes whose major surface has an (001) orientation. Details of this calculation which used the BET value of 9.0 m^2/g as a measure of surface area, are given in Appendix I. Whether this is of significance, however, is speculative at this stage of the investigation.

If carbon contamination on individual Cr powder particles exists initially as multilayers of adsorbed atoms, the outer layers are undoubtedly bound by the relatively weak forces associated with physical adsorption. The innermost layer on the other hand would be affixed much more strongly by chemisorption. During cleaning, the weakly-bound outer layers would be easily removed by the CH_4 reaction. The inner layer, however, being in intimate contact with the metal itself, might even be in the form of a monolayer of carbide. Whether carbide or chemisorbed monolayer, however, the activity of the carbon atom would be much lower than that associated with the outer layers. Practically, this means that the H_2 environment must be kept very pure (low P_{CH_4}) or the CH_4 reaction will not proceed.

The fact that P_{H_2} did not show a strong effect on the carbon removal was quite surprising. During the early stages of the kinetic curve of Figure 13, a pressure effect is observed, but it is not as strong as originally anticipated. The lack of a strong pressure effect in the plateau region of Figure 13 is quite significant. Since the maximum allowable P_{CH_4} which will still allow cleaning to proceed is a function of P_{H_2}, this would seem to indicate that the cleaning in the plateau region is no longer governed

by thermodynamics associated with adsorbed C. The appearance of this barrier indicates a drastic change in activity of the adsorbed carbon. Although this could be due to strong bonding of the innermost chemisorbed layer of carbon, carbide formation seems more compatible with the observed results. Removal of carbide, for example, would necessitate an increase of several orders of magnitude in the purity (P_{CH_4}) of the cleaning environment while a more gradual transition in the carbon activity with successively lower layers of adsorbed carbon would be expected. Carbide formation would also depend upon pre-cleaning thermal history of the sample as is suspected in sample 8.

The fact that number of pressure cycles had no effect on the observed results (Figure 13) indicates that reaction products are removed from the powder voids by gaseous diffusion. As the CH_4 reaction progresses within the voids, pressure diminishes since 2 moles H_2 form one mole CH_4. Pressure is equilibrated by a flow of fresh hydrogen into the voids. This is a diminishing process and as the methane pressure within the void approaches the external P_{H_2}, the reaction will become dependent upon counter diffusion of CH_4 out of, and H_2 into, the voids. Calculations show that only 1.5% of the C contamination may be converted to methane without removing reaction products from the voids. This would predict a large number of pressure cycles necessary for cleaning if gaseous diffusion were not effective.

6. COMPACTION OF THE CLEANED BLEND TO HIGH DENSITY

6.1 GAS PRESSURE BONDING - (Submicron Blends Cleaned Carbothermically)

The high pressure, high temperature autoclave used for compaction consists of three major parts: 1) the 10,000 psi, H_2O cooled pressure vessel which contains a 3000°F three zone, molybdenum wound, electrical resistance (1-1/2 inch I.D.) furnace; 2) four-stage compressor capable of compressing helium to 10,000 psi; and 3) the control panel which houses temperature, pressure controllers and indicators. Furnace temperature is monitored at each of the three furnace zones by platinum-platinum rhodium thermocouples.

Densification of the powders occurs as a result of gas pressure transmission to the powders through the encapsulating material. Figure 17 illustrates the degree of densification by a comparison between the capsule dimensions before and after autoclaving. The wire bail seen in the Figure was tack welded onto the capsule to promote ease of handling in the autoclave. The major problems encountered in this technique were lack of densification as a result of defects in the sealing welds and collapse of the capsule into an irregular shape during compaction. In order to avoid leakage problems, the capsules were leak tested by pressurizing in 30 psi helium for fifteen minutes and checked for helium "weepage" in a vacuum system connected to a helium leak detector. Just before charging into the autoclave, the capsules were wrapped in tantalum foil which acted as getter during the high temperature exposure.

The autoclaving conditions used for densifying powders prior to extrusion were selected on the basis of 98% density, minimum interparticle spacing (IPS), and general microstructure of three different compactions. The contract specifies density of more than 98% theoretical and IPS of

less than 1.5 microns for the submicron blends. As may be seen in Figure 18 the optimum autoclaving conditions were 2000°F/2 hrs/ 10 ksi He. The temperature for the extrusion operation was also selected as 2000°F.

6.2 EXTRUSION - (Submicron Blends)

Extrusion of the Cr-4Mo-5 $v/_o$ MgO-0.25 each Hf, Th, Y alloy (5MO-2 of Table 14) was carried out at 2000°F in the two types of low carbon steel extrusion capsules shown in Figure 19. The precompacted material was obtained by autoclaving at 2000°F/2 hrs/10 ksi He and the densified capsule machined down to 0.90 inch diameter. A two-inch bar of this material was then placed in the extrusion can and the can electron beam seal welded under vacuum.

Loose elemental powder of the 5Mo-2 alloy was encapsulated in the extrusion can (Figure 19) using the same outgassing and powder handling procedures as described earlier. After filling the capsule, the piston was sealed to the body of the can by TIG welding with very light penetration. The final vacuum seal was again accomplished by EB welding of an axial hole in the piston.

Extrusion was carried out at the Research and Development Center of General Electric Company using an 18/1 extrusion ratio at 2000°F. The design of the loose powder capsule was such that movement of the piston relative to the container body precompacted the powders prior to extrusion through the die. The extruded rod emerged in three pieces which are shown in Figure 20. Extrusion of the autoclaved powders yielded similar results and are also illustrated in Figure 20. In this case breaks in the extruded rod were observed at regular four-inch intervals.

Upon removal of the steel jacket by acid pickling in a 50% HCl, 50% HNO_3 solution, it was found that the chromium alloy core was not in the shape of a rod, as expected, but consisted of small (10 gram), tear-drop shaped buttons. These buttons were located at the breaks in the extruded rod seen in Figure 20. This phenomena was originally thought to result from a poor matching of strengths between the soft thick-walled can and the chromium alloy core, and later extrusions were therefore canned in unalloyed molybdenum capsules.

In an attempt to salvage material for mechanical testing, several of the above buttons were drop forged (one blow at 2000°F) followed by hot rolling at 2000°F and 2200°F. The forging, which was done in air, was quite successful, with only small amounts of edge cracking. These cracks were benched off on a wet 180 grit emery paper prior to hot rolling. The unclad specimens were heated in hydrogen and given a 20% reduction in one pass. Severe cracking occurred at both 2000° and at 2200°F, rendering these specimens useless for future mechanical testing.

After autoclaving, the 5 $v/_o$ Y_2O_3 alloys containing variations in reactive element additions (5 YO series, Table 14) had irregular cross sections which were not completely removed by machining for encapsulation in the extrusion cans. These irregularities, therefore, were still evident in the extruded product of alloy 5YO-2 (0.25 REA) thereby reducing the number of tensile specimens attainable form this alloy. As in the 5Mo-2 alloy, the 5YO-3 (0.3 REA) extruded into short segments. Tensile test results in this series of alloys indicated that this segmentation was probably the result of intergranular failure of an ultrafine grained structure. Since extrusion is normally used to break up coarse, segregated, as-cast structures, which are not present in these ultrafine grained compacts, the next series of alloys was processed by autoclaving and swaging, omitting

the extrusion step. This series was to include the base-line alloy (Cr-3Mo), 2YO, 2MO, 3YO, 3MO, 7YO, and 7MO alloys of Table 14, all encapsulated in unalloyed molybdenum cans. The molybdenum cans in this series, however, were very poor quality and wall movement during autoclaving caused cracking. The first and second autoclave attempts in this series were, therefore, unsuccessful. After superposing a tantalum jacket over the molybdenum can, these alloys densified successfully on the third attempt. Since the capsules were buried in Ta "gettering" powder during autoclaving, the leakage to the powder was not considered to be a source of interstitial contamination.

Swaging was initiated on the base-line alloy but was aborted as a result of cracks and checks in the molybdenum jacket with subsequent exposure to possible embrittlement by nitrification. The remaining alloys were therefore impact extruded at 2000°F using a 4/1 extrusion ratio at Superalloy Forge, Hamburg, Michigan. Of the four alloys extruded (2MO, 2YO, 7MO, and YO) only the alloy with 2.5 $v/_o$ Y_2O_3 dispersoid was sound. Both 7MO and 7YO contained numerous transverse cracks and 2MO contained only a small amount of sound material. The extrusions are shown in Figure 21. A summary of thermo-mechanical processing is documented in Table 15.

6.3 COMPACTION OF COARSE PREALLOYED FLAKES

Successful dispersion strengthening is thought to depend (at least in part) upon achievement of a strong crystallographic texture.[16,17,18]. Since the as-milled flakes (50% less than 2μ) have a strong (001) texture, compaction was done in such a way as to preserve this preferred orientation. As-milled flakes have a large diameter/thickness ratio and thus align themselves in parallel layers. If the powders are compacted without disturbing this flake alignment, the as-compacted alloy should exhibit a preferred crystallographic texture. Enhancement of this

crystallographic texture by secondary working should thus be greatly facilitated. The technique which seemed most promising for producing and maintaining flake alignment during processing was hot pressing. Four separate unsuccessful attempts were made initially to produce a sound compact of Cr-4Mo-.15 (LA + Y) for use in thermomechanical processing (TMP). The starting material in each case was H_2 cleaned at 800°F/ 200 psi H_2/ 40 hrs. The cleaned powders were transferred between cleaning system and the vacuum hot press in "Transfer/Hot Press" capsules in which they were cleaned. Pressing conditions and capsule design used with each of the compacts are given in Table 16. Subsequent rolling was conducted at 2000°F without decapsulating. The thick end closures of mild steel capsule #1 and #2 caused irregular flow during hot pressing which resulted in substantial variations in thickness in the as-pressed compact. This undesirable phenomenon was further exaggerated during hot rolling at 2000°F. To eliminate this problem, a capsule with thin sheet end closures was used in Hot Press #3. This configuration compacted well but suffered an "alligator" type fracture during rolling as a result of inadequate strength in the end closure. Use of higher strength capsule (304 stainless tubing) in Hot Press #4 yielded a product which was similar to that of capsule #1. These results indicated that the encapsulation requirements for hot pressing and for hot rolling were divergent and that different encapsulation should be used in each process.

The difficulties encountered in the first four attempts to produce sound Cr-4Mo-4 $v/_o$ ThO_2 compacts by hot pressing were overcome in the fifth attempt (Hot Press #5). The earlier failures were the result of inadequate encapsulation which was circumvented by using two types of encapsulation, one for hot pressing and the other for hot rolling. After vacuum hot pressing to full density (7.26 g.cc) at 2200°F/2 hrs/10 ksi in a stainless steel capsule with thin end closures, the compact was decapsulated and sectioned in preparation for hot rolling.

6.4 SECONDARY WORKING

Attempts at secondary working of the submicron blend compacts met with little or no success. These trials which are summarized in Table 15 included hot rolling, swaging, and drop forging. Secondary working of the coarse (2μ) flake-shaped prealloyed powder, on the other hand, was quite successful. In this case, the decapsulated hot press compact (Hot Press #5) was sectioned as shown in Figure 22 and a cursory study of the rolling temperature was conducted on the scrap pieces (Figure 22). The results of this study are reported in Table 17. Rolling was conducted with 8" diameter rolls at a roll surface speed of 480 inches/minute. These samples were sandwiched between 60 mil hastelloy X sheet and rolled in the same direction each of the three passes. Density measurements indicate that the compacts were fully dense both before and after rolling. Preliminary texture measurements show that the rolled sheet has a strong (001) texture which increases intensity with increasing rolling strain. This is reported in Table 18 where the intensities of the (110), (200), and (211) planes are shown as a ratio between the intensities from the sheet material and from a randomly oriented ASTM standard. The larger pieces of Hot Press #5 were encapsulated in a Hastelloy X picture frame compact (Figure 23) after which they were rolled to sheet according to parameters selected from the data of Tables 17 and 18. The large pieces were successfully rolled 84% at 1800°F and decapsulated in preparation for further evaluation. All subsequent test material was produced by these same processing procedures.

7. ALLOY EVALUATION

7.1 DISPERSOID STABILITY

7.1.1 Alloys Compacted From Submicron Blends

Although the ball milled submicron blends resulted in relatively fine as-densified dispersions, thermal exposure of such alloys causes severe dispersoid agglomeration. Alloy 5MO-1, for example, has a particle size of $< .1\mu$ after compaction by autoclaving. Thermal exposure of this compact, however, causes drastic coarsening of the MgO and an associated increase in IPS. Examples of this phenomenon, which is common to all three (MgO, Y_2O_3, and ThO_2) dispersoid oxides used, is shown in Figures 24 through 27. Tabulation of this instability is given in Table 19. Several notable features of this instability are listed as follows:

1) Dispersoid particles grow from $< .1\mu$ to $> 1.0\mu$ upon extended thermal exposure at 2600°F.

2) The coarsened particles are not spherical but have a very irregular, elongated morphology (Figure 24).

3) Initially, oxide particles are relatively equiaxed and are located in grain boundaries. After thermal exposure, matrix grain growth occurs leaving a few particles behind which are not associated with boundaries. These particles are usually very fine.

4) The major fraction of oxides, however, are still associated with grain boundaries after grain growth. These are segregated in cuspoidal shapes at triple points.

5) The final morphology gives a vague outline of the matrix grain boundaries, with a resulting increase in IPS of more than one order of magnitude. (Figure 25)

6) In the alloys containing Y_2O_3 and MgO, x-ray diffraction studies indicate that excess oxygen was present initially as Cr_2O_3 but after extended thermal exposure combined with the Y_2O_3 or MgO to form a spinel.

7) The spinel/matrix interfacial energy is approximately the same as the Cr grain boundary energy. This is evidenced by the contact angle between $YCrO_3$ and Cr at a grain boundary triple point and is shown in Figure 26.

8) Instabilities seem to be independent of the ability of the oxide to resist spinel formation since ThO_2 which is reported to be inert to Cr_2O_3[3] shows the same behavior as MgO and Y_2O_3 which readily form such complex oxides.

Existing theoretical treatments of such instabilities such as those by Wagner [19], Lifshitz and Slyozov[20], and Oriani[21], are based on dissolution of fine particles and reprecipitation on coarse ones. Such instabilities could occur utilizing grain boundary diffusion as transport, but in this case, it does not seem likely that the resulting coarse particles would have such irregular shapes. Aust[22] and Beamond, et al[23] have proposed the possibility of particle movement without dissolution. In both cases, it was proposed that particles moved with the grain boundary.

As the grain boundary migrates, more and more particles are swept up, until local contact is made between adjoining particles. Such a mechanism would explain the non-random location of dispersoids, their highly irregular shapes and their location at grain boundaries and triple points. A schematic representation of such instabilities in various stages of completion is shown in Figure 28.

According to this model, one of the ultrafine grains grows at the expense of neighboring grains. Growth may be the result of differences in strain energy (from ball milling) between adjoining grains or it may reflect a variation in vapor pressure as a function of crystallographic orientation. In the latter case, atom movement across the boundary would occur by vapor transport, while surface diffusion of Cr both on the oxide and along the grain boundary would fill the area shadowed from the vapor by the oxide.

7.1.2 ALLOYS COMPACTED FROM PREALLOYED FLAKE-SHAPED POWDERS

The relative stability of oxides in a Cr matrix compacted from flake-shaped powders lends further credence to this theory. In the photograph of Figure 29, Y_2O_3 oxides which are almost in contact with each other appear to be quite stable. In this case, the preferred orientation of the flakes promotes formation of a low energy grain boundary which is quite resistant to migration. Similar coarse prealloyed (Cr-4Mo-.15 (La + Y) compacts containing 4 $^{V}/_{o}$ ThO_2 are also resistant to dispersoid coarsening. After 2600°F/10 hour exposure for example, the fine ThO_2 particle extractions shown in Figure 30 are relatively unchanged in size when compared to those in the as-compacted alloy of Figure 31. The massive ($\geq 1\mu$ diameter) particles seen in both photographs are evidently Cr_2O_3 which originates from the .55 w/o excess oxygen which was picked up

in powder handling. As is evident here, the fine ThO_2 particles are quite resistant to agglomeration even in the presence of large excesses of oxygen contamination. The coarse Cr_2O_3 particles are unstable at 2600°F in vacuum and may actually disappear as shown in Figure 30. This depletion of Cr_2O_3 seems to be completely independent of the ThO_2 particles since the change in ThO_2 particle size here is from 700Å to 800Å during the 2600°F exposure. Whether or not this is a real change in ThO_2 particle size is questionable, however, since the 100Å change is probably just slightly larger than the limits of accuracy of the technique (estimated to be $\pm$ 10%). In either case, however, this is a major improvement over the stability exhibited by the submicron blends (Table 19) where particles grew to ~1μ sizes during similar exposures. The type of instability which caused the drastic particle growth shown in Table 19 seems to be independent of the properties of the dispersoid since it occurs in a similar fashion to alloys containing ThO_2, MgO, and Y_2O_3. In addition, it seemed to occur whether or not large excesses of oxygen were present and also whether or not double oxide formation occurred. On the other hand, these drastic instabilities disappeared in alloys which contained a strong preferred orientation in the matrix.

7.2 CHEMICAL AND MICROPROBE ANALYSES

Chemical analysis for sulfur and metallic elements (with the exception of molybdenum) was done at Ledoux and Company, by both wet chemical and spectrographic techniques. Oxygen, hydrogen and nitrogen in the compacted alloys were analyzed by gas fusion techniques at the Material and Process Technology Laboratories (MPTL) of General Electric Company. The molybdenum and carbon content were determined from powders; details of these techniques were reported in Section 4.3. These results are tabulated in Tables 20 and 21 The semi-quantitative analysis of Table 20 was conducted at MPTL as a monitor to process contamination. As may be seen here, metallic element contamination (with the exception of Mo) was not a problem.

In order to determine if molybdenum concentration gradients existed in the autoclaved material, line profile microprobe traces were carried out on an ARL (Applied Research Laboratories) electron microprobe analyzer in MPTL. The specimens were mounted in an electrically conducting material (Copper Diallyl Phthalate) and metallographically polished. After calibrating the system with a pure molybdenum standard peaked on K_{α_1} with a LiF crystal, the samples were analyzed with a one micron diameter beam at scanning speeds of 8 and 96 microns per minute. Results of these analyses are shown in Figure 32. The high molybdenum alloy (5M23-2) autoclaved at 2000°F/2 hrs/8 ksi shows variations in molybdenum content from 10 to 45%. The low molybdenum alloy 5MO-2, however, shows a homogenous structure after autoclaving at 2000°F/2 hrs/10 ksi. In addition to the microsegregation seen in Figure 32, the 23% molybdenum alloy also exhibited macrosegregation, which could be visually detected on a polished surface as small circular areas varying from 1/16" to 1/8" in diameter. These isolated areas were low (less than 10%) in molybdenum content and constituted less than 10 v/o of the alloy.

7.3 DENSITY

Density of the compacted alloys was measured with an analytical chainomatic balance using Archimedes principle.

Density measurements of the compacted alloys in the as-compacted condition and after various thermal exposures are tabulated in Table 22. In most cases, systematic variation in density as a function of exposure conditions was masked by wide scatter in the density of as-compacted alloys.

When exposed in the as-autoclaved condition, which was uniformly dense, the 5MO-2 alloy showed a decrease in density with increasing exposure temperature. During exposure at 2400°F/1 hr/vac, for example, this alloy expands approximately 4% in volume (Figure 33).

7.4 OXIDATION/NITRIDATION CHARACTERISTICS OF Cr ALLOYS

Static air oxidation tests were conducted for 10 and 100 hours at 2000°, 2400°, and 2600°F. The samples, which were ground and polished through 400 grit paper, had surface to volume ratios in the range from .2 to 2.0 and weighed approximately .3 grams. Exposure was conducted in zirconia crucibles using a furnace with SiC heating elements and natural convection. After weight gain determination, the samples were prepared for metallographic and microhardness measurements. Specimens were mounted at such an angle that the oxidized surface has a mechanical magnification factor of 4/1. The results of these tests are summarized in Tables 23, 24, 25, and 26.

Weight Gain - At 2000°F the alloys showed weight gains that varied from 0.14 to 4.2 mg/cm^2 after 10 and 100 hour exposures. Weight gain varied considerably from alloy to alloy but two general trends emerged. First, addition of an oxide dispersoid decreases both weight gain and oxide thickness. Secondly, comparison of oxide thickness and weight gain at 10 and 100 hours indicates that in all alloys except 7TO, volatilization losses are occurring simultaneously. Such behavior is typical of Cr alloys and has been reported in detail previously by Tedmon [24], Clark[25], and Chang[26]. At higher temperatures this behavior is more pronounced and several samples actually showed weight loss. Above 2400°F, the metal oxide interface shows indication of direct Cr volatilization. An example of this phenomenon, which is common to all alloys, is shown in Figure 34A. A more detailed view of a similar region is shown at higher magnification in Figure 34B.

During early stages of scale growth at 2000°F the oxide layer on all alloys is quite adherent. Oxide separation was observed at longer times at 2000°F in some alloys and at 2400°F and 2600°F, all alloys showed this behavior. The initial stages of separation may be seen in Figure 34. The raised portion of the scale appears as a small blister when viewed macroscopically as in Figures 35 and 36. Large cracks and spalling of some blisters is evident in the 5YO-1 alloy exposed for 100 hours at 2000°F. (Figure 36).

Nitridation - Exposure of Cr to hot air results in nitridation in addition to scaling by oxidation. Nitridation may occur as a continuous nitride layer beneath the oxide scale, grain boundary nitride network and/or matrix contamination by nitrogen dissolution. Each of these causes serious embrittlement which constitutes the major deterrent to the use of Cr-base alloys as high temperature structural materials. Degree of nitridation, as determined by metallography is reported in Tables 23, 24, and 25. Results of air exposure at 2000°, 2400°, and 2600°F were measured metallographically as thickness of the continuous nitride layer, and as depth of hardening (depth to which nitride particles or grain boundary films were visible in the microstructure). Depth of hardening is also reported in Table 26 where it was determined by Knoop hardness traverse on exposed samples.

As may be seen in Table 23 all alloys were resistant to nitridation for 100 hours at 2000°F except the base line alloy and 2MO. The Cr-Mo alloy without dispersoid (base line alloy) had a .2 mil thick continuous nitride layer and was hardened by grain boundary nitride network to depths of 18 mils after 10 hours and to 24 mils after 100 hours at 2000°F. Although 2MO showed no grain boundary network at either 10 or 100 hours, a .4 mil nitride layer was formed during air exposure for 100 hours at 2000°F.

At 2400°F and 2600°F, on the other hand, nitridation was severe in all alloys and network nitrides were observed throughout the entire sample after 100 hours at 2400°F and after both 10 and 100 hours at 2600°F. Volatilization from the internal interface is evidently a competitive process to formation of a continuous nitride layer since nitride layers were found only in a few instances when vaporization such as that shown in Figure 34 was observed.

7.5 RECRYSTALLIZATION BEHAVIOR

Recrystallization phenomenon in the flake compacts were very difficult to observe metallographically because the microstructure consistently overetched around the large Cr_2O_3 particles before the grain boundaries became visible. As a result Laue diffraction patterns were used to determine the onset of recrystallization. A comparison of the recrystallization behavior of the as-hot pressed, the hot pressed plus warm rolled Cr-4Mo-.15 (La + Y) - 4v/o ThO_2 alloy and the warm rolled Cr-4Mo-.15 (La + Y)-0v/o ThO_2 alloy is shown in Figure 37. Note that both the 0v/o ThO_2 alloy and the 4v/o ThO_2 as-pressed alloy are recrystallized after one hour exposure at 2200°F. The strongly textured (Table 18) 4v/o ThO_2 alloy on the other hand was only partially recrystallized after 10 hours at 2600°F.

7.6 TENSILE PROPERTIES

7.6.1 ALLOYS PRODUCED FROM SUBMICRON BLENDS

Most tests at both high and low temperatures were made on specimens annealed for one hour at 2000°F. Low temperature tests were conducted on double-reduced button head specimens (Figure 38) ground to .120" diameter by .25" long gage dimensions. Elevated temperature testing was conducted on ground button-head specimens with an overall gage length of 1.1" and a diameter of .160". All testing was conducted on an Instron tester at a nominal strain rate of .01 per minute.* High temperature testing was conducted in vacuum at pressures of 10^{-5} torr or below.

* Actual strain and, therefore, strain rate was not measured. All data reported herein was measured as cross-head movement.

Yield strengths of the alloys tested are shown as a function of temperature in Figures 39 and 40. At temperatures of 800°F or less, the 2YO alloy exhibits a pronounced yield point. Samples which were prestrained 1% in tension and aged one half hour prior to testing also showed a pronounced yield point drop, but it was less severe and depended on the aging and test temperature as shown in Table 27 and Figure 42. The 5YO-1 alloy did not exhibit this yield drop phenomenon when tested under the same conditions (Figure 41). In addition to a higher content of oxide dispersoid, the 5YO-1 alloy has much lower carbon and Mo content (Table 21). Higher carbon level alone, however, does not seem sufficient to explain the difference since both alloys are sufficiently high in interstitials to cause yield drop in relatively pure Cr[27]. Perhaps a more important consideration in this phenomenon is the difference in oxide dispersion parameters between the two alloys. Alloy 5YO-1 has an IPS of 1.6μ while 2YO has a much poorer spatial distribution of oxides with IPS of 10.8μ.

Ductile to brittle transition temperature (DBTT) was investigated using slow strain rate (0.5%/min) tensile loading to 1% plastic strain. After 1% plastic strain, the load was released, the temperature reduced 100°F, and the sample was again loaded to 1% strain. This procedure was repeated at 100°F increments until failure occurred. In the as-extruded 5YO-1 alloy the test was initiated at 800°F and fracture occurred at 600°F. A very severe surface defect in the gage length, however, undoubtedly caused premature failure. The second sample was heat treated at 2000°F for one hour in vacuum prior to testing. A summary of the DBTT test of the second 5YO-1 sample is shown in Figure 41, which is a reproduction of the Instron load versus extension chart. The test was initiated at 600°F where the flow stress was 87 ksi. Fracture occurred at room temperature after a total plastic strain of 5% resulting from five increments of 1% strain each. Chromium alloy 2YO exhibited a DBTT of approximately 500°F, Figure 42, while 5YO-1 had a transition temperature of approximately 200°F. Such behavior is not

unexpected since the former was initially higher in Mo, C, and N (Table than the latter. In addition, 5YO-1 contains .15% each of the reactive elements Y, Th, Hf as well as a finer IPS and particle size.

High temperature properties of alloys processed from submicron blends were extremely low in all alloys tested. The best 1900°F strength (Table 28) was found in the 2MO and 2YO alloys, but these properties are not as high as would be expected from wrought alloys without ThO_2. Tensile properties as a function of temperature may be seen in Figures 39 and 40. Increasing the dispersoid content from 2.5 $v/_o$ Y_2O_3 was quite effective in improving strength at lower temperatures. In spite of the fact that the Mo content was more than double that in 5YO, the finer particles and better dispersion of 5YO approximately doubles the 800°F strength of 2YO (87 vs. 36.1 ksi). At high temperatures, however, the grain boundary weakness in the 5YO alloy drastically diminished tensile strength. Flow stress of the two 5YO alloys with .15 and .25 REA alloys was approximately 90 ksi at 800°F. At 2000°F, however, intergranular fracture occurred at 2.2 ksi for the 0.15% REA alloy and 5.7 ksi for the 0.25% Rea alloy. Both alloys showed considerable ductility (45% and 26% elongation respectively) but contained many transverse intergranular surface cracks as shown in Figure 43. Such high temperature behavior is typical of many high strength ultrafine grained alloys. Disappointingly, extrusion did not produce a texture or a fiber shaped grain morphology which might minimize this grain boundary weakness. In addition, since the extrusions were unworkable, such a microstructure could not be produced by thermomechanical processing (TMP).

7.6.2 ALLOYS PRODUCED FROM PREALLOYED FLAKES

Testing procedures for the alloys produced from coarse (50% < 2μ thickness) flakes were identical to those used with the submicron blend buttonhead specimen reported in the previous section. In this case, however, the

mechanical test specimens were cut from 50 mil sheet and, therefore, contained a rectangular gage cross section (Figure 44). Elevated temperature tensile properties of the Cr-4Mo-.15(La+Y)-$4^{V}/oThO_2$ alloy were extremely high (Table 29). At 2100°F for example, UTS is approximately four times as great as would be expected from a wrought matrix alloy of similar composition* and is more than a factor of 10 better than the best of the submicron blend alloys. Extreme difficulties were encountered in machining this material and several test samples were lost during the "Elox"ing operations. In addition, several samples fractured in the tabs during high temperature tests. In at least two instances this was the result of cracks which were evidently initiated during machining. While the tensile properties were extremely good at high temperature, stress rupture properties of material from the same sheet were very low. At 2100°F/2.5 ksi for example, fracture occurred upon loading. At 1900°F/15 ksi rupture life was .25 hours. Comparison of the fractured tensile sample which had a 81 ksi UTS and the stress rupture samples by optical microscopy gave indications that grain boundary separation may be the cause of the poor rupture properties. (Figure 45) Laue transmission x-ray photographs of the 2100°F tensile and the 2100°F rupture samples indicates that recrystallization was beginning during the rupture test while the tensile sample gives no indication of recrystallization. Partial recrystallization is indicated in the Laue transmission photographs of Figure 46 by the appearance of isolated bright spots in each of the continuous diffraction rings.

*Pure Cr + .1 Y - UTS = 9.2 ksi @ 2100°F
Cr + 7.1 w/o Mo + .1 Y - UTS = 31 ksi @ 2100°F
Interpolated UTS for Cr-4.0 w/o Mo-.1Y = 21 ksi @ 2100°F

Data taken from INTERIM SUMMARY REPORT NASA CONTRACT NO. NAS 3-7260, June 30, 1967. (J.W. Clark, Author)

Bend tests were conducted on the rolled sheet using a .040" x .100" cross section. Three-point loading tests were performed on an Instron machine, using a 75° V-block with a span of 1.5-inch and a bending die radius of approximately four times the thickness of the sheet. Tests were conducted above room temperature in an oven with forced-air circulation mounted on the frame. Temperature was controlled by a chromel-alumel thermocouple mounted in the female die. Load-deflection curves were recorded at a ram speed of .05 inches per minute. The results of these tests are listed in Table 31 and indicate a DBTT in the Cr-4Mo-.075 each La, Y-4V/oThO_2 (HP-5) alloy of approximately 900°F.

8. DISCUSSION OF RESULTS

The coarse flake approach appears to be the most promising process for producing oxide dispersion strengthened Cr alloys. Dispersoid agglomeration problems in the submicron blend alloys rendered them unworkable and thus prevented the TMP necessary to produce the desired texture, grain size, and grain morphology. The coarse prealloyed flakes on the other hand were easily workable to a strong deformation texture which imparted both dispersoid stability and a strong resistance to recrystallization. The as-worked microstructure consisted of a double dispersion of oxides. A fine (.07μ) ThO_2 dispersion which had an IPS of 1.0μ and a coarse Cr_2O_3 (> 1μ) dispersion with a 15μ IPS. The stability of these dispersions seemed to be independent of one another. The Cr_2O_3 for example, disappeared in high temperature vacuum while the ThO_2 remained essentially unchanged in size. While this alloy (Cr-4Mo-.15(La+Y)-4$v/o$$ThO_2$) showed excellent high temperature tensile properties (81.3 ksi @ 2100°F), it had a high DBTT (~ 900°F) and was very sensitive to variations in strain rate. The strain rate sensitivity was exhibited by exceptionally low stress rupture properties. Recrystallization occurred during these tests and was evidently the cause of the short rupture lives. Resistance to recrystallization in other of the same type specimens was shown to be a function of degree of texture. In addition, the rupture specimen (HP-8) was only lightly textured when compared to the recrystallization resistant alloy shown in Figure 37, (HP5-2). It therefore seems likely that optimization of TMP to produce either a stronger texture and/or a larger grain size would alleviate this strain rate sensitivity.

The high DBTT poses a more serious problem. If the postulate of Hahn and Rosenfield [2] is correct however, then a reduction in volume fraction of dispersoid, a decrease in the size and volume fraction of the corase Cr_2O_3 particles, and/or a change in grain size might enhance the ductility. In the present alloy, two factors would tend to increase DBTT. The first was a high interstitial content while the second was the presence of Mo as a solid solution strengthener. A fine grain size, coupled with a more reasonable volume fraction of dispersoid might overcome this problem.

The results obtained using coarse prealloyed powders were quite promising. Since these data were generated on compacts in which TMP was not optimized, it seems reasonable to expect that further developments in TMP would improve resistance to recrystallization and thereby overcome the low creep strength of this alloy. In addition, recent work reported by Bullens[27] indicates that a fine substructure in pure Cr decreased the ductile to brittle transition temperature to -120°F.

Thus one might expect that a heavily textured Cr alloy with fine substructure would provide a significant improvement both in high temperature performance and in low temperature fracture behavior. It is therefore, strongly recommended that NASA investigate the potential of TMP in oxide dispersion strengthened Cr alloy in much greater detail.

9. SUMMARY OF RESULTS

A powder metallurgy process was investigated in this contract for the production of oxide dispersion strengthened Cr-Mo alloys with metallographic parameter goals of 1.5 microns interparticle spacing (IPS) and 0.1 micron particle size (PS). Ball milled blends of metal and oxide powder mixtures were densified by several techniques and the resulting compacts evaluated. Three different types of blends were used in an effort to achieve the microstructural parameter goals. These were: 1) an elemental metal/oxide blend in which particle size was 99% $< .5\mu$; 2) a prealloyed metal flake/oxide blend in which the metal flakes were 99% $< 1\mu$ in thickness; and 3) a prealloyed metal flake/oxide blend in which the flakes were 50% $< 2\mu$ in thickness.

The microstructural parameters of as-compacted submicron blend alloys which were not exposed to an interstitial cleaning step, were quite fine. Severe dispersoid instability, however, caused an increase in these parameters by more than one order of magnitude above the program goals during a one-hour vacuum exposure at 2600°F. Dispersoid instability occurred in alloys containing MgO, Y_2O_3, or ThO_2 and appeared to be the result of cooperative movement of grain boundaries and oxide particles rather than by dissolution and reprecipitation of the particles. Since these blends contained excessive quantities of interstitial contamination, (both carbon and oxygen), a carbothermic cleaning method was developed which was shown to be capable of reducing oxygen contamination in the as-milled submicron Cr powders to 130 ppm and carbon to less than 500 ppm. Sintering of the powders during cleaning, however, was accompanied by dispersoid agglomeration which was severe enough to preclude achievement of the interparticle spacing and particle size goals for the consolidated alloy. Tensile properties of this class of alloys fell in the range from 40-100 ksi at room temperature, but high temperature properties were not as high as would

be expected from wrought alloys without ThO_2. Ductile to brittle transition temperature of the submicron blend alloys were measured by slow strain rate (.05/min) tensile testing and did not show an improvement over wrought Cr alloys of comparable Mo content.

Oxidation/nitrification resistance of the alloys processed from submicron blends was quite good at 2000°F and compared favorably with the best cast Cr alloys. At 2400°F and 2600°F, however, 100 hour air exposures caused severe attack, both by oxidation and nitridation.

In an effort to avoid the O_2 contamination problems associated with fine elemental metal starting powders used to produce the ball milled submicron blends, the investigation was continued with a blend of flake-shaped, low oxygen, prealloyed Cr powders with 4 v/o of ultra-fine ThO_2. Arc melted 50 gram button of Cr-4Mo-.15 (La+Y) were made from iodide Cr. After crushing of the buttons, comminution to flakes was accomplished in a Mo-lined ball mill at -50°F using toluene milling liquid with an argon cover. Although the starting powders were very low in interstitial content, carbon contamination occurred during ball milling as a result of adsorption of toluene. Since ball milling of these coarse high purity powders took much longer times, the blend goals were changed to 99% < 1μ (flake thickness). This particle size goal was achieved by ball milling 800 hours at -50°F in toluene. Ball milled prealloyed Cr powders took on a flake shape during milling. The particles were heavily cold worked and had a strong deformation texture. The large flake surface had a strong tendency for {001} orientation after milling. This orientation became much less pronounced in compacts made up of particles with an average flake thickness of less than .1μ. Carbon contamination of these powders amounted to 1.4%C. Removal of this carbon without destroying the ball milled blend was attempted by low temperature H_2 cleaning. A unique closed powder cleaning system was developed in which ultra-pure high pressure H_2 was generated and cleaned internally. This system was used in an attempt to reduce C, O, H, and N to less than 100 ppm each. The efficiency of this system for removal of carbon from ball milled metal/oxide powder blends was investigated in a detailed kinetic study.

This kinetic study of carbon removal was made using matrix powders without the dispersoid oxide addition. The best results were an order of magnitude above the target concentration of 100 ppm C. (Carbon level in as-milled powder was reduced from 1.4% to .09% during a 800°F/250 psi H_2/2500 min. exposure). Four cleaning temperatures were investigated, 400°F, 600°F, 800°F, and 1000°F. Carbon removal was most efficient at 800°F. A variation of cleaning time at 800°F showed that most of the carbon was removed during the first hour of exposure to high pressure hydrogen. Subsequent removal occurred at a steadily decreasing rate. Final carbon content approached a barrier C concentration asymptomatically at long times. Increasing the hydrogen pressure was not as effective in accelerating the reaction as was originally anticipated. The barrier concentration, for example, was completely independent of P_{H_2}. A moderate increase in rate was seen in the early stages of cleaning, e.g. doubling the P_{H_2} from 250 to 500 psi increased the C removal from 53.4% to 60.4% during a 800°F/60 min. exposure. Removal of reaction products from powder voids by cycling the H_2 pressure proved difficult experimentally and its effect was relatively inconclusive. Necessary gas flow into and out of the voids was evidently accomplished by gaseous diffusion. The C barrier observed was probably caused by carbide formation during cleaning. Thermodynamics of carbide removal predict that the achievement of the desired 100 ppm C content is not likely in the existing apparatus.

The third blend (50% < 2μ flake thickness) was a further increase of the blend flake size which was made in order to ease the contamination/cleaning problem and to take advantage of the strong texture observed in the coarse ball milled flakes. Powder processing steps in this case were the same as those used for production of compacts from the 99% < 1μ blends. The desired microstructural parameters of 1.5μ IPS and 0.1μ particle size were to be achieved by thermomechanical processing the densified alloy. The coarse flakes present in the as compacted alloy were thus elongated by rolling. Dispersoid particles, present in the flake surfaces boundaries were thus brought closer together as the flake became thinner. This improved the general dispersion parameters and also retained the elongated grain shape and preferred orientation which existed in the original flake particles.

Although the contamination goal of < 100 ppm each of C, O, H, N, and S could not be achieved, the third approach yielded by far the most encouraging results, which are briefly recounted as follows:

1) Hot pressed compacts of Cr-4Mo-.15(La+Y)-4$^{v}/_{o}ThO_2$ had excellent workability.

2) Dispersoid stability was sufficient in the as-pressed compact to prevent agglomeration during the thermomechanical processing (TMP) steps necessary to promote good high temperature properties.

3) TMP produced a strong texture and enhanced the ThO_2 dispersion, (1.0μ IPS - .07μ PS).

4) After rolling 84% at 1800°F a Cr-4Mo-.15(La+Y)-4$^{v}/_{o}ThO_2$ alloy had good dispersoid stability, was resistant to recrystallization and had a 2100°F tensile strength of 81.3 ksi ($\sim$ 4X the strength of the undispersed matrix).

5) The DBTT of this alloy was approximately 900°F.

6) Elevated temperature tests indicated that the strength of Cr Alloy/ThO_2 sheet was very sensitive to strain rate.

A summary of the interstitial contents and dispersion parameters which were achieved by the various processes investigated are shown on the following page.

	Powder Type	Dispersoid Type	Powder Blend Size	Cleaning Method	Interstitial Content After Cleaning (%) C (%)	O (2) (%)	N (%)	S (%)	Dispersion Parameters (1) As-Compacted PS (μ)	IPS (μ)	After Working 2600F/10hrs PS (μ)	IPS (μ)	PS (μ)	IPS (μ)
1	Elemental	MgO, Y_2O_3	99% <.5μ	None	.6	.5	.005	.008	.07	1.6	-	-	1.4	12.0
2	Elemental	MgO, Y_2O_3	99% <.5μ	Carbo-Thermic	.04	.01	.005	.008	.39	5.1	Alloys Not Workable		1.5	12.5
3	Elemental	MgO	99% <.5μ	Low Press High T - H_2	1.4	-	-	-	-	-	-	-	-	-
4	Prealloyed	MgO, Y_2O_3	Failed Submicron Blend Goal	-	-	-	-	-	-	-	-	-	-	-
5	Prealloyed	ThO_2	99% < 1μ	High Press Low T - H_2	.09	.397	.0001	.008	-	-	-	-	-	-
6	Prealloyed	Y_2O_3 ThO_2	50% < 2μ	High Press Low T - H_2	.04	.55	.019	-	-	-	.07	1.0	.08	-

(1) See Appendix II for details of the Quantitative metallographic analysis used.

(2) O_2 in excess of that combined as dispersoid.

REFERENCES

1. J.W. Clark, NASA Interim Summary Report, Contract NAS 3-7260 (June, 1967).

2. G.T. Hahn and A.R. Rosenfield, TR AFML-TR-65-409 (January, 1966).

3. R.F. Bunshah and C.G. Goetzel, WADC TR-59-414 (March, 1960).

4. R.W. Fraser, B. Meddings, D.J.I. Evens, and V.N. Mackiw, Modern Developments in Powder Metallurgy, Vol. 2, H.H. Hausner, Editor, Plenium Press, p. 87 (1966).

5. G.S. Ansell, Paper intended for publication in the Proceedings of the Bolton Landing Conference on Oxide Dispersion Strengthening, Bolton Landing, New York, on June 27-29, 1966.

6. A.L. Mincher, Report, AFML-TR-65-442, Part II, E.I. du Pont de Nemours & Company, Inc., Wilmington, Del., Contract AF-33(615)-1680 (March, 1967).

7. J.L. Walters, Trans. AIME, 239, 12, p. 1979 (December, 1967).

8. A. von Zeerleder; Z. Metallkunde, 41 (1950) 228.

9. W.S. Cremens; PhD Thesis, MIT (1957).

10. E.A. Calnan and C.J.B. Clews, Phil Mag., Ser 7, Vol. 42, No. 329, p. 616, (June, 1951).

11. R.J. Bacigalupi and H.E. Neustadter, NASA Technical Note TN D-3141 (December, 1965).

12. W.H. Chang, Welding Research Supplement, 622 (December, 1966).

13. J.F. Elliot and M. Gleiser, "Thermo-Chemistry for Steel Making," Addison-Wesley Pub. Co., (1960).

14. W.L. Worrell, Trans AIME, 233, No. 6, 1173 (1965).

15. D.F. Stein, Private Communication.

16. G.F. Doble, PhD Thesis, Case Institute of Technology, (June, 1968).

17. D.H. Killpatrick and J.D. Young, McDonnell Douglas Corp. Internal Report 4843, (February, 1968).

18. W.M. Baldwin, R.E. Cairns, H.G. Marsh, and R.E. Wilson, U.S. Patent 3,346,427, (October 10, 1967).

19. C. Wagner, Z. Elektrochem, 65, 581, (1961).

20. I.M. Lifshitz and V.V. Slyozov, J. Exp. Theor. Phys., USSR, 35, 479 (1958).

21. Che-Yu Li and R.A. Oriani, Paper intended for publication in the Proceedings of the Bolton Landing Conference on Oxide Dispersion Strengthening, Bolton Landing, New York on June 27-29, 1966.

22. E.F. Koch and K.T. Aust, Acta Met. 15, 405, (1967).

23. T.W. Beamond and D.H. Houseman, Powder Metallurgy, Vol. 7, No. 14, (1964).

24. C.S. Tedmon, Jr., "The Effect of Oxide Volatilization on the Oxidation Kenetics of Cr and Fe-Cr Alloys," G.E. Internal Report 66-C-094, (April, 1966).

25. J.W. Clark, First Semi-Annual Report, NASA Contract NAS 3-7260, (October, 1965).

26. W.H. Chang, "Microstructures and Properties of Some Experimental Cb-base and Cr-base Alloys," G.E. Internal Report R66FPD102, (April 1, 1966).

27. F. P. Bullen, Technical Presentation at the Round Table Discussion on Cr, held at Battelle Memorial Institute Columbus, Ohio, May 9, 1969.

TABLE 1

CHEMICAL ANALYSIS OF FRENCH* CHROMIUM POWDERS USED IN THE ELEMENTAL POWDER APPROACH

Chromium	99.04%
Oxygen	0.40
Carbon	0.08
Nitrogen	0.005
Iron	0.20
Aluminum	0.02
MgO	0.25

*Aciéries de Gennevilliers 119 Av Louis Roche Paris, France.

TABLE 2

INTERSTITIAL CONTENT AND PARTICLE SIZE OF STARTING MATERIALS FOR ELEMENTAL POWDER APPROACH

Material	Material Source	O	H	N	C	S	Analytical Source	Powder Size
Cr	Aciéries de Gennevilliers	5570	10	24	600[1]	100[1]	MPTL	FSS[2] 1.6μ
Cr	Aciéries de Gennevilliers	4000		50	800		M&R[3]	FSS 1.6μ
Y, Th, Hf Hydrides	Metal Hydrides, Inc.							-60 mesh
Mo	M&R Refractory Metals, Inc.	431			60	< 10	M&R[3]	FSS 1.6μ

[1] Ledoux

[2] Fisher sub-sieve size

[3] M&R Refractory Metals, Inc.

TABLE 3

CHEMICAL ANALYSIS OF MELTING STOCK FOR THE PREALLOYED POWDER APPROACH

Element	Purity	Form	Impurities (ppm) O	N	H	C	Fe	Ni	Al	Si	S	Other
Chromium [1]	99.94%	H_2 Reduced Flake	42	100	3	80	75	25	10	70	75	-
Chromium [2]	99.997%	Iodide Crystal	7	1	.5	9	13	1	.3	10	-	2Ca
Molybdenum	99.9%	Pellet	105	12	-	-	160	61	25	55	-	435W
Yttrium	99.9%	Sponge	890	8	-	-	20	-	5	50	-	10Ca400RE[3]
Lanthanum		Ingot	300	10	-	-	10	1	1	50	-	200Ca500RE[3]

[1] Used as starting material for induction melting

[2] Used as starting material for arc melting (60g buttons)

[3] Rare earth impurities, principally Yt, Ho, Ce, Pr, Nd

TABLE 4

CHEMICAL ANALYSIS OF MgO POWDER (.04μ Diameter)

MgO	98.97%
NH_4OH	0.02
Barium	0.005
Calcium	0.05
Chlorine	0.010
Heavy Metals (as lead) Insol. in dilute HCl	0.02
Iron	0.01
NO_3	0.005
Potassium	0.005
Sodium	0.50
Sol. in H_2O	0.40
Strontium	0.005
Sulfate & Sulfide	0.005

TABLE 5

CHEMICAL ANALYSIS FOR Y_2O_3 POWDER (1μ Diameter)

Dysprosium Oxide	0.039%
Holmium Oxide	0.0052
Erbium Oxide	0.017
Thulium Oxide	0.002
Other Rare Earths	below limit of detection
Calcium	0.0150
Silicon	0.0065
L.O.I. *	0.400
Y_2O_3	balance

* Ignition Loss

TABLE 6

X-RAY TEXTURE ANALYSIS OF BALL MILLED Cr POWDERS*

Ball Milling Time (hours)	Relative Diffracted Intensity I/I_{ASTM}					
	As Milled			Annealed 2400°F/1 hr/Vac		
	{110}	{200}	{211}	{110}	{200}	{211}
0 (ASTM Standard)	1.0	1.0	1.0	1.0	1.0	1.0
69	1.0	1.4	1.3	-	-	-
207	1.0	35.4	4.3	1.0	10.4	7.9
300	1.0	29.0	2.5	-	-	-
600	1.0	3.6	1.2	1.0	7.0	3.0

*Cold pressed in cylindrical steel dies at 100 ksi.

TABLE 7

INTERSTITIAL ANALYSIS OF CRUSHED PREALLOYED BUTTONS

Number	Alloy Composition (w/o)	Impurities (ppm) C	O	H	N	Powder Size
PA-1	Cr-3Mo-.25 ea Th Hf Y[1]	150	168	6	71	-6 mesh
PA-2A	Cr-2.5Mo-.075 ea La, Y[2]	40	7	5	13	-60 mesh
PA-2B	Cr-2.5Mo-.075 ea La, Y[2]	80	43	1	3	-60 mesh
PA-2C	Cr-2.5Mo-.075 ea La, Y[2]	50	36	3	< 1	-60 mesh

[1] Induction Melted

[2] Arc Melted

TABLE 8

Mo CONTENT OF AS-MILLED Cr POWDERS

Alloy No	Ball Mill Time (hrs)	Mo Added (%)	Mo Pick Up From Liner (%)	Total Mo (%)
Pure Cr	232	0	5.9	5.9
2 MO	232	0	5.9	5.9
2 YO	448	0	2.4	2.4
3 MO	407	0	2.5	2.5
3 YO	407	0	2.1	2.1
5 MO-2	472	0	3.15	3.15
5 YO-1	500	0	1.0	1.0
7 MO	312	0	4.5	4.5
7 YO	490	0	2.3	2.3
7 TO	290	0	6.2	6.2
Prealloyed	918	3.0	.9	3.9
HP 5	200	2.5	1.7	4.2
HP 6	200	2.5	1.5	3.8

TABLE 9

CARBON CONTENT OF AS-MILLED M&R Cr POWDERS AFTER APPLICATION OF VARIOUS TOLUENE DISPLACEMENT SOLVENTS

Solvent	ppm C
Trichloroethylene	5700
Xylene	6100
Benzene	6000
Hexane	7800
Ethyl Alcohol	6200
Acetone	6100

TABLE 10

CARBON CONTENT OF FRENCH Cr POWDERS AFTER HYDROGEN CLEANING*

Run No.	Environment	Temp °F	No. of Cycles (1 hr H_2 +1/2 hr vac)	% C Final	Remarks
1	H_2 (99.999%)	1800	4	1.04	No He used-capsule backfilled directly with H_2
2	H_2 (99.999%)	1800	3 hr H_2 + 2 cycles	1.34	Thin layer of powder on Mo tray
3	H_2 (99.92%)	1800	4 hr H_2	1.92	Thin layer of powder on Mo tray

* Starting powder - Cr-2.8Mo-5 v/o MgO-0.25 each Hf, Th, Y. Ball milled 500 hrs/-50°F/toluene (7300 ppm C).

TABLE 11

GAS ANALYSIS OF LOOSE Cr POWDERS AFTER CARBOTHERMIC CLEANING

No	Elemental Powder	Cleaning Conditions (temp °F/time min/powder depth/type getter)	C (%) Initial	C (%) Final	O (1) (%) Initial	O (1) (%) Final
1	As-milled Cr	2070/50/.05/Zr	0.124	0.006	0.4030	0.555
2	As-milled Cr	2070/5/.275/Zr	0.124	0.006	0.4030	0.557
3	As-milled Cr	2350/50/.275/Zr	0.124	0.007	0.4030	0.637
4	As-milled Cr	1800/10/.275/Zr	0.124	0.008	0.4030	0.477
5	As-milled Cr	1600/10/.275/Zr	0.150	0.131	0.6750	0.2610? 0.6520
6	As-milled (Cr+graphite)	1800/5/.275/Zr	0.5750	0.5520	0.580	0.697
7	As-milled (Cr+graphite)	2070/5/.275/Zr	0.5750	0.3250	0.580	0.424
8	As-milled (Cr+graphite)	2400/33/.275/Zr	0.6150	0.1460	0.6080	0.2125
9	As-milled (Cr+graphite)	2400/50/.275/Zr	0.6150	0.0645	0.608	0.0130
10	As-milled (Cr+5v/o MgO+ 0.25 each Y,Th,Hf)	2000/5/.05/Ta	0.570	0.0600	0.460	0.670
11	As-milled (Cr+MgO+Y,Th,Hf) (same as No. 10)	2200/5/.05/Ta	0.570	0.0445	0.460	0.10 0.47(2)
12	As-milled (Cr+MgO+Y,Th,Hf)	2400/5/.05/Ta	0.570	0.0360	0.460	0.40(2)
13	As-milled (Cr+Mgo+Y,Th,Hf)	2400/5/.275/Ta	0.570	0.0950	0.460	0.36
14	As-milled (Cr+MgO+Y,Th,Hf)	2100/50/.05/Ti	0.570	0.0425	0.460	-0.006(3)
15	As-milled (Cr+MgO+Y,Th,Hf)	2000/50/.05/Zr	0.570	0.0160	0.460	-0.022 0.32(2)
16	As-Milled (Cr+MgO+Y,Th,Hf)	2400/50/.05/Zr	0.570	0.0204	0.460	-0.48
17	As-Milled (Cr+MgO+Y,Th,Hf)	2000/50/.05/Ta	0.570	0.0140	0.460	-

(1) Oxygen is reported as that which is not combined with MgO. (As-purchased French Cr powders contain 0.25% MgO)

(2) After compaction by autoclaving at 2000°F/2 hrs/10 ksi He.

(3) Negative sign indicates total oxygen by chemical analysis is less than oxygen added as MgO.

TABLE 12

FREE ENERGY OF REACTION AS A FUNCTION OF TEMPERATURE

FOR SEVERAL POSSIBLE CLEANING REACTIONS

I $C + 2\ H_2 \rightarrow CH_4$

II $C + 23/6\ Cr \rightarrow 1/6\ Cr_{23}C_6$

III $CH_4 + 23/6\ Cr \rightarrow 1/6\ Cr_{23}C_6 + 2\ H_2$

IV $C + 7/3\ Cr \rightarrow 1/3\ Cr_7C_3$

V $CH_4 + 7/3\ Cr \rightarrow 1/3\ Cr_7C_3 + 2\ H_2$

VI $C + 3/2\ Cr \rightarrow 1/2\ Cr_3C_2$

VII $CH_4 + 3/2\ Cr \rightarrow 1/2\ Cr_3C_2 + 2\ H_2$

	$\Delta F^\circ_{reaction}$, Kcal/mol C						
T°K	I	II	III	IV	V	VI	VII
298	-12.1	-16.8	- 4.7	-14.5	- 2.4	-11.7	+ 0.4
400	-10.0	-17.0	- 7.0	-14.7	- 4.7	-11.8	- 1.8
600	- 5.5	-17.3	-11.8	-15.1	- 9.6	-12.0	- 6.5
800	- .55	-17.6	-17.0	-15.5	-15.0	-12.2	-11.6
1000	+ 4.6	-17.9	-22.5	-16.0	-20.6	-12.6	-17.2
1200	+ 9.8	-18.3	-28.1	-16.4	-26.2	-13.1	-22.9

TABLE 13

H_2 CLEANING OF PREALLOYED Cr-4Mo-.15 (La + Y)

POWDERS WITHOUT ThO_2

Run No.	Hydride Temp. T_S - °F	Sample Temp. T_C - °F	H_2 Press. psi	Number of Pressure Cycles	Time @High pressure Cycle (min)	Total Time at Temperature	% Carbon* Removed
1	1360	1000	205	1	30	120	40.3
2	1300	1000	300	2	30	360	63.0
3	1400	800	200	2	30	600	80.4
4	1650	800	50	2	30	480	77.6
5	1650	600	350	1	30	360	13.6
6	1650	400	200	1	90	120	4.8
7	1650	800	250	1	60	60	53.4
8	1650	800	250	1	2500	2500	94.0
9	1650	800	250	6	300	1800	78.9
10++	1650	800	500	1	60	60	60.4
11++	1650	800	300	2+	2500	2560	80.2

* GOAL = > 99.3% Removed or < 100 ppm C.

+ Ball Milled 24 hours - between cycles to breakup agglomerates.

++ 100 gram samples

TABLE 14

COMPOSITION OF ALLOYS PROCESSED FROM SUBMICRON BLENDS

Alloy No.	Dispersoid v/o	Mo %	Reactive Element Addition % each of Hf, Th, Y
Base Line Alloy	0	5.9	0
2 MO	2.5 MgO	3.3	0
2 YO	2.5 Y_2O_3	2.4	0
3 MO	3.5 MgO + 4.0ThO_2	2.5	0
3 YO	3.5 Y_2O_3 + 4.0ThO_2	2.1	0
5 MO-1	5.0 MgO	3.91	.25
5 MO-2	5.0 MgO	3.91	.25
5 MO-3	5.0 MgO	3.91	.25
5M23-1	5.0 MgO	23.0	.25
5M23-2	5.0 MgO	23.0	.25
5 YO-1	5.0 Y_2O_3	.9	.15
5 YO-2	5.0 Y_2O_3	1.0	.25
5 YO-3	5.0 Y_2O_3	1.0	.30
5 YO-4	5.0 Y_2O_3	3.45	0
7 MO	7.5 MgO	4.5	0
7 YO	7.5 Y_2O_3	2.35	0
7 TO	7.5 ThO_2	6.2	0
Prealloyed	5.0 MgO	3.9	.25
HP 5	4.0 ThO_2	3.8	.075*
HP 6	0.0 ThO_2	4.2	.075*
HP 7	4.0 ThO_2	4.0	.075

*La and Y instead of Hf, Th, Y.

TABLE 15

SUMMARY OF SUBMICRON BLEND ALLOY PROCESSING

Alloy No.	Carbothermic Clean Cond. (°F/Min)	Autoclave (°F/Hr/ksi)	Secondary Working	Results of Working
Base Line Alloy	2400/50	2000/2/10	Swage 2000°F → 1600°F	Mo jacket badly cracked and checked. Exposed powder.
2MO	2400/45	2000/2/10(1)	Impact Extrude-2000°F-4/1	Transverse cracks.
2YO	2400/50	2000/2/10(1)	Impact Extrude-2000°F-4/1	Sound
5MO-1	-	1900/3/10	-	-
5MO-2	-	2000/2/10	Extrude 2000°F-18/1	Segmented
5MO-3	-	2400/2/10	-	-
5M23-1	-	1900/2/10	Swage 2500°F	Severe cracks
5YO-1	2000/45	2000/.75/10	2000°F Extrude-14/1	Sound
5YO-2	2000/45	2000/.75/10	2000°F Extrude-14/1	Irregular corss section
5YO-3	2000/45	2000/.75/10	2000°F Extrude-14/1	Extrude to short segments
3MO	2400/50	2000/2/10	Hot roll-2000°F → 1400°F	Severe cracks
3YO	2400/50	2000/2/10(1)	Hot press-2000°F	Severe cracks
7MO	2400/50	2000/2/10(1)	Impact extrude-2000°F-4/1	Transverse cracks
7YO	2200/50	2000/2/10(1)	Impact extrude-2000°F-4/1	Transverse cracks
7TO	2400/50	Hot Press 2400/.25/5	Hot roll-2000°F → 1400°F	Severe cracks
918	2200/20	2000/2/10	Hot roll-2000°F → 1400°F	One large edge crack

(1) First and second attempts unsuccessful as a result of capsule weld cracks. Capsules resealed and compacted according to conditions shown.

TABLE 16

HOT PRESSING CONDITIONS AND CAPUSLE DESIGN FOR COMPACTION OF Cr-4Mo-.15(La+Y)-4v/o ThO_2 POWDERS

	Temperature (°F)	Pressure (ksi)	Time (hours)	Vacuum (torr)
H.P. #1	2000	10	2	10^{-5}
H.P. #2	2000	10	2	10^{-5}
H.P. #3	2000	10	2	10^{-5}
H.P. #4	2200	10	2+	10^{-5}

+Capsule was soaked at 2200°F/1 hour prior to application of the load.

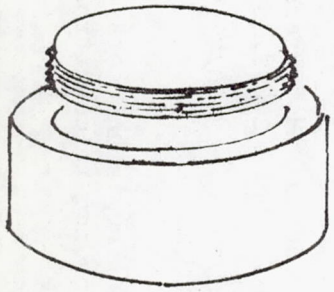

Mild Steel
Thick End Closure
HP1 - HP2

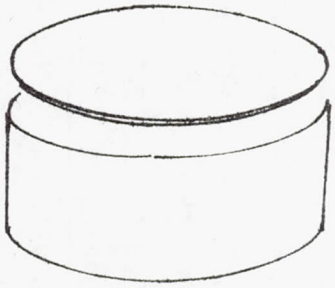

Mild Steel
Thin Sheet End Closure
HP3

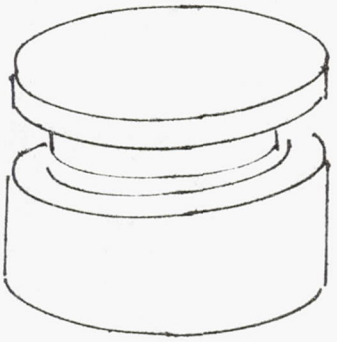

Stainless Steel
Thick End Closure
HP4

TABLE 17

ROLLING PARAMETERS FOR Cr + 4 Mo + .15 (La + Y) + 4 v/o ThO_2

ALLOYS PRODUCED FROM COARSE FLAKES

Sample No.	Rolling Temperature °F	Reduction in Thickness %	No. Passes	Appearance
HP5-5	1600	84	3	Very Slight Edge Cracking
HP5-4	1700	84	3	Very Slight Edge Cracking
HP5-2	1800	83	3	Very Slight Edge Cracking
HP5-7	1800	84	3	Fracture in Hast X Rolling Pack - Cr Sound
HP5-8	1800	85	7	Slight Edge Cracking
HP6*	1800	85	7	Delamination-No Sound Material
HP7	1800	84	7	Slight Edge Cracking

* 0v/o ThO_2

TABLE 18

TEXTURE OF HOT PRESSED AND HOT ROLLED

Cr-4Mo-.15(La+Y)-4v/o ThO_2 SHEET

Sample Number	Rolling Temperature °F	Rolling Reduction %	X-ray $I_{Sheet}/I_{ASTM\ Stand}$ Diffraction Intensity (110)	(200)	(211)
HP5	-	0	1.0	2.1	2.2
HP5-5	1600	84	1.0	830	16.4
HP5-4	1700	64	1.0	21.6	6.6
HP5-4	1700	84	1.0	299	10.3
HP5-2	1800	83	1.0	1,340	19.4
HP5-2 + 2600°F/10hrs/VAC	1800	83	1.0	122	25.0
HP5-8*	1800	84	1.0	6.7	2.4

* Encapsulated in Hastelloy X Rolling Pack

TABLE 19

QUANTITATIVE METALLOGRAPHY DATA[1] OF AS-AUTOCLAVED ALLOYS

BEFORE AND AFTER THERMAL EXPOSURE

Alloy No.	As Autoclaved			Hrs.	Thermal Exposure Conditions								
					2000°F			2400°F			2600°F		
	PS μ	IPS μ	f v/o		PS μ	IPS μ	f v/o	PS μ	IPS μ	f v/o	PS μ	IPS μ	f v/o
2 MO	.81	27.6	2.9	10	.9	23.8	2.4	.69	18	2.5	1.9	50	2.7
				100	.98	25.6	2.7	.59	24	2.4	1.4	63	2.15
2 YO	.51	10.8	4.8	10	.8	20.8	2.7	.6	15.6	2.9	1.5	38.4	2.3
				100	1.2	41.0	2.9	.54	25	2.4	1.8	46.8	2.5
3 MO	.39	5.1	7.6	10	.51	4.2	7.2	.6	4.9	7.7	1.5	12.5	7.6
				100	.30	6.0	5.0	.66	8.0	8.2	.54	7.6	7.1
3 YO	.42	5.9	7.2	10	.85	7.1	7.9	1.49	12.2	6.8	3.0	25	7.4
				100	.53	9.7	5.5	.69	21.7	3.17	----	----	---
7 MO	.70	5.3	13.2	10	.76	6.25	7.6	1.74	14.3	7.8	2.0	16.7	7.9
				100	.84	8.7	9.6	1.93	20.3	9.5	5.8	48.6	7.5
7 YO	.61	7.1	8.6	10	.82	6.7	7.6	1.5	12.6	7.5	2.34	19	7.5
				100	.49	7.9	6.1	.98	22.5	4.41	1.67	13.6	7.5
7 TO	.76	12.3	6.2	10	1.6	13.1	8.5	----	----	----	2.7	21.8	6.2
				100	.87	10.5	8.3	1.62	22.0	4.5	----	----	----
5M23-1	.86	9.2	9.4	----	----	----	---	----	----	----	----	----	----
5M23-2	.54	8.1	6.64	----	----	----	---	----	----	----	----	----	----
HP 5[1]	.08[2]	1.0	6.3	10	----	----	---	.07	1.0	6.2	.08	----	----

(1) Details of the Quantitative Metallography Methods given in Appendix II.

(2) Densified by hot pressing rather than autoclaving. Quantitative Analysis was conducted after 84% rolling reduction rather than in the as-hot pressed condition.

TABLE 20

SPECTROGRAPHIC ANALYSIS OF COMPACTED ALLOYS

Alloy No.	Al	Ca	Cr	Cu	Fe	Mg	Mn	Mo	Ni	Si	Y	Th	Hf
Pure Cr	T	T	Major	T^-	T	T	T	Minor	T	T	0	0	-
2 Mo	T	T^-	Major	T^-	T	Minor	T	Minor	T	T	0	0	-
2 YO	T	T	Major	T^-	T	T	T	Minor	T^-	T	Minor	0	-
3 Mo	T	T	Major	T^-	T	Minor	T	Minor	T	T	0	T	-
3 YO	T	T	Major	T^-	T	T	T	Minor	T	T	Minor	T	-
5 Mo-2	-	-	Major	-	T	Minor	-	Minor	-	-	T	T^-	T
5 YO-1	T^+	T	Major	T	T	T^+	T	Minor	T	T	Minor	T	T
7 Mo	T	T	Major	T^-	T	T	T	Minor	T	T^-	0	0	-
7 YO	T	T	Major	T^-	T	T	T	Minor	T	T	Minor	0	-
7 TO	T	T	Major	T	T	T	T	Minor	T	T	T^-	Minor	-
Prealloyed	T	T^-	Major	T^-	T^-	T^-	T^-	Minor	T^-	T	T	0	-
HP 5	T	T	Major	T	T^+	T	T	Minor	T	T	T	-	-
HP 6	T	T	Major	T	T	T	T	Minor	T	O	T	-	-

100-10% - Major

10-1% - Minor

1-0% - Trace

T^- - Light

T^+ - Heavy

TABLE 21

INTERSTITIAL ANALYSIS OF COMPACTED ALLOYS

Alloy	Condition	C	O	H	N	S	Mo	Dispersoid v/o
Base Line Alloy	Swaged	.0470	.2890	.0009	.0041	.0080	5.90	0
2 MO	Impact Extruded	.280	.421	.0003	.0118	.0090	3.30	2.5 MgO
2 YO	Impact Extruded	.088	.538	.0018	.0107	.0080	2.40	2.5 Y_2O_3
3 MO	Hot Rolled	.081	1.568	.0026	.0110	.0080	2.50	3.5 MgO + 4 ThO_2
3 YO	Autoclaved	.096	1.66	.0025	.0015	.0110	2.10	3.5 Y_2O_3 + 4 ThO_2
5 YO-1	Extruded	.0066	1.55	----	.0029	----	.90	5.0 Y_2O_3
5 MO-2*	Autoclaved	.23	1.53	----	.0040	----	3.91	5.0 Y_2O_3
7 MO	Impact Extruded	.180	2.09	.0027	.0023	.0160	4.50	7.5 MgO
7 YO	Impact Extruded	.270	2.17	.0030	.0030	.0090	2.35	7.5 Y_2O_3
7 TO	Hot Rolled	.0190	1.80	.0026	.0033	----	6.2	7.5 ThO_2
Prealloyed	Hot Rolled	.223	1.54	.0260	.0260	----	3.90	5.0 MgO
HP 5	Hot Rolled	.040	1.19	.0020	.0190	----	4.2	4.0 ThO_2
HP 6	Hot Rolled	.042	.410	.0005	.0038	----	3.8	0

*Not Cleaned

TABLE 22

DENSITY DATA FROM ARGON THERMAL STABILITY TESTS

Alloy[1]	Initial[2]	2000°F		2400°F		2600°F	
		10 Hrs	100 Hrs	10 Hrs	100 Hrs	10 Hrs	100 Hrs
Base Line Alloy	7.20	7.26	7.21	6.90	7.07	7.21	7.23
2MO	7.02	7.05	7.01	7.11	6.83	7.00	6.82
2YO	7.04	6.79	6.16	6.29	6.58	6.60	-
3MO	6.69	7.35	6.70	6.98	6.98	7.01	7.06
3YO	7.13	7.21	6.66	6.96	7.12	7.34	-
7MO	6.84	7.04	6.81	6.60	6.39	6.65	6.61
7YO	6.88	6.95	7.12	6.55	6.50	6.55	6.57
7TO	6.95	8.27[3]	8.0[3]	6.33	6.87[3]	7.76	-
Prealloyed	7.21	7.12	7.34	6.91	7.26	7.46	-

(1) Alloys processed as shown in Table 10.

(2) Density = $\frac{\text{weight in air}}{\text{weight in air - weight in water}}$

(3) Test accuracy questionable as a result of extremely small sample size.

TABLE 23

2000°F OXIDATION AND NITRIDATION DATA ON PROCESSED Cr ALLOYS

Alloy	Initial Condition	Time Hours	Weight Gain Mg/Cm^2	Oxide Thickness Mils	Nitride Layer Mils	Depth Of Hardening Mils
Base Line Alloy	Swaged	10	3.64	.1	.2	18
		100	4.20	.45	.2	24
2YO	Impact	10	.99	.03	0	0
	Extrude	100	.86	.02	0	0
2MO	Impact	10	1.89	.05	0	0
	Extrude	100	.16	.25	.4	0
3YO	Autoclaved	10	.507	.01	0	0
		100	1.16	.01	0	0
3MO	Hot Rolled	10	2.60	.03	0	0
		100	2.87	.05	0	0
5YO-1	Autoclaved	10	2.21	.5	0	0
		100	-3.53	-		0
7MO	Impact	10	3.90	.03	0	0
	Extrude	100	2.24	.5	0	0
7YO	Impact	10	1.92	.03	0	0
	Extrude	100	1.03	.08	0	0
7TO	Rolled	10	.89	.03	0	0
		100	3.80	.15	0	0
Prealloyed	Rolled	10	.14	.02	0	0
		100	.30	.03	0	0

TABLE 24

2400°F OXIDATION AND NITRIDATION DATA ON PROCESSED Cr ALLOYS

Alloy	Initial Condition	Time Hours	Weight Gain Mg/Cm^2	Oxide Thickness Mils	Nitride Layer Mils	Depth Of Hardening Mils
Base Line Alloy	Swaged	10	-14.2	.76	0	All-GB
		100	16.8	1.1	0	All
2MO	Impact	10	10.2	1.4	0	All
	Extrude	100	48.4	1.2	0	12
2YO	Impact	10	3.4	.76	0	All
	Extrude	100	1.68	.5	0	All
3MO	Hot Rolled	10	45	.29	0	All
		100	36.1	11.5	45	26
3YO	Autoclaved	10	1.9	.1	0	All
		100	24.2	-	0	20
7MO	Impact	10	-18.5	.61	.76	.76
	Extrude	100	14.8	5.8	11.4	All
7YO	Impact	10	20	.86	.62	.62
	Extrude	100	48.2	17.3	0	All
7TO	Rolled	10	-	-	-	-
		100	-	-	-	-
Prealloyed	Rolled	10	.3	.14	0	All-GB
		100	- 2.84	-	0	16
5YO-1	Autoclaved	10	2.36	-	0	-
		100	-9.45	-	0	-

TABLE 25

2600°F OXIDATION AND NITRIDATION DATA ON PROCESSED Cr ALLOYS

Alloy	Initial Condition	Time Hours	Weight Gain Mg/Cm²	Oxide Thickness Mils	Nitride Layer Mils	Depth Of Hardening Mils
Base Line Alloy	Swaged	10	-50.2	.48	0	All
		100	91.0	17	19	All
2MO	Impact	10	-10.3	.67	0	All
	Extruded	100	-----	22.6	0	All
2YO	Impact	10	-8.7	.38	0	All
	Extruded	100	75.0	-----	0	
3MO	Hot Rolled	10	45.0	.91	0	All-GB
		100	27.0	-----	-----	-----
3YO	Autoclaved	10	-----	.48	0	All
		100	126	83	0	-----
5YO-1		10	109	-----	-----	-----
7MO	Impact	10	-30	.57	0	All
	Extruded	100	121	9.5	0	
7YO	Impact	10	-----	3.8	0	All-GB
	Extruded	100	130	60	0	All
7TO	Rolled	10	-----	-----	-----	-----
		100	-----	-----	-----	-----
Prealloyed	Rolled	10	-----	.67	-----	All
		100	58.0	Consumed	-----	-----

TABLE 26

HARDNESS DATA ON PROCESSED ALLOYS

Alloy	Initial Condition	Knoop Hardness			
		Center		Edge	
		Air	Argon	Air	Argon
Base Line Alloy	As Compacted		337		342
	2000°F/10 hrs	273	271	860	
	2000°F/100 hrs	360	278	1009	
	2400°F/10 hrs	276	263	276	
	2400°F/100 hrs	391	306	816	
	2600°F/10 hrs	833	255	1063	
	2600°F/100 hrs	740	229	740	
2MO	As Compacted		337		479
	2000°F/10 hrs	295	315	282	
	2000°F/100 hrs	336	324	360	
	2400°F/10 hrs	254	254	747	
	2400°F/100 hrs	259	255	638	
	2600°F/10 hrs	513	253	1163	
	2600°F/100 hrs	1273	191	1273	
2YO	As Compacted		337		361
	2000°F/10 hrs	219	189	168	
	2000°F/100 hrs	172	130	172	
	2400°F/10 hrs	296	134	296	
	2400°F/100 hrs	317	226	740	
	2600°F/10 hrs	175	137	1163	
	2600°F/100 hrs	-	188	-	
3MO	As Compacted		317		328
	2000°F/10 hrs	315	399	419	
	2000°F/100 hrs	370	273	370	
	2400°F/10 hrs	317	310	1163	
	2400°F/100 hrs	261	254	1003	
	2600°F/10 hrs	996	231	996	
	2600°F/100 hrs	Consumed	290	Consumed	
3YO	As Compacted		305		305
	2000°F/10 hrs	326	272	326	
	2000°F/100 hrs	276	314	276	
	2400°F/10 hrs	289	277	289	
	2400°F/100 hrs	251	256	379	
	2600°F/10 hrs	326	261	925	
	2600°F/100 hrs	1270	—	1270	

TABLE 26 (CONT'D)

HARDNESS DATA ON PROCESSED ALLOYS

Alloy	Initial Condition	Knoop Hardness			
		Center		Edge	
		Air	Argon	Air	Argon
7MO	As Compacted		286		299
	2000°F/10	311	298	260	
	2000°F/100	246	190	246	
	2400°F/10	262	261	262	
	2400°F/100	309	158	309	
	2600°F/10	243	215	876	
	2600°F/100	1076	231	1076	
7YO	As Compacted		369		367
	2000°F/10	264	256	266	
	2000°F/100	248	188	248	
	2400°F/10	236	208	566	
	2400°F/100	212	160	1063	
	2600°F/10	1091	210	1091	
	2600°F/100	1132	215	1132	
7TO	As Compacted		367		367
	2000°F/10	312	348	303	
	2000°F/100	354	303	379	
	2400°F/10	-	-	-	
	2400°F/100	-	333	-	
	2600°F/10	-	329	-	
	2600°F/100	-	-	-	
Prealloyed	As Compacted		333		333
	2000°F/10	263	241	373	
	2000°F/100	315	253	300	
	2400°F/10	305	249	816	
	2400°F/100	252	231	816	
	2600°F/10	277	230	989	
	2600°F/100	Consumed	-	Consumed	

TABLE 27

UPPER AND LOWER YIELD STRENGTH OF Cr-2.4%Mo-2.5$^{V}/_{O}Y_2O_3$ At INTERMEDIATE TEMPERATURES

Spec. No.	Initial Condition	One-Half Hour Aging Temp. °F	UYS Ksi	LYS Ksi	Test Temp °F
2YO-1	As extruded	None	53.2	47.3	800
2YO-2	As extruded	700	58.3	Fracture	700
2YO-3	Extruded + 2400°F/2 hr/vac Anneal	None	43.5	36.1	800
2YO-4	Extruded + 2400°F/2 hr/vac Anneal	700	51.5	50.7	700
2YO-5	Extruded + 2400°F/2 hr/vac Anneal	600	54.8	53.0	600
2YO-6	Extruded + 2400°F/2 hr/vac Anneal	500	55.9	55.2	500
2YO-7	Extruded + 2400°F/2 hr vac Anneal	400	58.1	Fracture	400

TABLE 28

TENSILE PROPERTIES OF PROCESSED ALLOYS

Sample No.	Composition	Temp (°F)	UTS (ksi)	Yield Str. (ksi)	Elong. Total (%)
2 YO	Cr-2.5$^{V}/_{O}$-Y_2O_3-2.4Mo-OREA	800	(1)	53.2	-
2 YO	" " " "	700	58.3	-	4.7
2 YO	" " " "	800	(1)	43.5	-
2 YO	" " " "	700	(1)	51.5	-
2 YO	" " " "	600	(1)	54.8	-
2 YO	" " " "	500	(1)	55.9	-
2 YO	" " " "	400	58.1	-	8.8
2 YO	" " " "	1900	16.82	-	11.8
2 MO	Cr-2.5MgO-3.3Mo-OREA	1900	20.1	-	2.0
5 YO-1	Cr-5$^{V}/_{O}$-Y_2O_3-1Mo-0.15REA	800	(1)	85.1	-
5 YO-1	" " " "	700	(1)	89.7	-
5 YO-1	" " " "	600	90.5	-	2.6
5 YO-1	" " " "	600	(1)	87.0	-
5 YO-1	" " " "	500	(1)	91.5	-
5 YO-1	" " " "	400	(1)	94.5	-
5 YO-1	" " " "	300	(1)	97.5	-
5 YO-1	" " " "	200	(1)	101.3	-
5 YO-1	" " " "	R.T.	98.5	-	5
5 YO-1	" " " "	2000	2.2	-	45.5
5 YO-2	Cr-5$^{V}/_{O}$-Y_2O_3-1Mo-0.25REA	2000	5.76	-	25.8

(1) Not tested to failure.

TABLE 29

TENSILE PROPERTIES OF THORIATED Cr SHEET PRODUCED FROM COARSE PREALLOYED POWDERS

Spec No.	Test Temp (°F)	.2YS (ksi)	UTS (ksi)	Elong (%)	RA (%)
HP5-8	800	-	> 73.4	Failed in Upper Tab	
HP5-8	1900	-	> 27.5	Failed in Lower Tab	
HP5-8	2100	75.8	81.3	2.3	2.8
HP5-8	2400	-	> 24.9	Failed in Upper Tab	

TABLE 30

STRESS RUPTURE PROPERTIES OF THORIATED Cr ALLOY SHEET PRODUCED FROM COARSE PREALLOYED POWDERS

Sample No	Temperature (°F)	Stress (ksi)	Rupture Time (hours)	Elong (%)	RA (%)
HP5-8-5	2100	2.5	.01	10.2	4.9
HP5-7-2	1900	15.0	.25	8.8	6.3
HP5-7-3(1)	1900	15.0	.06	-	-

(1) Heat Treated - Rapid Heat up to 1900°F
1900°F → 2600°F @ 50°F/hr - Furnace Cool

TABLE 31

BEND TEST DATA FOR DISPERSION STRENGTHENED ALLOYS PRODUCED FROM COARSE FLAKES

[Cr-4Mo-.15(La+Y)-4^{v}/oThO_2]

Spec No	Test Temp (°F)	Bend Ratio[1]	Bending[2] Yield Strength (ksi)	Fracture Bend Angle (degrees)
HP5-8-3	800	4.57	148	.2
HP5-7-5	1000	3.48	115.3	9.5
HP5-7-4	1000	3.41	119	5.5

(1) Bend Ratio = $\frac{\text{Ram Radius}}{\text{Specimen Thickness}}$

(2) Test conducted with a .05 ipm ram speed and a 1.5" span.

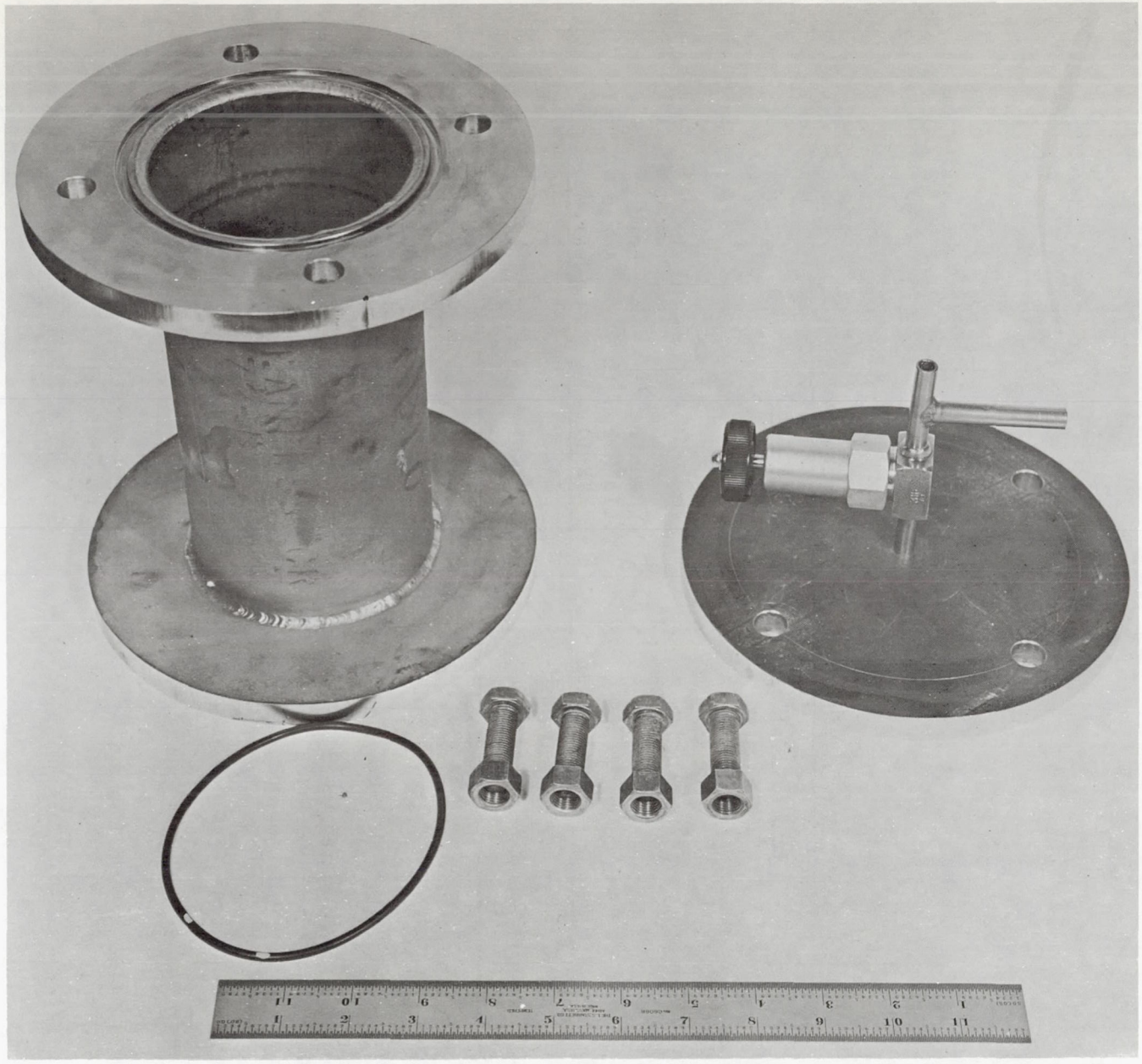

FIGURE 1 Controlled Environment, Molybdenum-lined, Ball Mill Used to Comminute Powders at -50°F in a Toluene Media.

C65121648

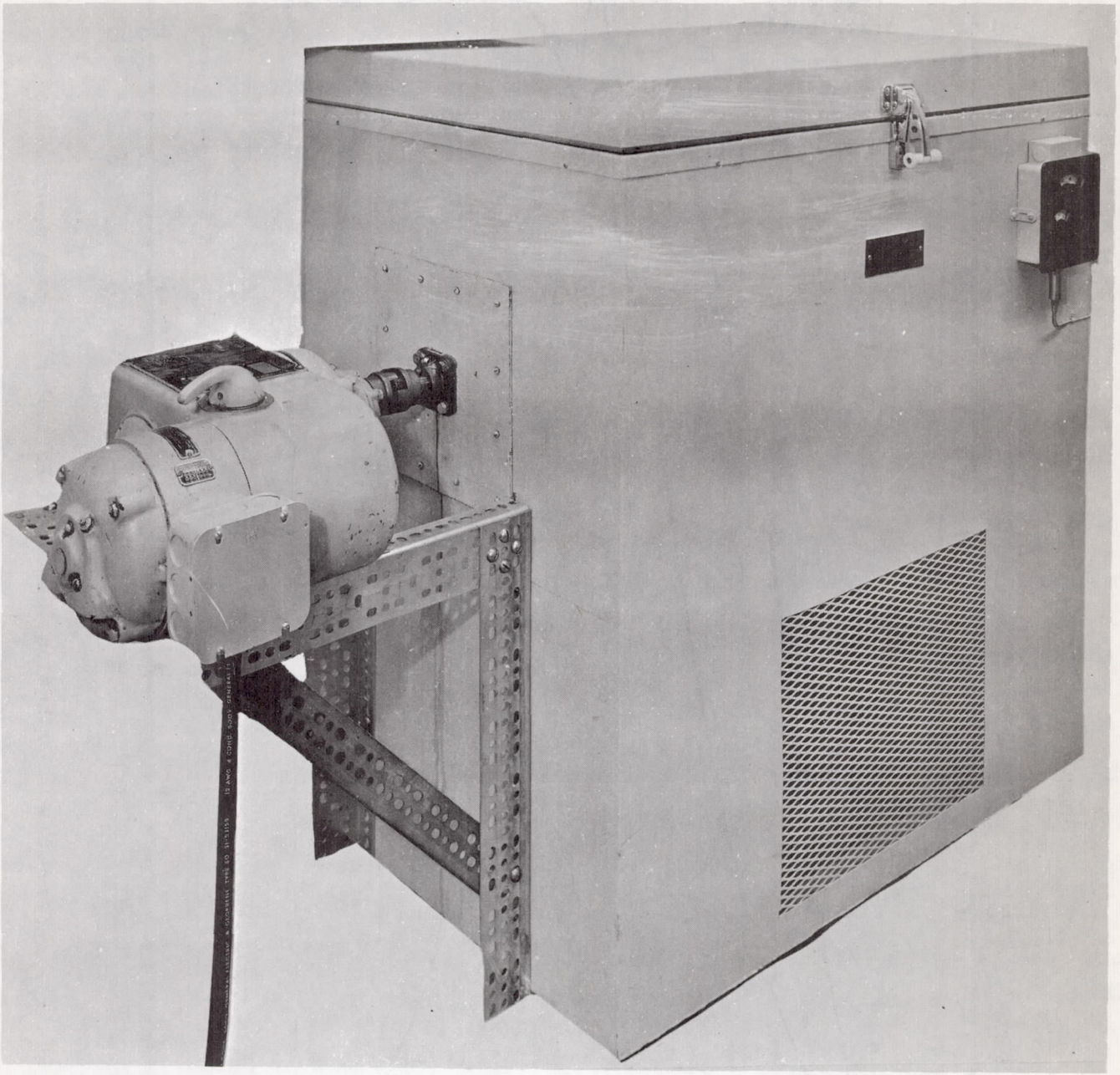

FIGURE 2 Cold Chamber for Low Temperature Ball Milling

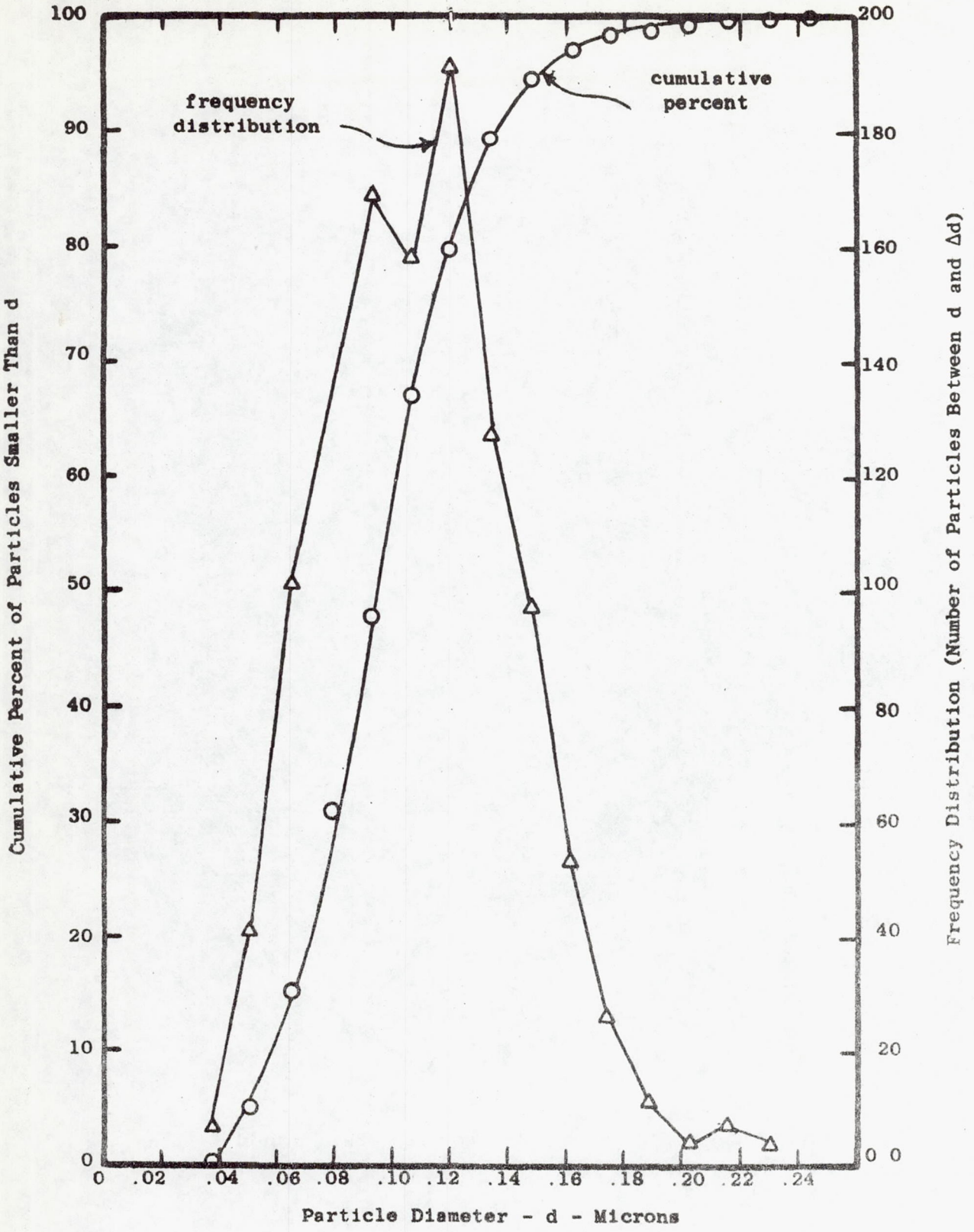

FIGURE 3 Particle Size-Frequency Distribution and Cumulative Percent for MgO Starting Powder

C65122802

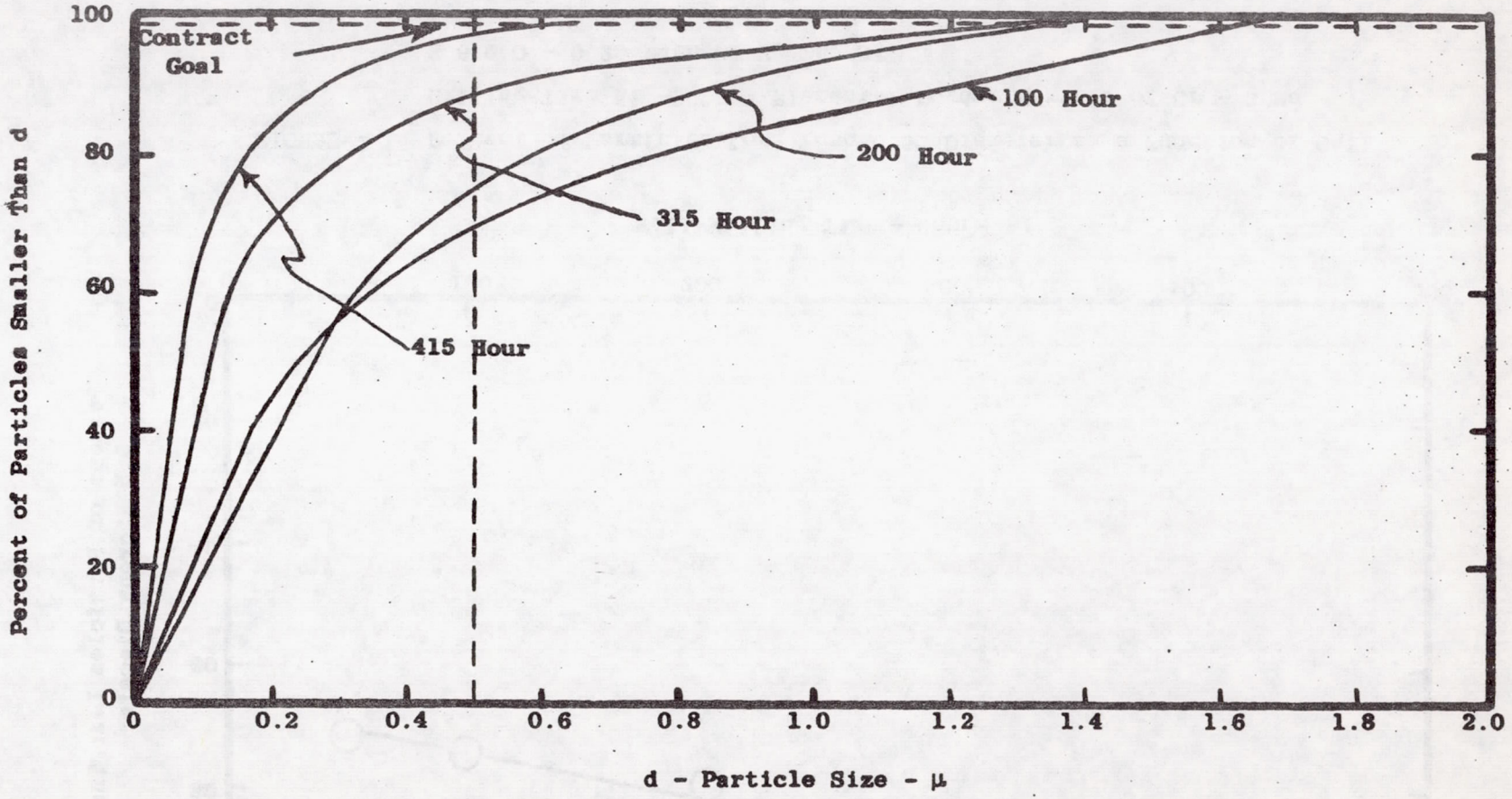

FIGURE 4 Cumulative Percent of Particles Smaller than Particle Diameter d as a Function of d with Ball Milling Time at -50°F as a Parameter. Elemental Powder Mixture of Cr - 3 Mo - 2.6 MgO - 0.25 each of Y, Th, Hf.

C65122803

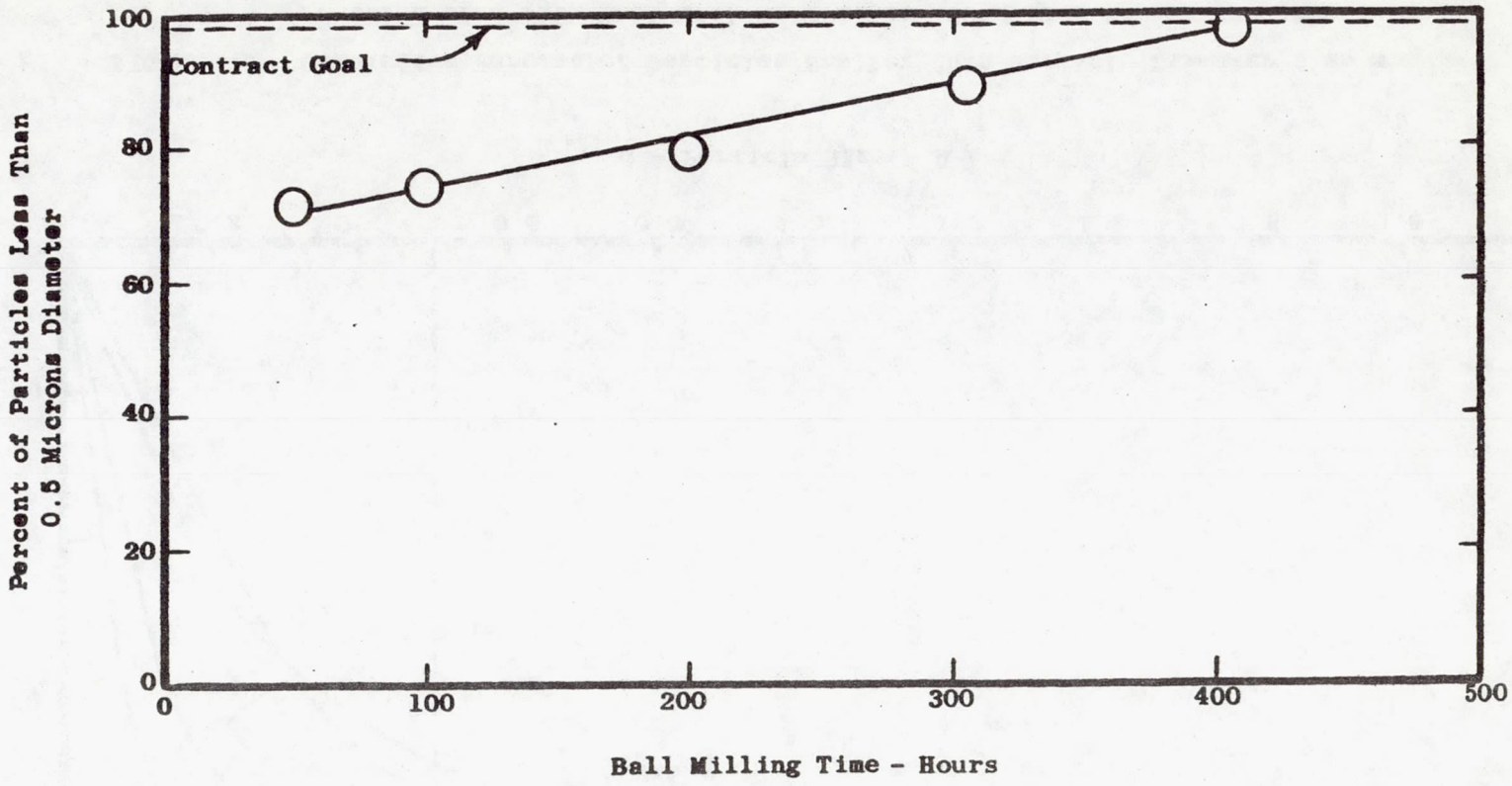

FIGURE 5 Percent of Particles Less Than 0.5μ Diameter as a Function of Ball Milling Time at -50°F. Elemental Powder Mixture of Cr - 3 Mo - 2.6 MgO - 0.25 Each of Y, Th, Hf.

C65121636

A

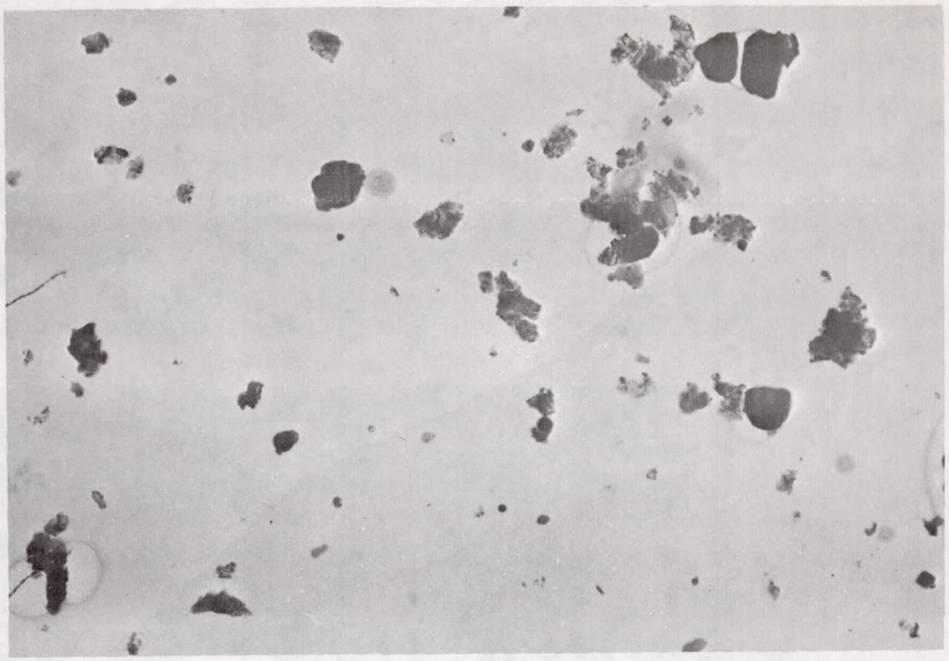

B

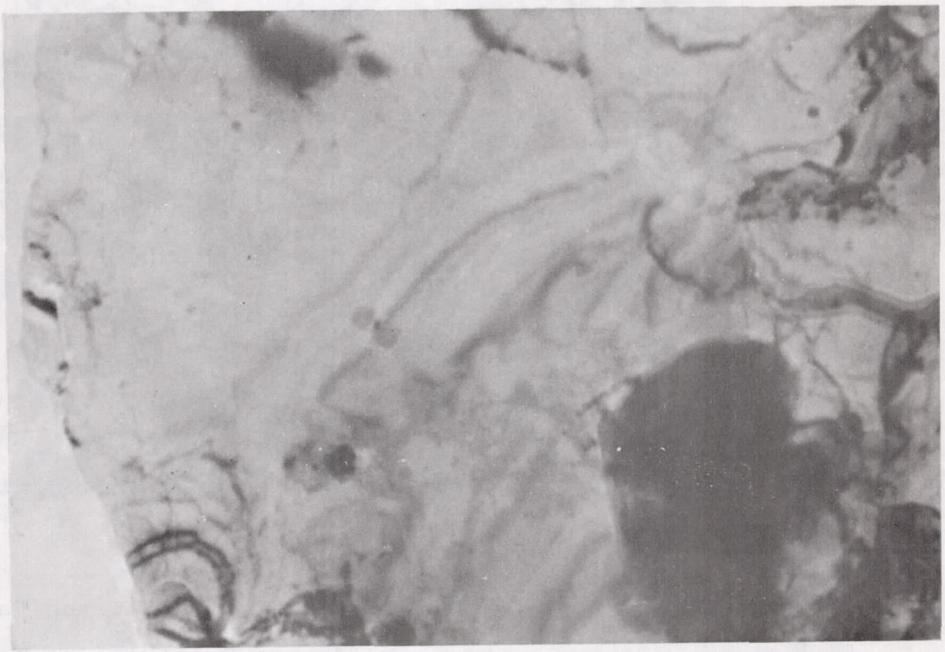

FIGURE 6 Electron Photomicrographs of the Elemental Powder Mixture Of Cr - 3 Mo - 2.6% MgO and 0.25 each Y, Th, Hf After 500 Hour Ball Milling Time

A - 10,000X B - 100,000X

A

L3310

B

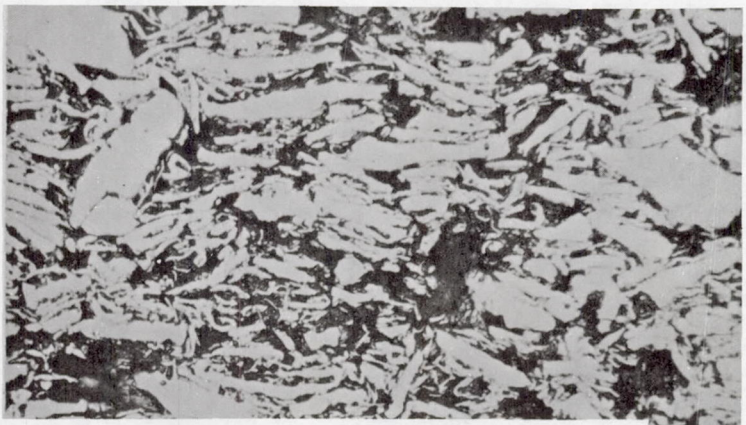

L3309

C

L4562

FIGURE 7 Photomicrographs of Prealloyed Powders Showing Particle Size and Shape at Three Different Ball Milling Times.

A) Heat No. 1 After 300 Hours Ball Milling Time - 500X

B) Heat No. 1 After 540 Hours Ball Milling Time - 500X

C) Heat No. 3 After Ball Milling 980 Hours - 1000X

C65121649

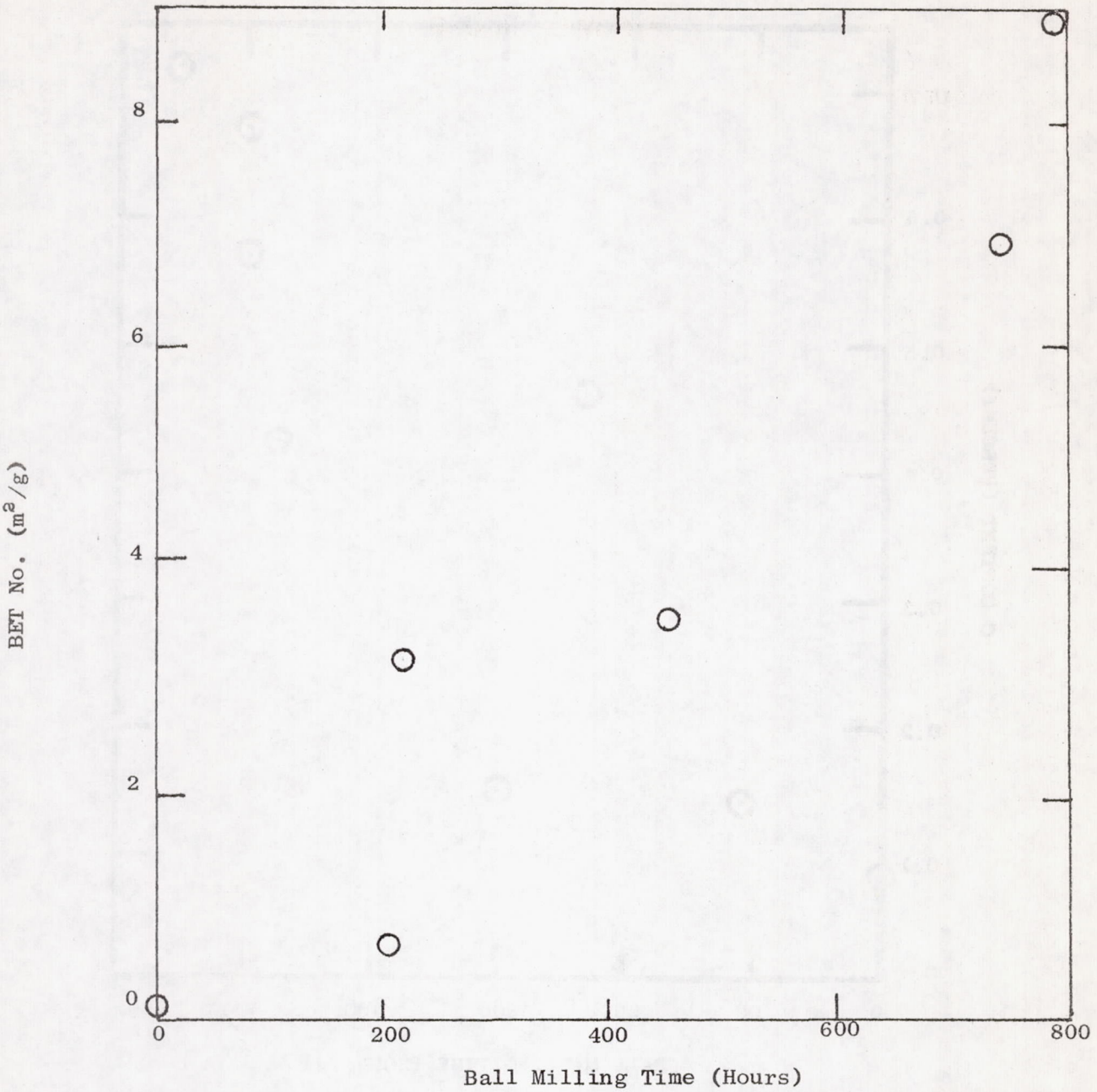

FIGURE 8 Surface Area of Prealloyed Flake Powder as a Function of Ball Milling Time. Ball Milling Conducted at -50°F with a Toluene Milling Liquid.

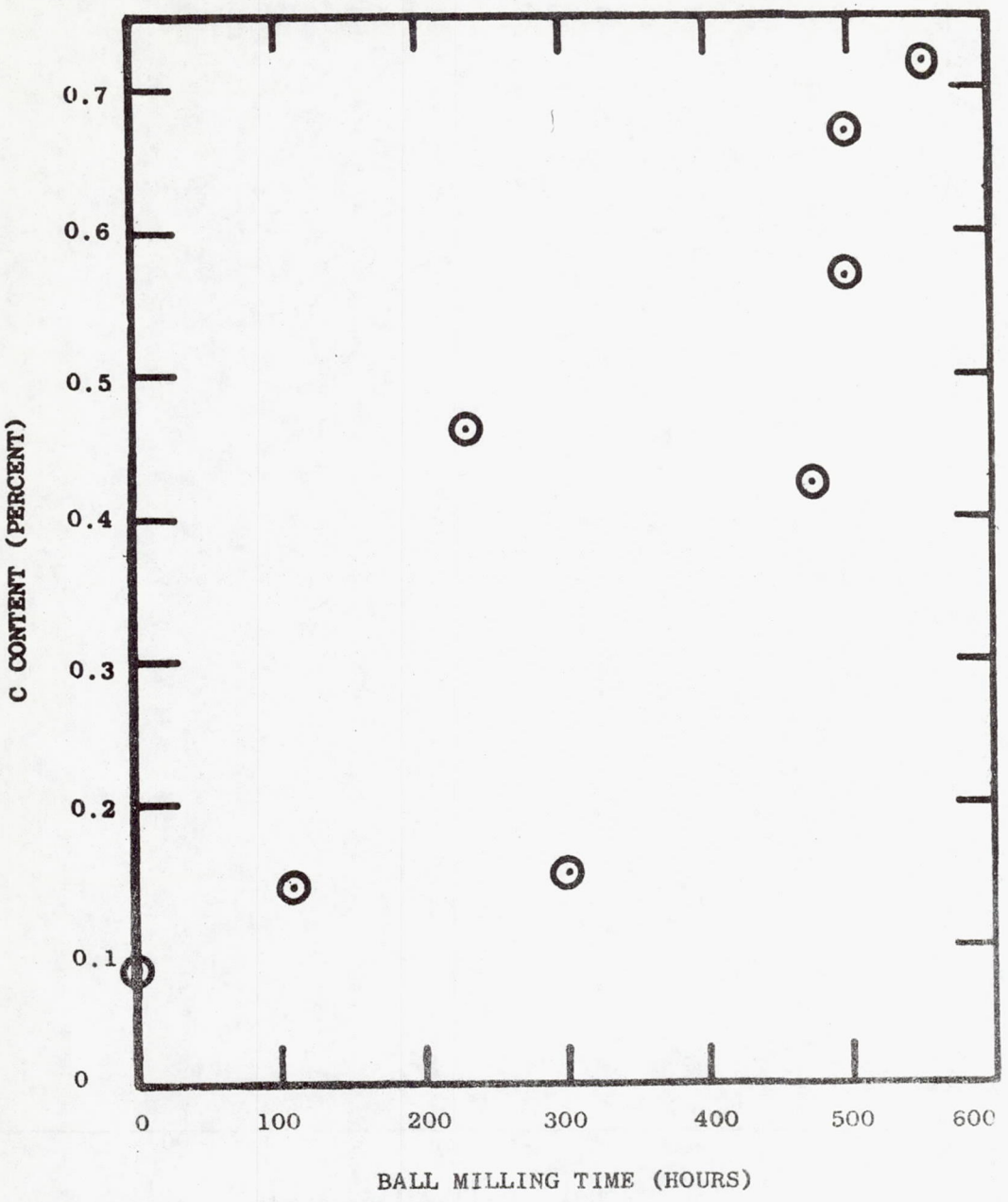

FIGURE 9 Carbon Content of Elemental Cr Powders + Oxide Dispersoid As a Function of Ball Milling Time.

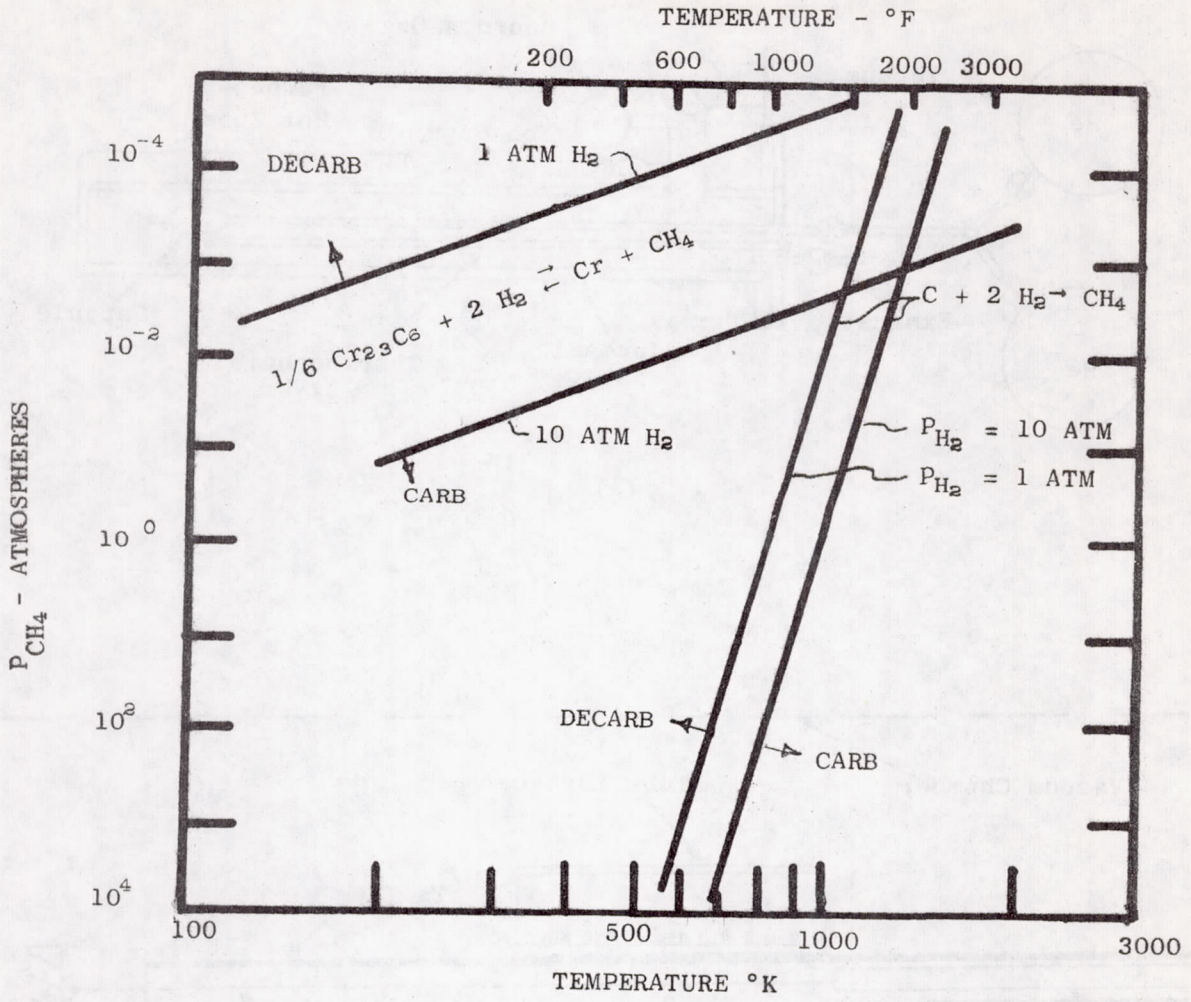

Figure 10 Thermodynamic Consideration of H_2 Cleaning for Carbon in Cr Powders.

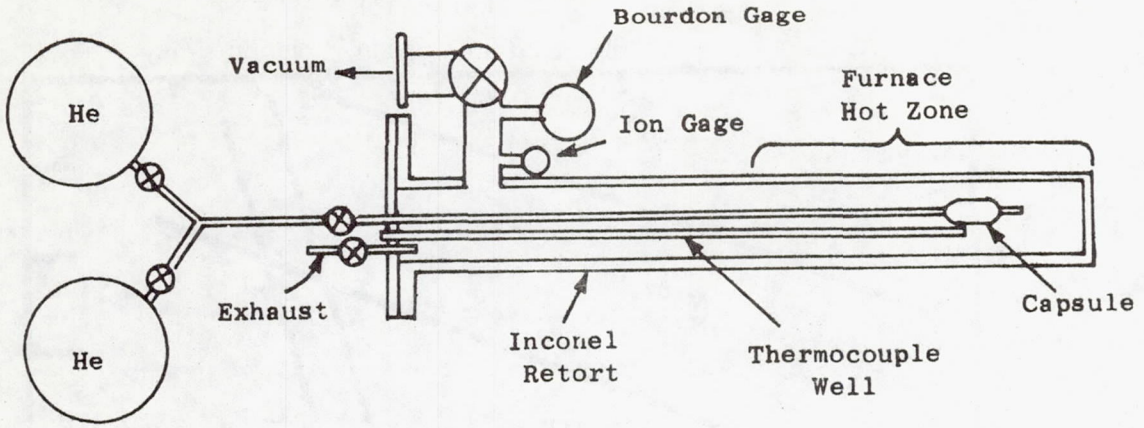

(a)

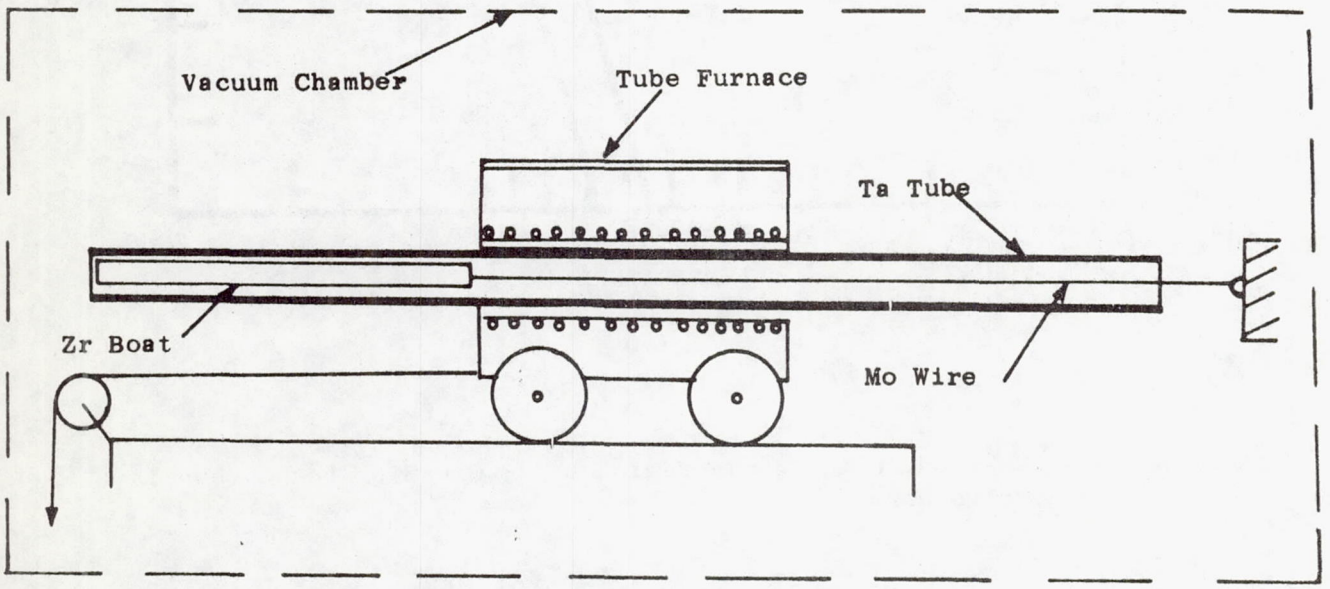

(b)

FIGURE 11 Schematic Diagrams of Experimental Equipment Used for:

(a) H_2 Cleaning, and (b) Continuous Carbothermic Cleaning of Elemental Submicron Blends.

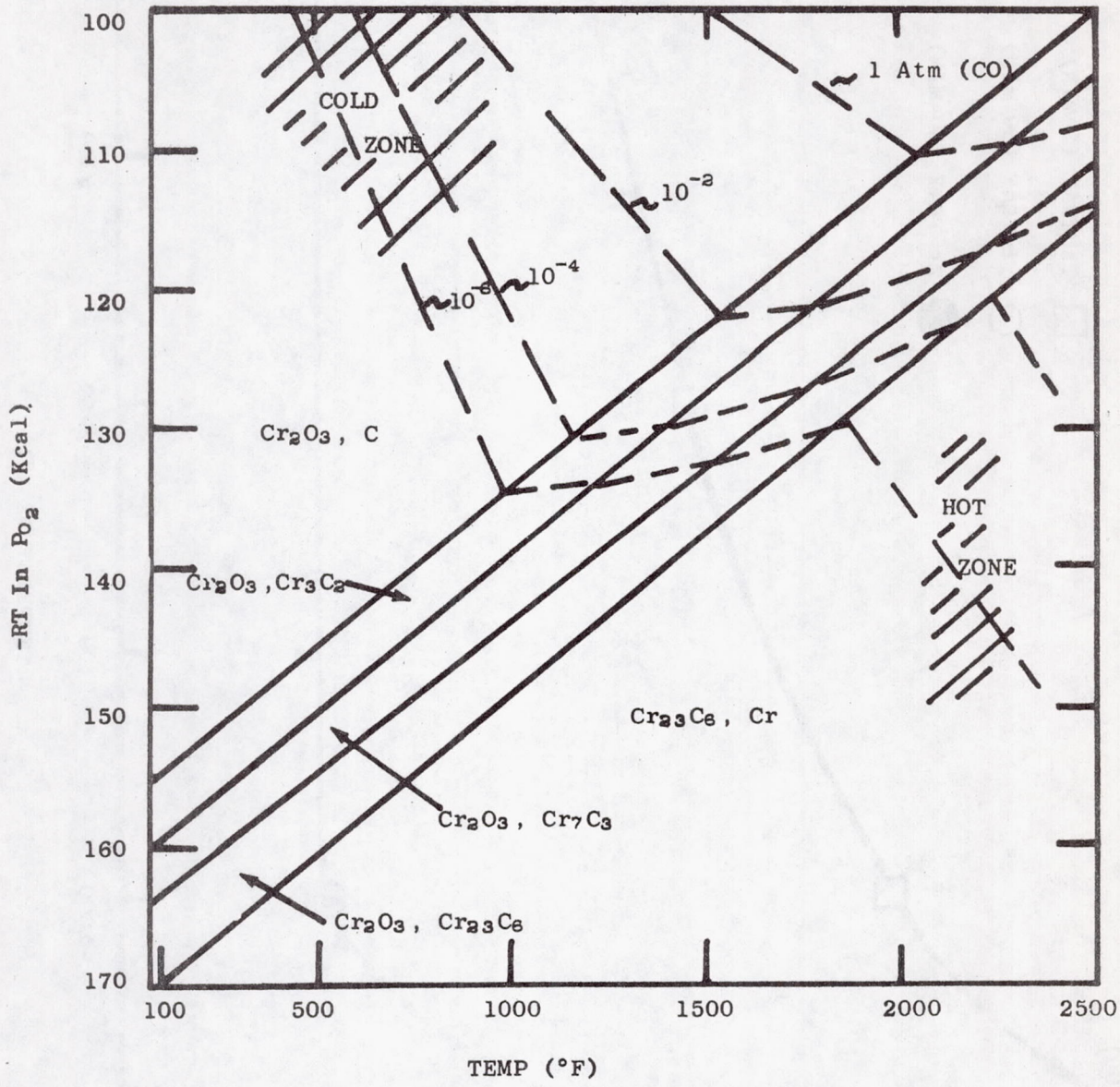

FIGURE 12 Pourbaix-Ellingham Diagram for the Cr-C-O System.

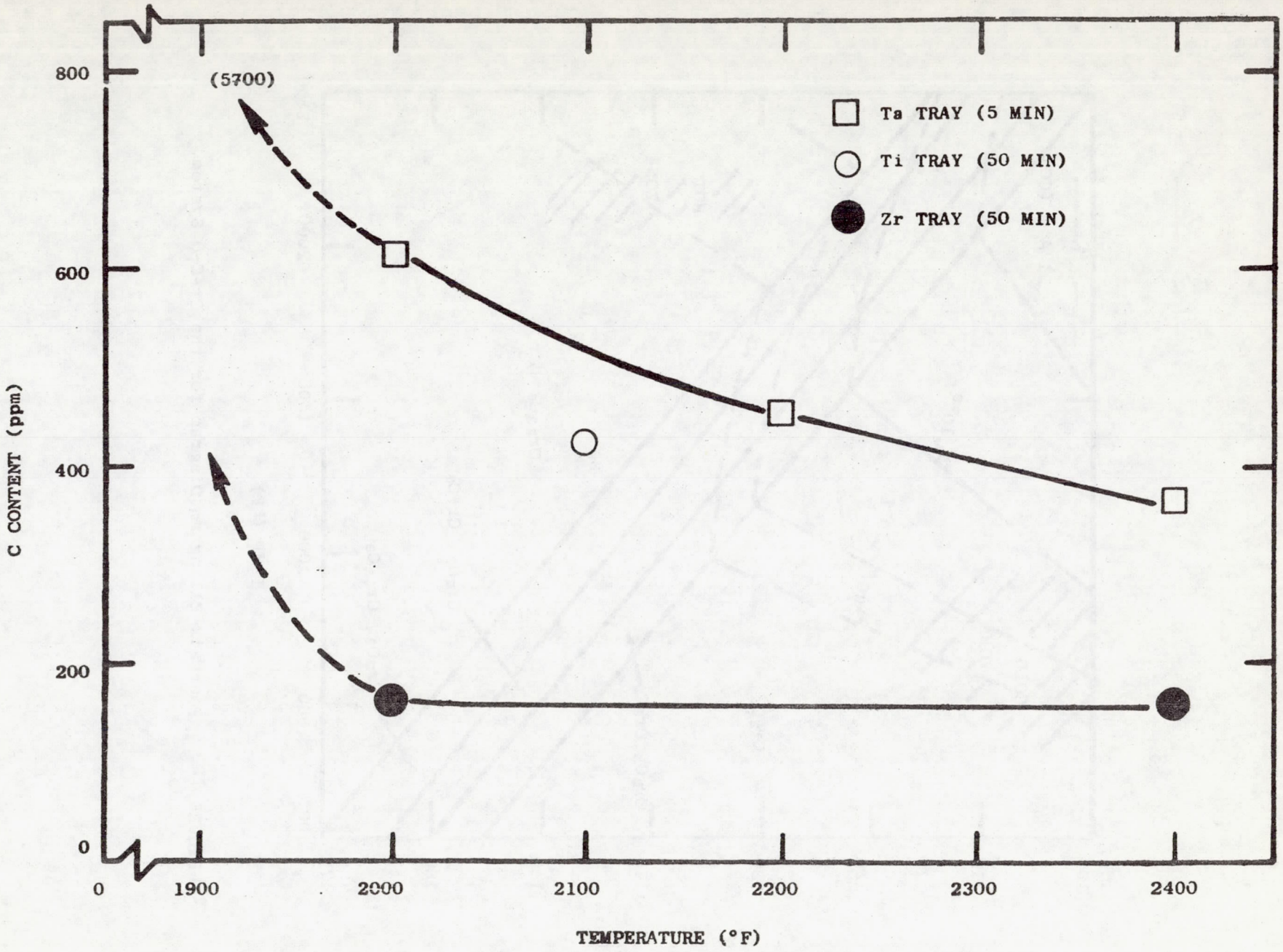

FIGURE 13 Carbon Content as a Function of Temperature for Carbothermic Cleaning of M&R Cr Powders Containing 5 $^{V}/o$ MgO.

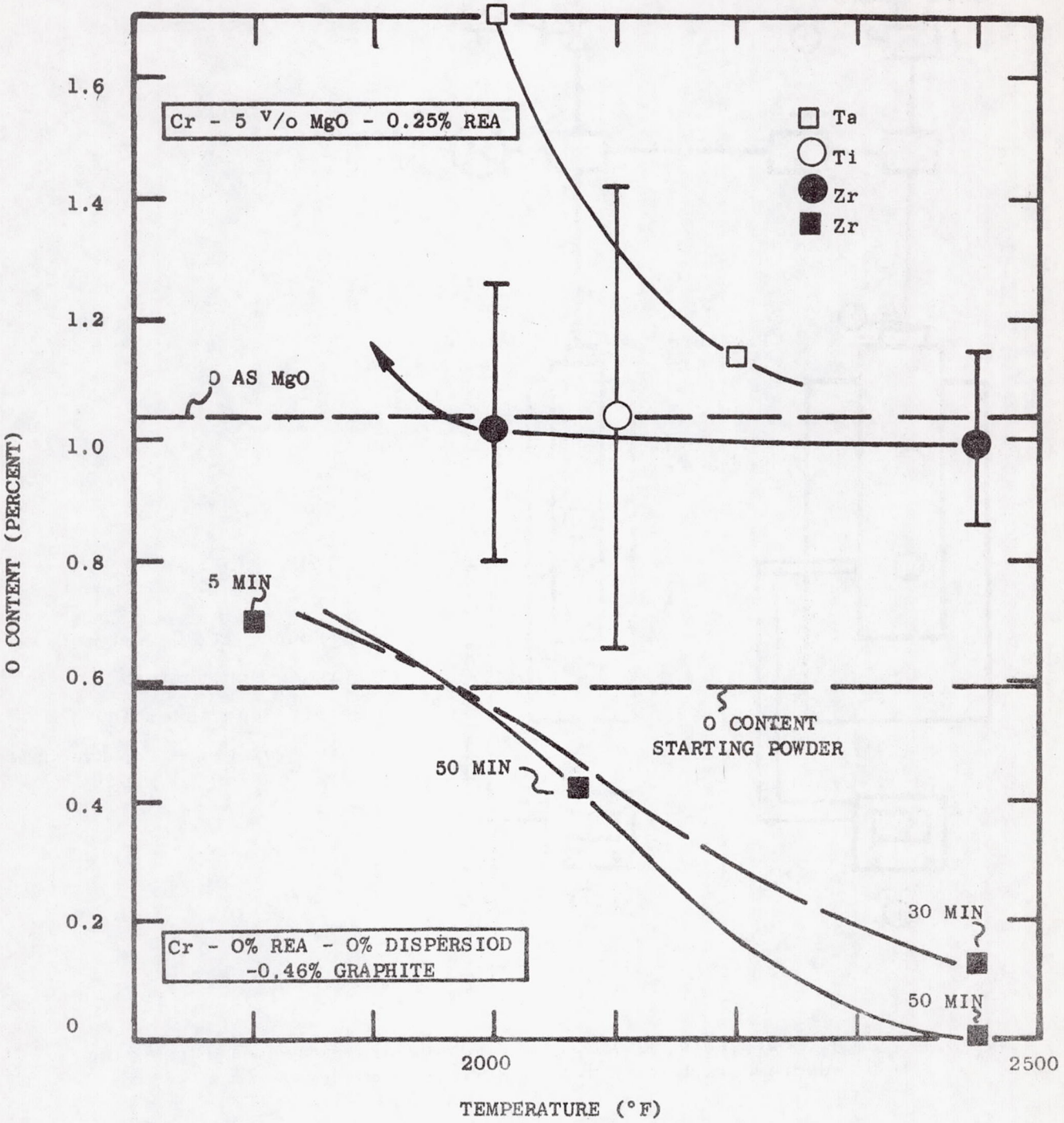

FIGURE 14 Reduction of O in Cr Powders during Carbothermic Cleaning At Various Temperatures.

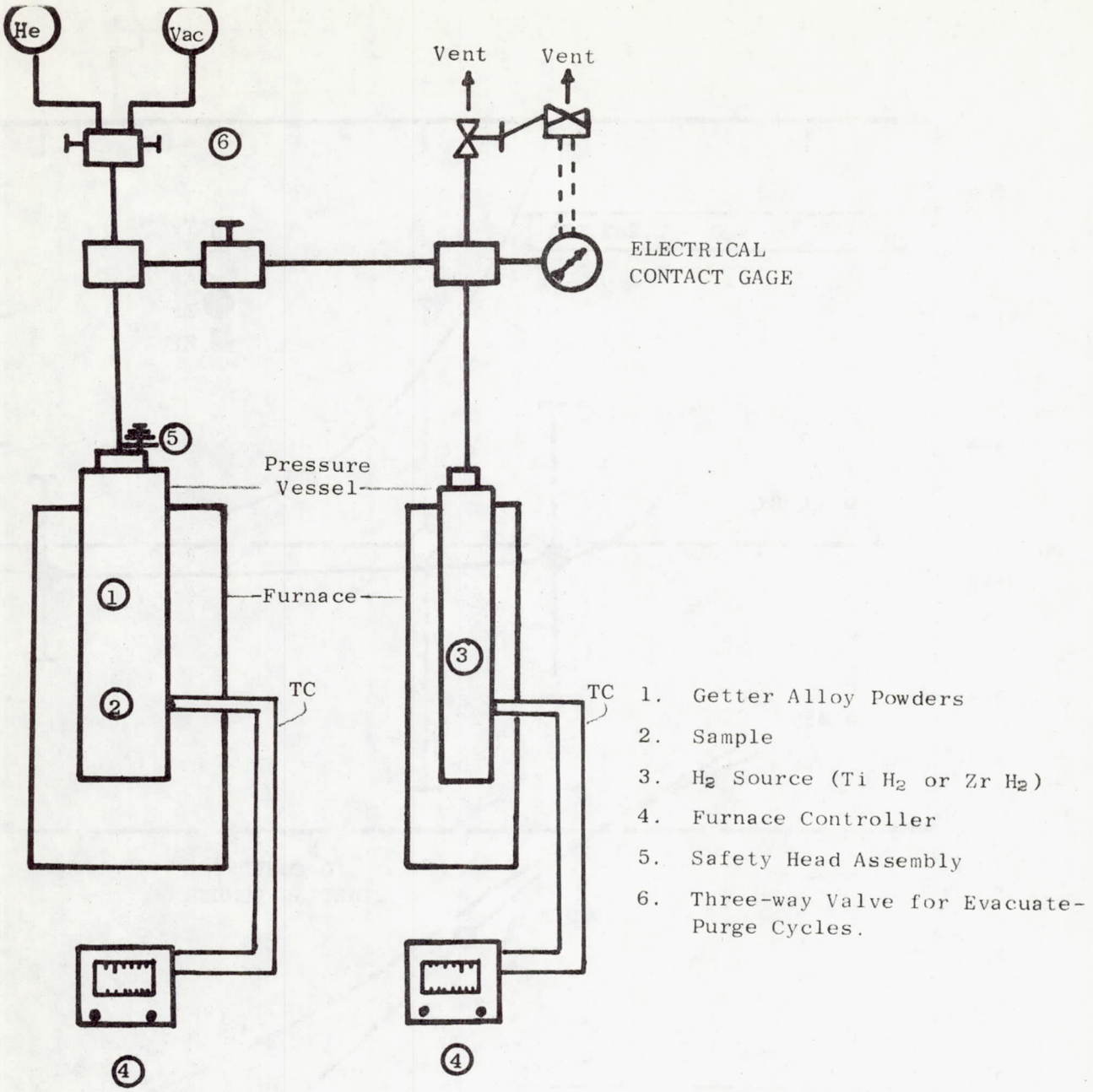

Figure 15 High pressure, closed, H_2 cleaning system used for removing adsorbed carbon from ball milled Cr powders.

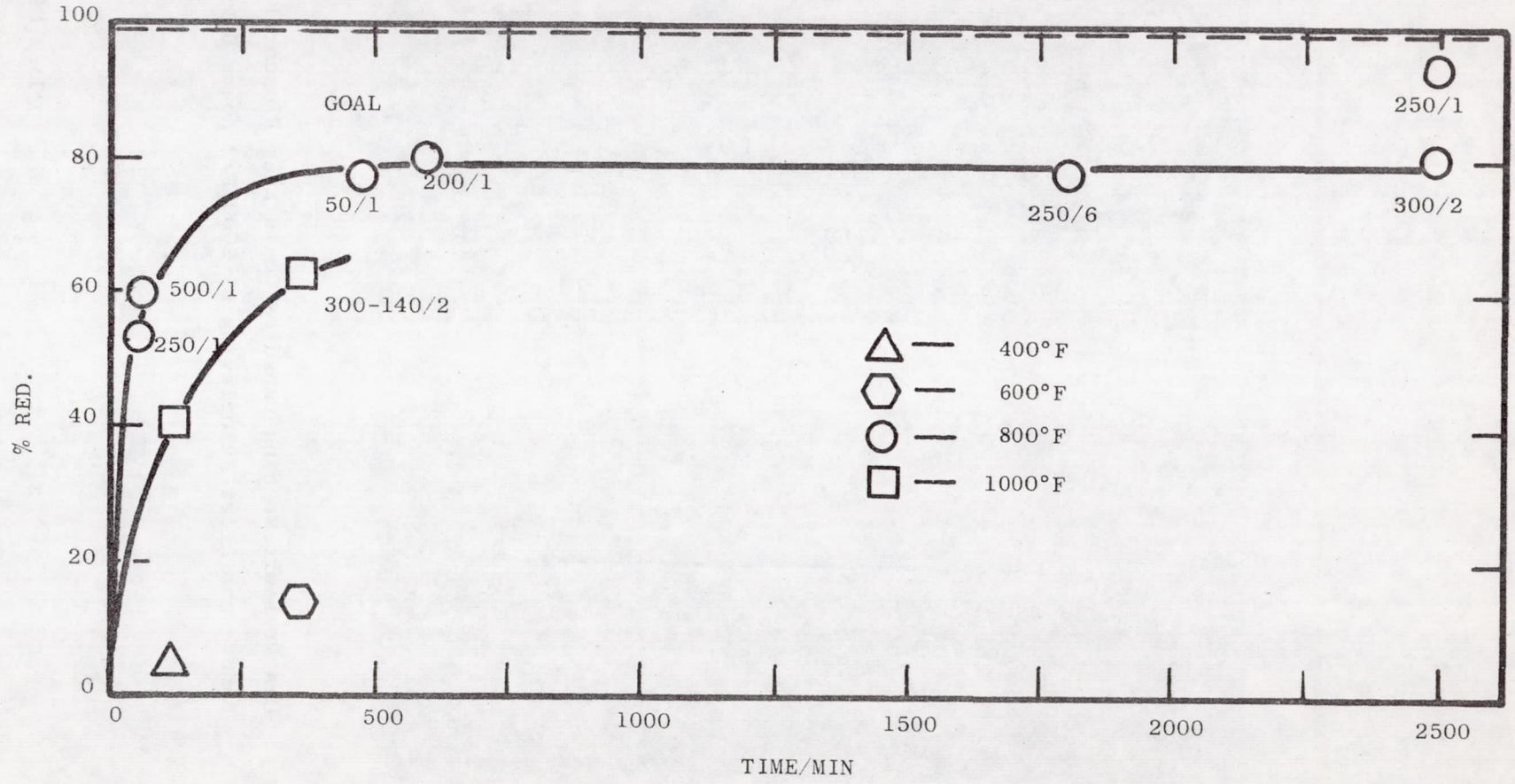

Figure 16 Percent Carbon Removed as a Function of Cleaning Time With Temperature as a Parameter. Hydrogen pressure and number of hydrogen pressure cycles are shown as P_{H_2} (psi)/N adjacent to each data point on the figure.

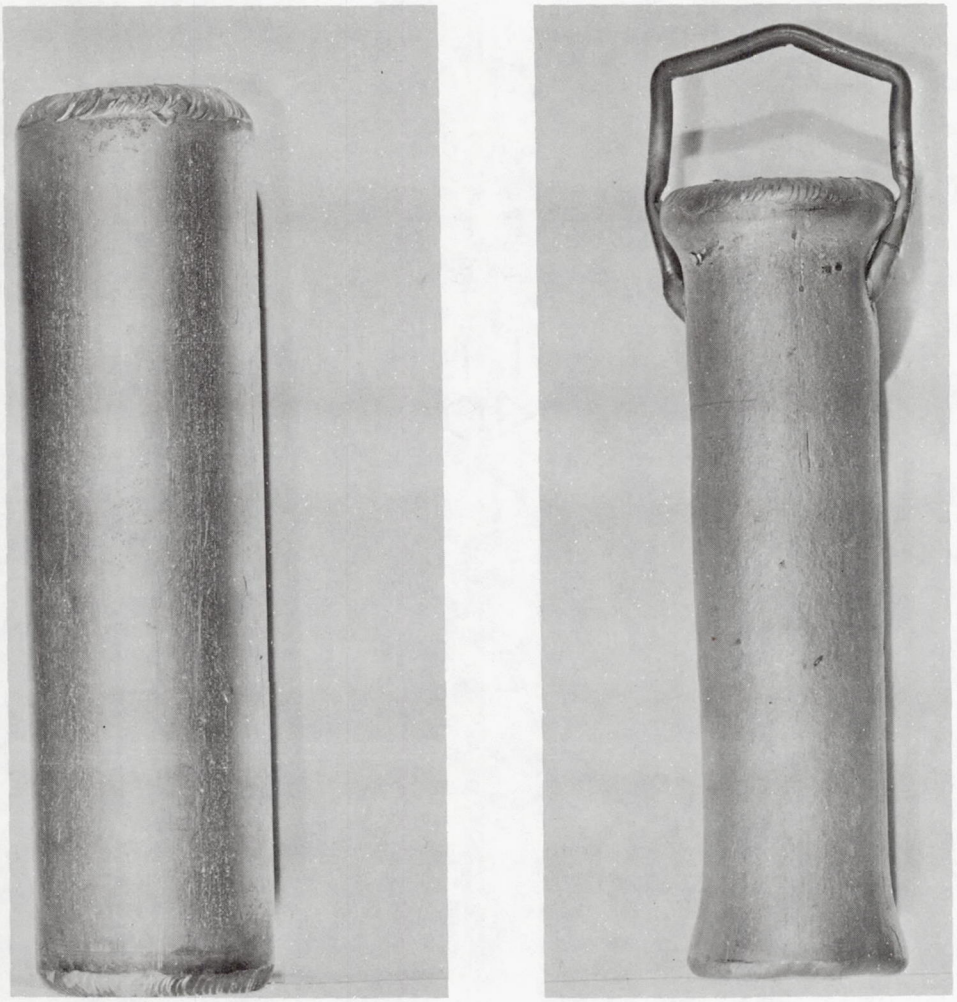

FIGURE 17 Gas Pressure Bonding Capsules Containing Elemental Powders Before and After Autoclaving at 2000°F/2 hours/8 ksi He

C65121644

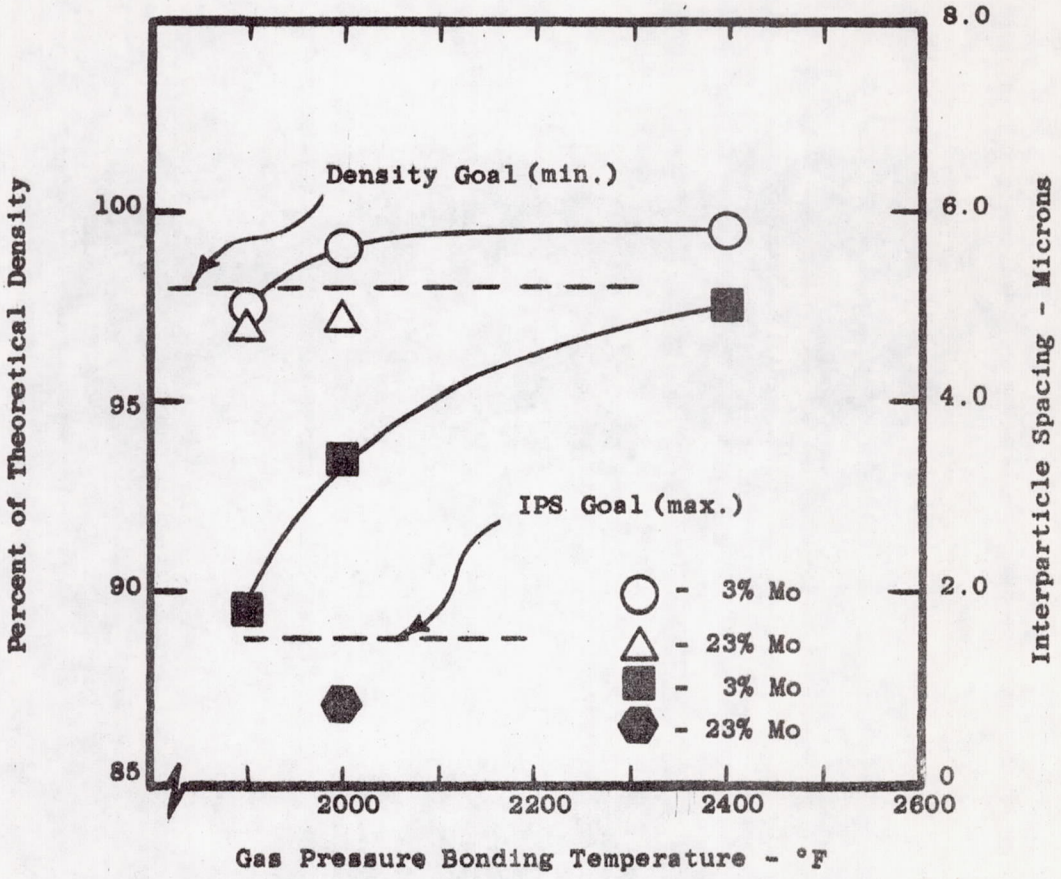

FIGURE 18 **Density and Interparticle Spacing as Related to Gas Pressure Bonding Temperature for Cr - Mo - 5 V/o MgO - 0.25 each Hf, Y, Th Alloys** prepared from elemental powders.

C65122801

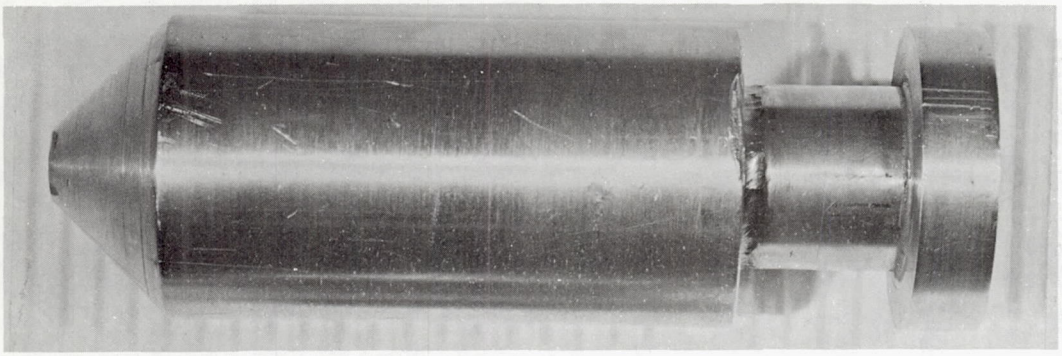

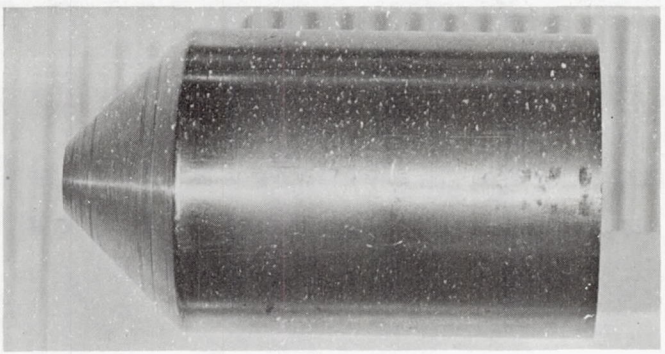

FIGURE 19 Extrusion Capsules for Direct Extrusion of Submicron Powders (Top) And for Extrusion of Gas Pressure Bonded Compacts (Bottom)

C65122807

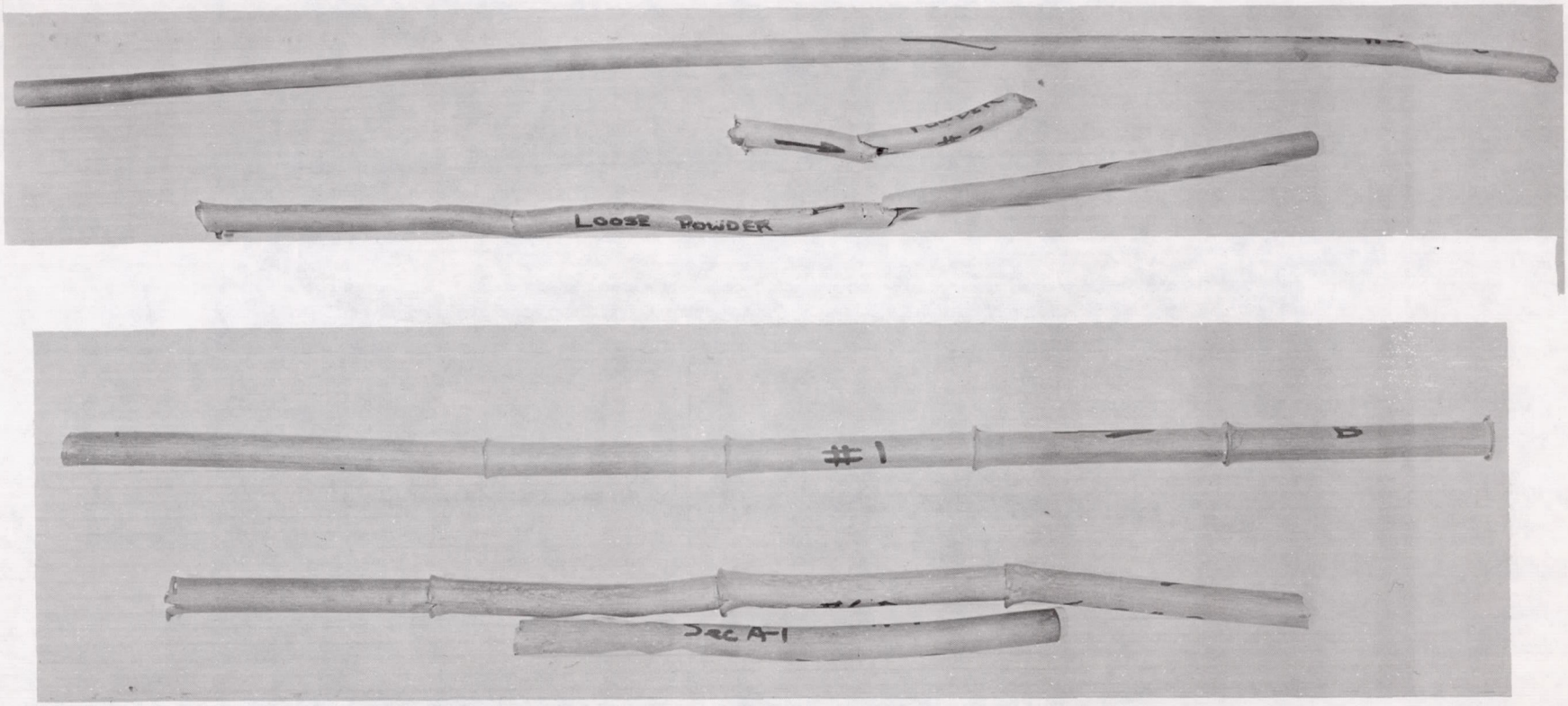

FIGURE 20 As-Extruded Billets Encased in the Low Carbon Iron Jacketing Material. Extrusion was Conducted At 2000°F With an 18/1 Extrusion Ratio

A) Extrusion of Loose Powders

B) Extrusion of Gas Pressure Bonded Compact

C65121650

C67022103

FIGURE 21 Cr Alloy Impact Extrusions After Removal Of Mo Extrusion Jackets.

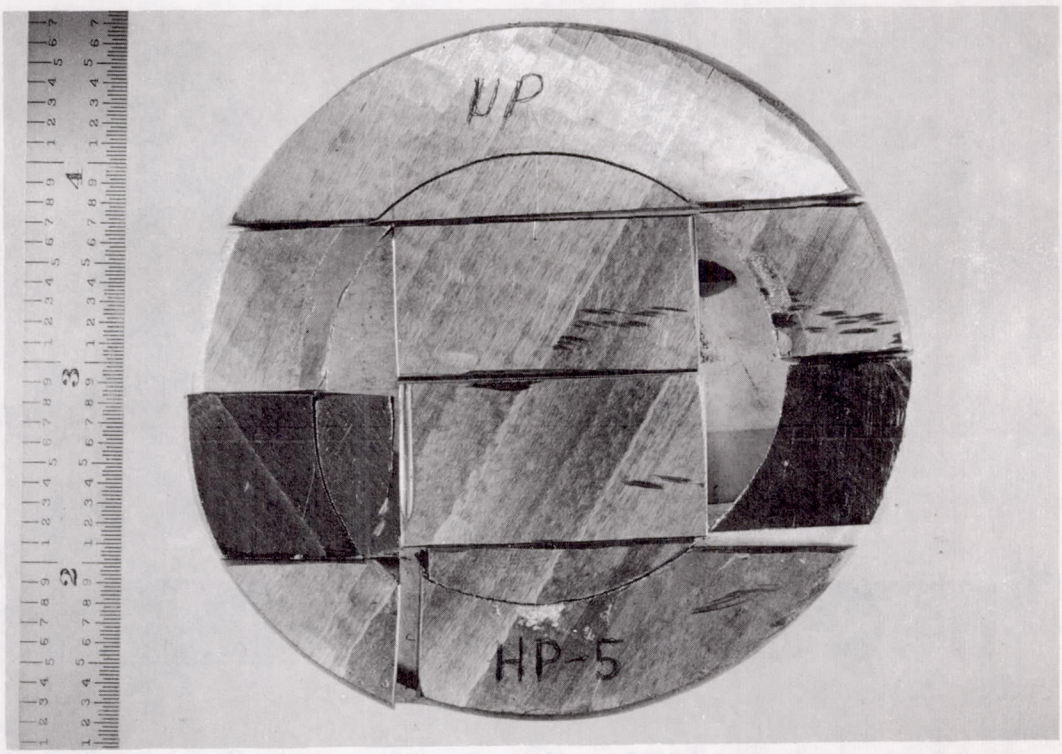

FIGURE 22 Sectioning of Hot Press Compact HP5. Hot Pressed at 2200°F/2 hrs/Vac from Prealloyed Flake Shaped Powders (Cr-4Mo-.15(La+Y)-4ThO_2) Small Pieces Were Used to Investigate Rolling Parameters

C68091748

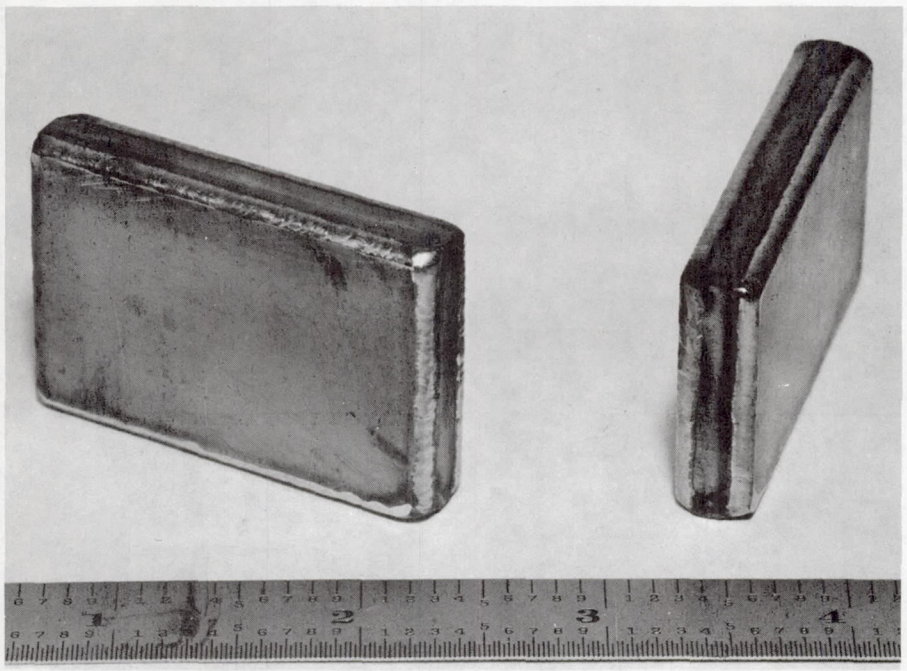

FIGURE 23 As-Pressed HP5 in Hastelloy X Rolling Packs Ready For Rolling.

C68092621

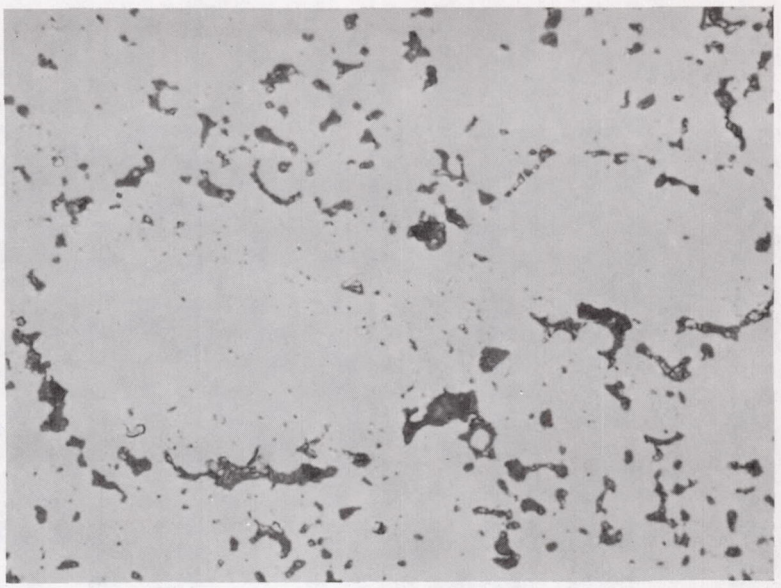

N2381

A) 2400°F/10 Hrs/Argon

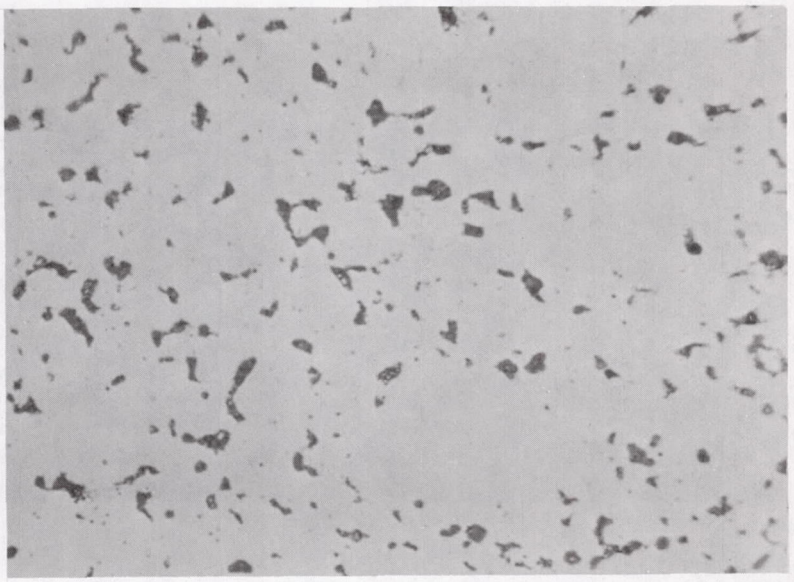

N2075

B) 2400°F/100 Hrs/Argon

FIGURE 24. Oxide Instability In 3YO Alloy After Exposure At 2400°F/Argon.

1,000X

A

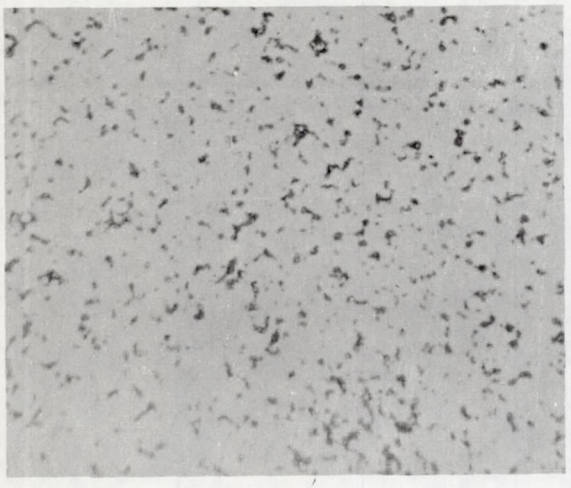

L4454

B

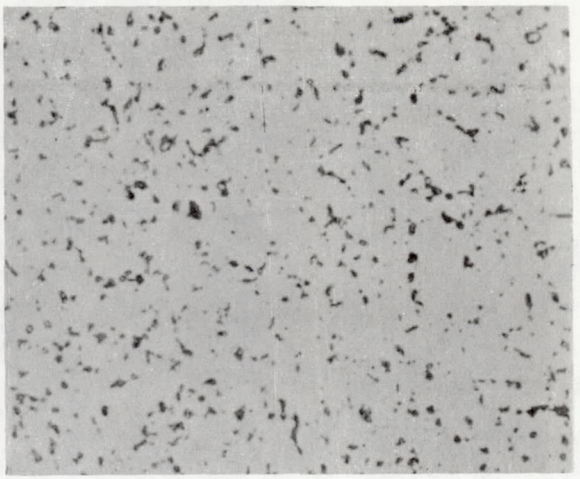

L4457

C

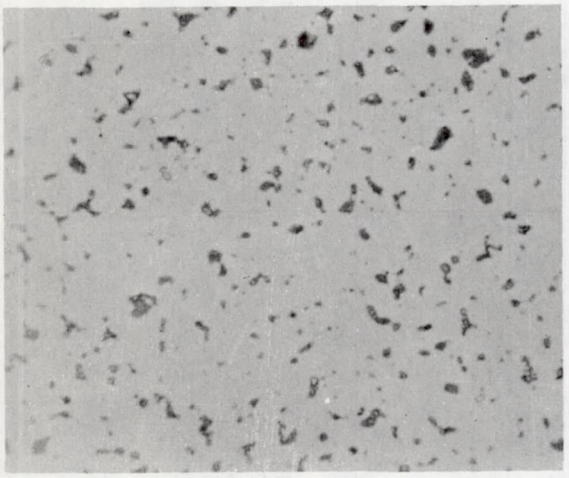

L4459

D

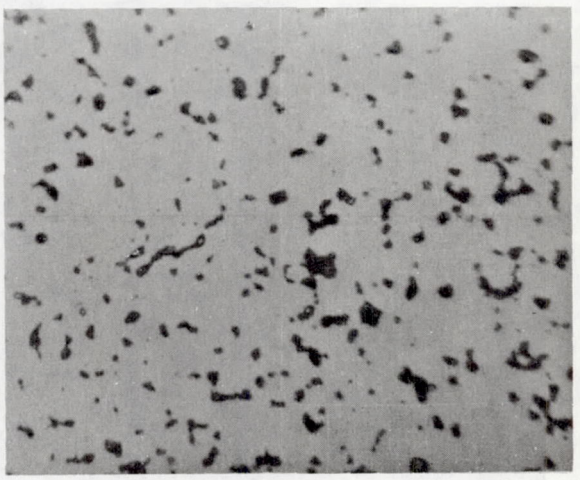

L4463

FIGURE 25 Cr - 3 Mo - 5 ^{v}/o MgO - 0.25 each Hf, Y, Th Alloy Compacted at 2000°F/2 Hours/10 ksi He after one Hour Vacuum Exposure at:

A - 2000°F B - 2200°F C - 2400°F D - 2600°F

1000X

C65122805

(a)

1000X

(b)

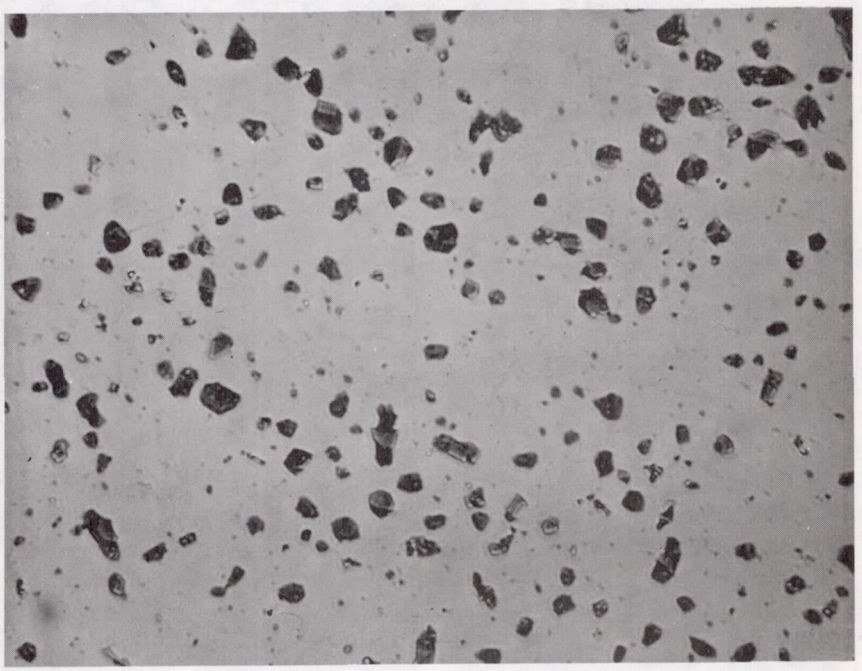

1000X

FIGURE 26 Dispersoid Stability of Chromium Alloy 5YO-4 Alloy Containing 60 ppm C and 1.3% Excess Oxygen. (a) As-Compacted. (b) As-Compacted + 2600°F/1 hr/vac.

A

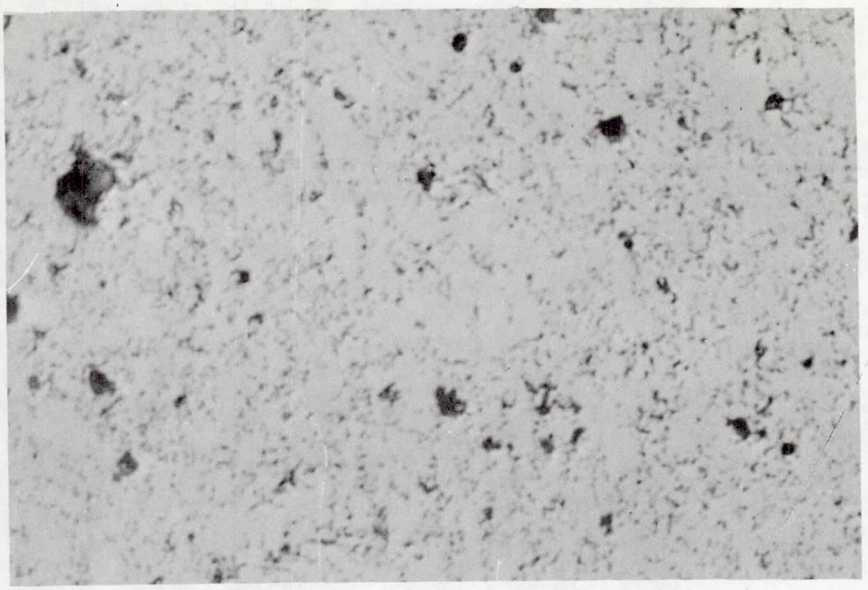

B

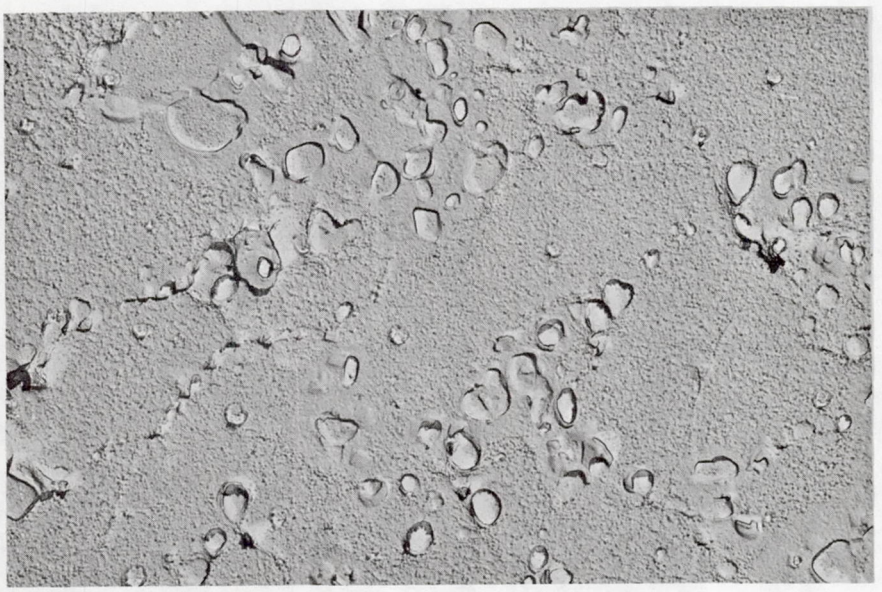

FIGURE 27 Cr - 3 Mo - 5 ^{v}/o MgO - 0.25 each Hf, Y, Th Alloy (5MO-1) Prepared by Ball Milling Elemental Powders 100 Hours And Subsequent 1900°F/3 hour/10 ksi He Autoclaving

A - 1000X Unetched

B - Electron Micrograph - Electrolytic Etch - 10,000X

C65121642

A) As Compacted

B) Early Stages Of Instability

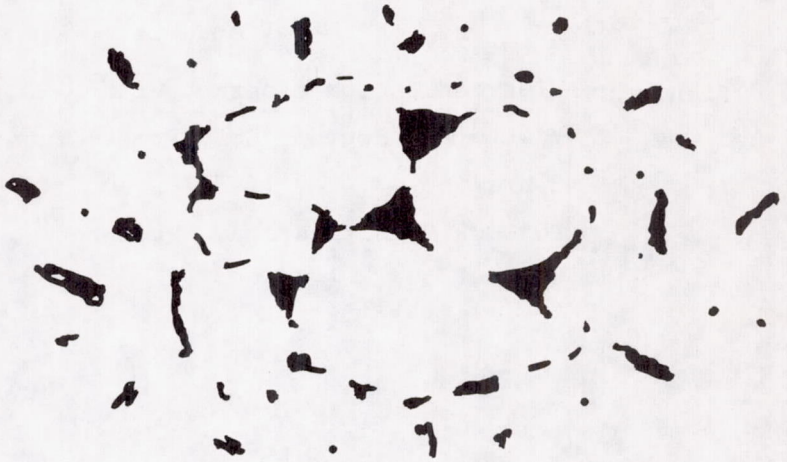

C) Late Stages Of Instability

FIGURE 28 Schematic Illustration Of Progressive Stages Of Dispersoid Instabilities.

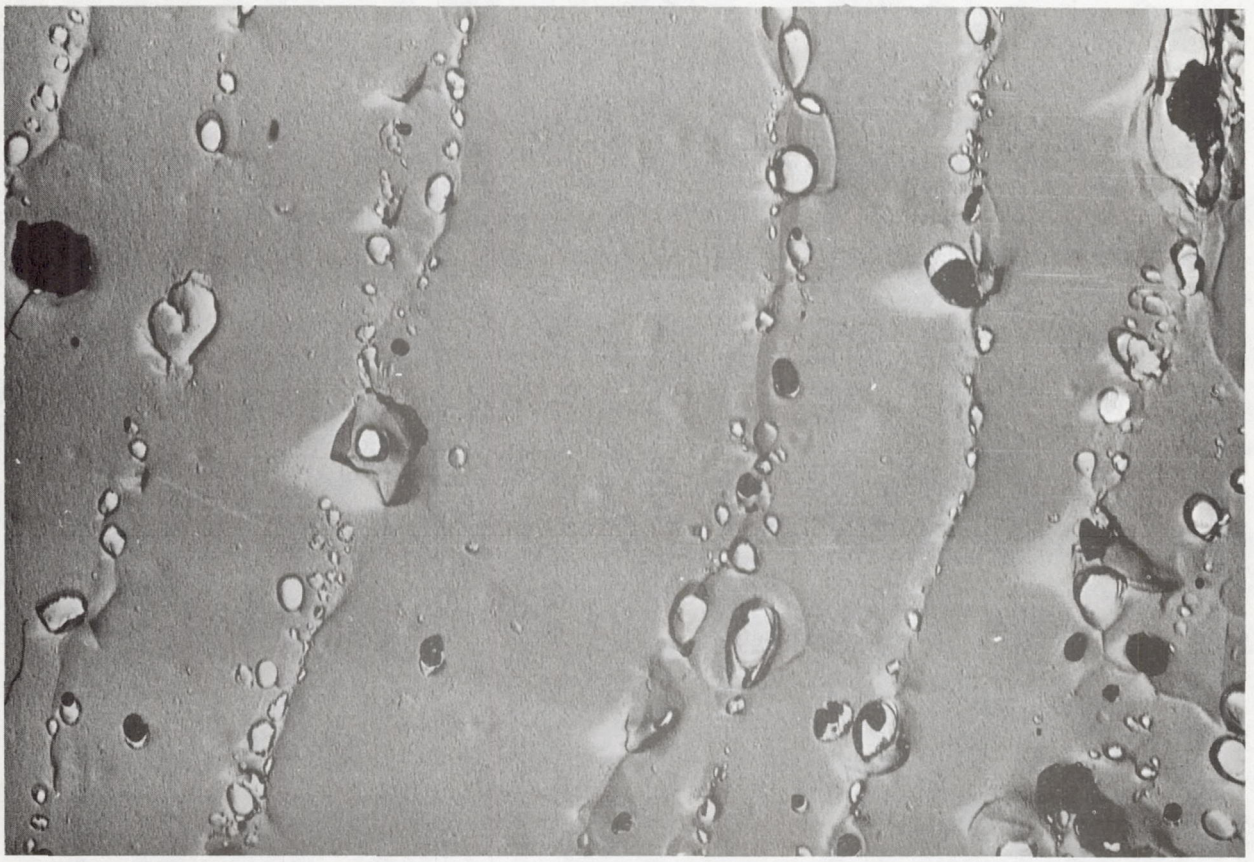

Figure 29 Electron Photomicrograph of Cr + 5 $^{V}/o$ Y_2O_3 Powder Ball Milled 207 Hours - Cold Pressed and Sintered at 2350°F/ 8 hrs/vac.
10,000X Magnification. Unetched.

A - 100X Unetched

P7978

B - Edge of (A) Unetched 1000X

P7980

C - Center of (A) Unetched 1000X

P7979

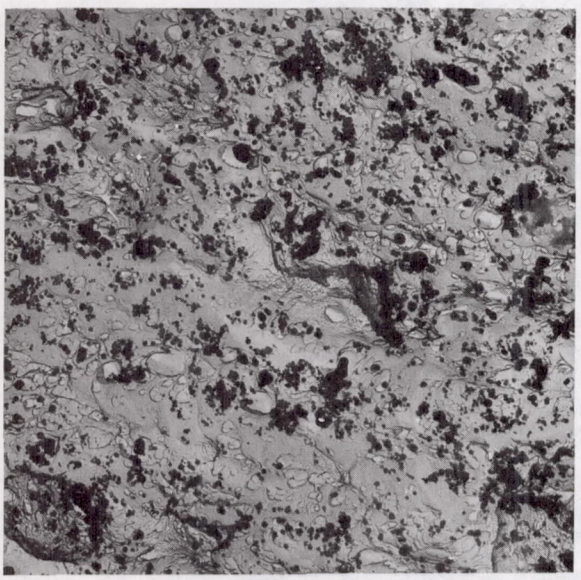

Extraction Replica - Edge of (A) 5000X Mag.

H-67-5

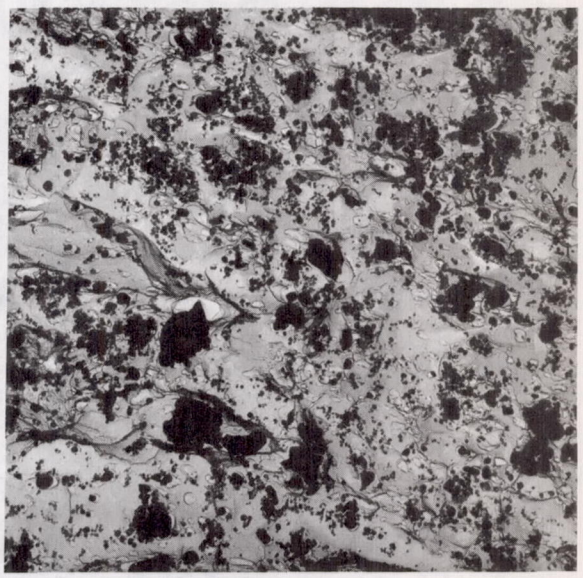

Extraction Replica - Center of (A) 5000X Mag.

H-67-7

FIGURE 30 Microstructure of Hot Rolled Sheet Produced from Coarse Prealloyed Flake Blends (HP5-8) after Thermal Exposure of 2600°F/10 hrs.

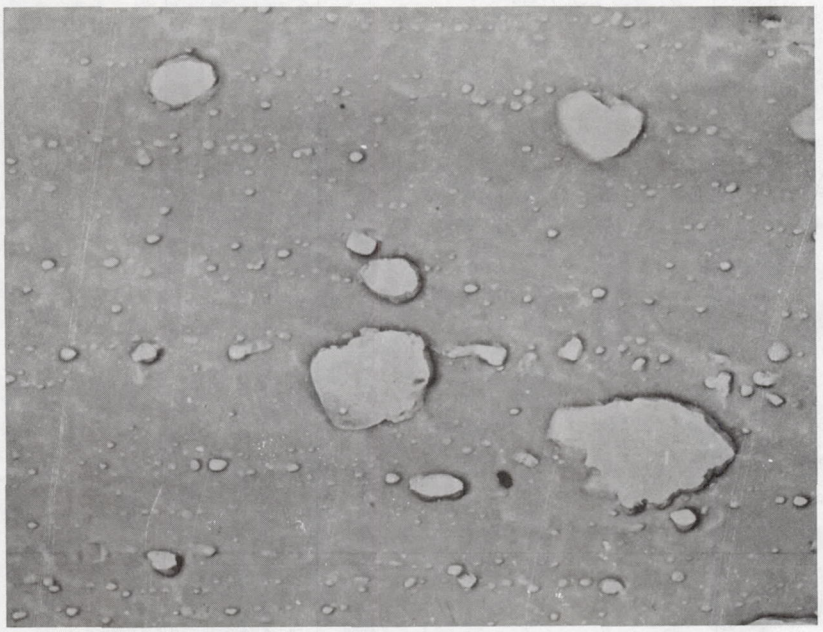

Unetched 10,000X Mag.

P8046

Extraction Replica 5000X Mag

H67-9

FIGURE 31 - As-Rolled Alloy HP5-8 Prior to Exposure (Fig. 30) to 2600°F/10 hrs./vac.

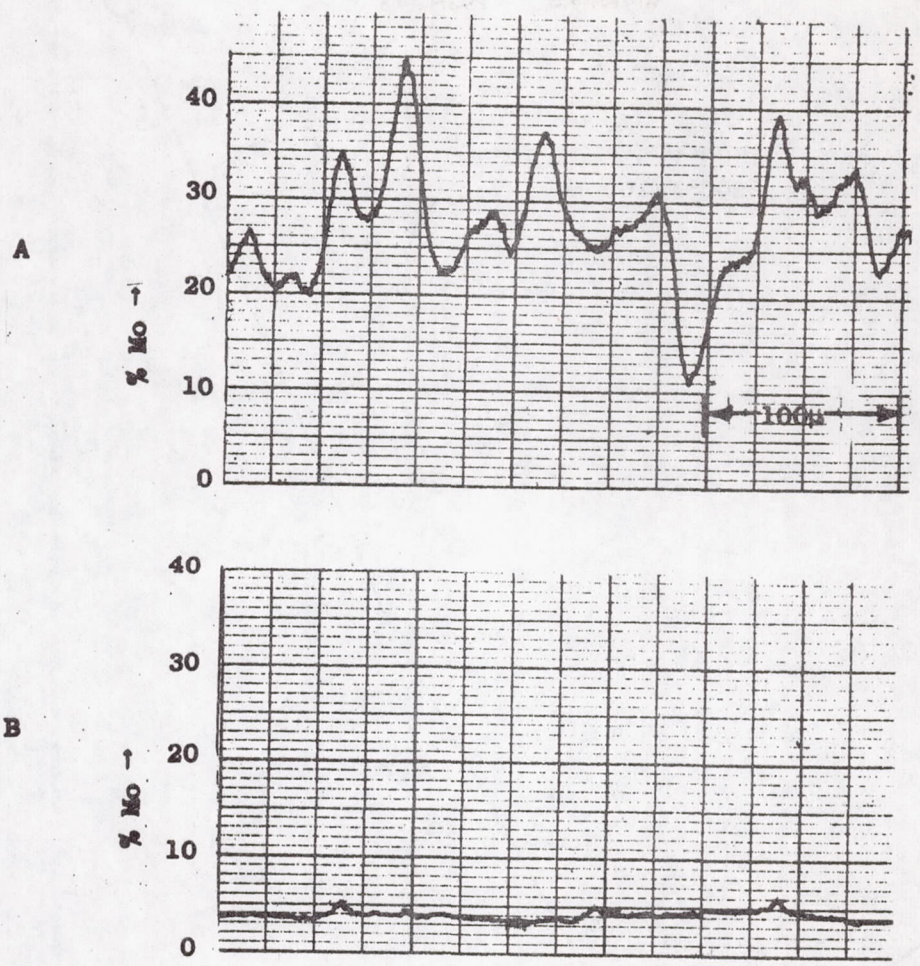

FIGURE 32 **Electron Microprobe X-Ray Emission for Molybdenum Analysis In Two Selected**, As-Compacted Elemental Powders. Analysis **Performed at 30 KV, 3.5 ma, and a Scanning Rate of 96 microns per Minute With a One Micron Diameter Beam.**

A - Cr - 23 Mo - 5 v/o MgO - 0.25 each Hf, Y, Th. **Compacted At 2000°F/2 hours/10 ksi He** (5M23-2)

B - Cr - 4 Mo - 5 v/o MgO - 0.25 each Hf, Y, Th. **Compacted At 2000°F/2 hours/10 ksi He** (5MO-2)

C65121651

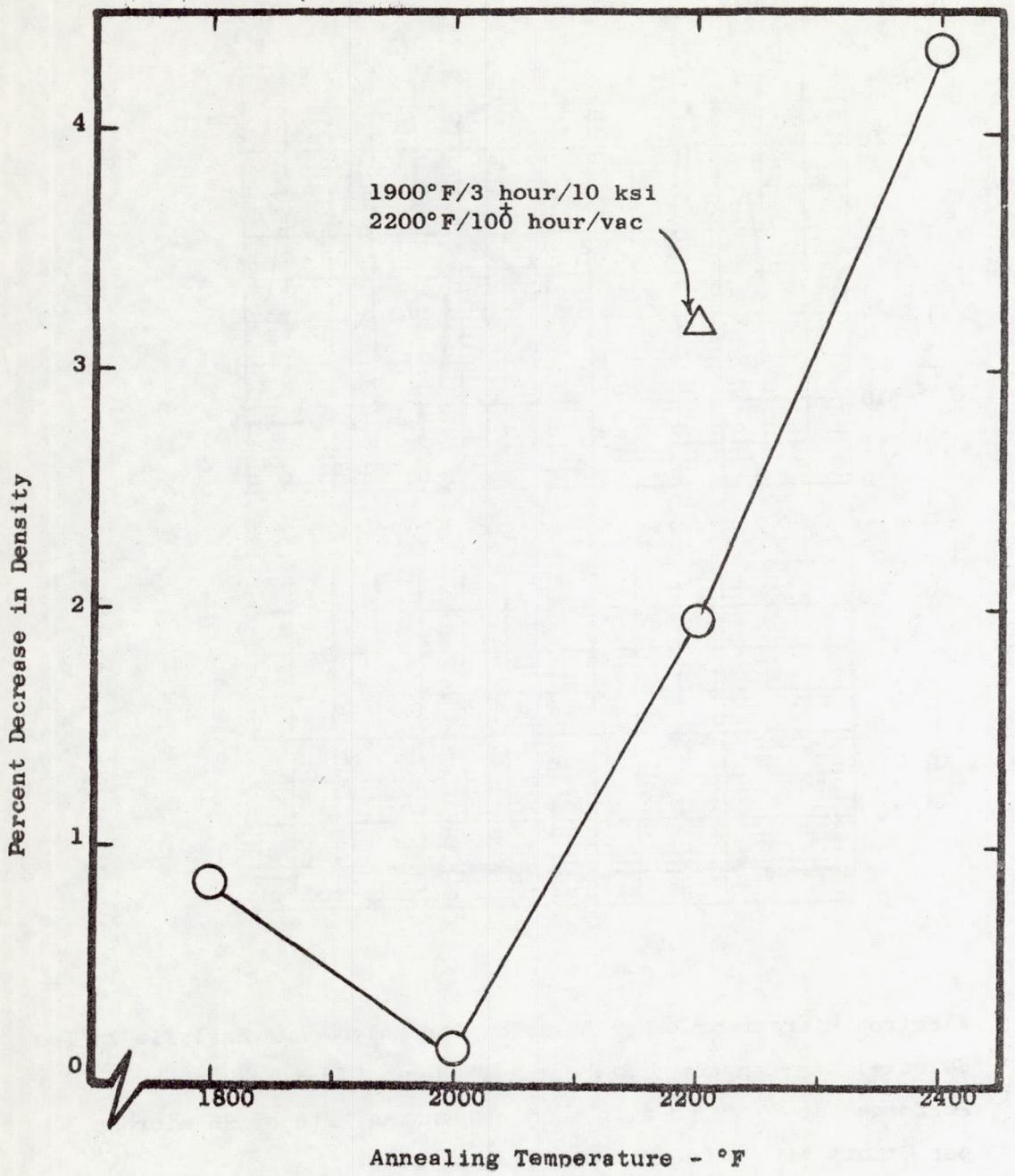

FIGURE 33 Decrease in Density of Cr - 3 Mo - 5 v/o MgO - .25 ea Hf, Y, Th (5MO-2) Alloy Autoclaved at 2400°F/2 hr/10 ksi And Annealed One Hour in Vacuum at Varying Temperature

C65121634

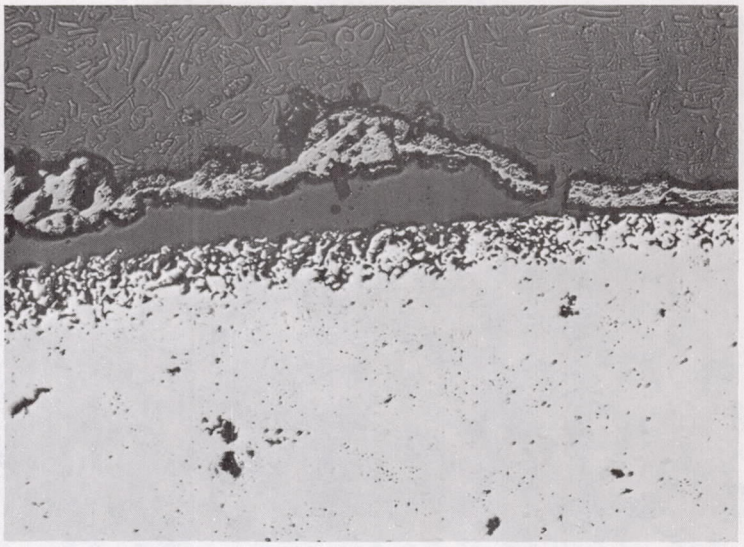

N2272

A) Oxide layer of 2MO after 2000°F/100/air exposure. 100X Mag.

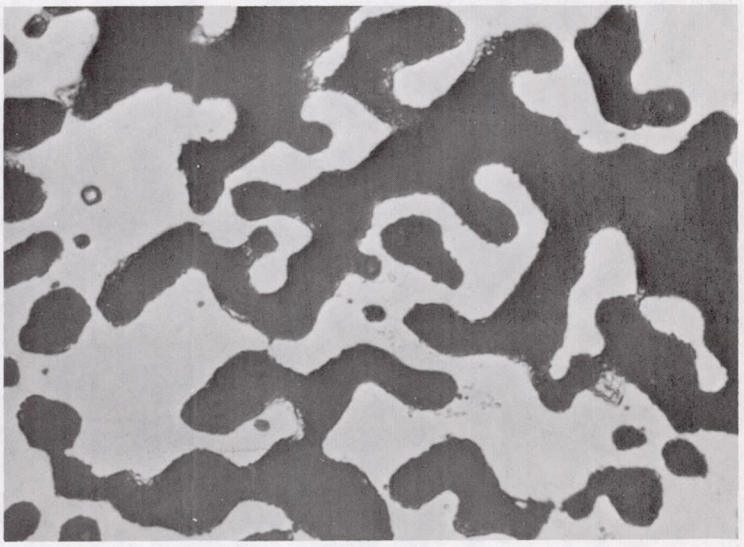

N2393

B) Internal interface beneath oxide layer showing evidence of Cr vaporization in 2Mo alloy. 1000X Mag.

FIGURE 34 Appearance Of The Oxide/Metal Interface Area Of 2MO Alloy After 2000°F Air Oxidation.

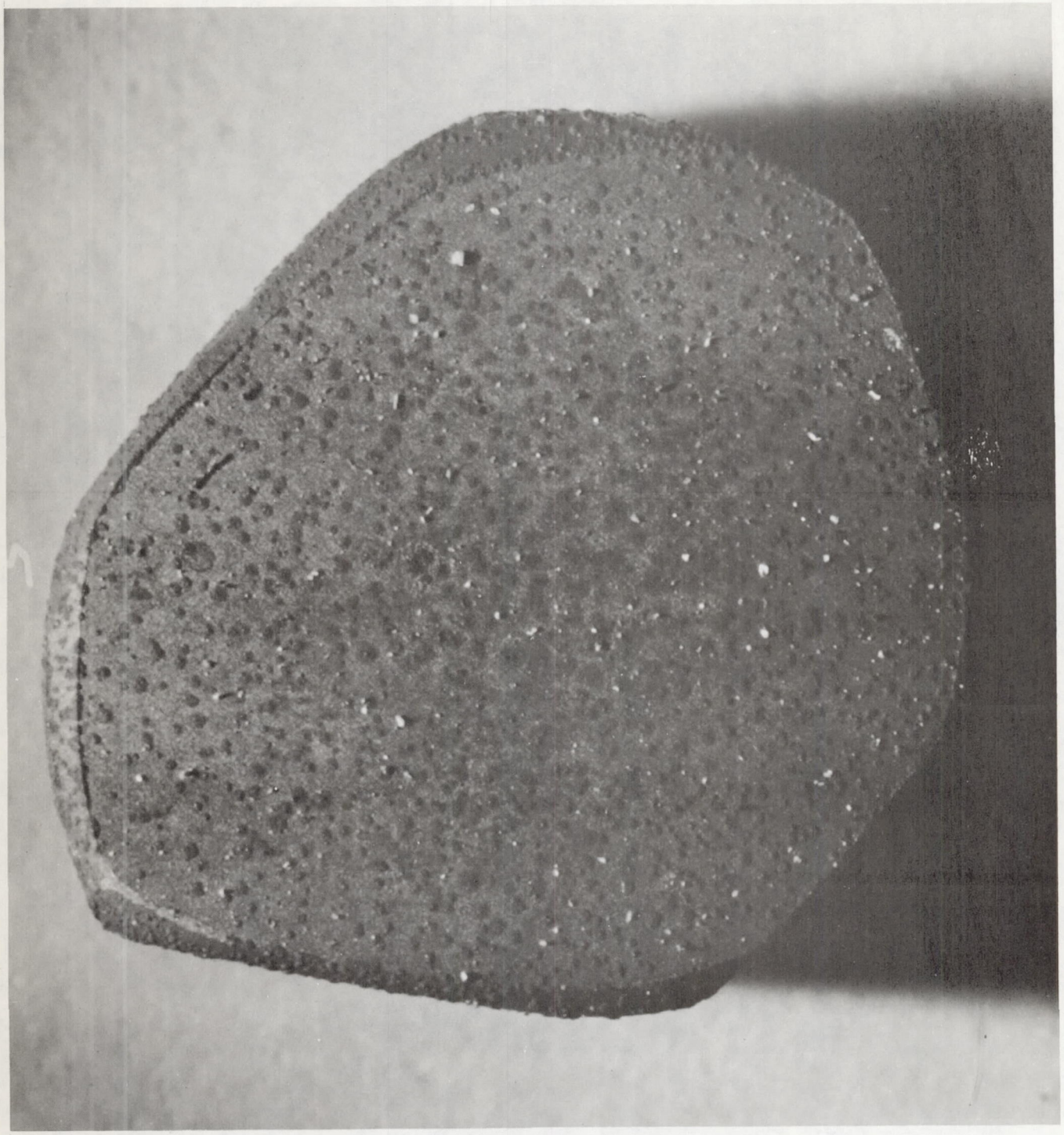

66072701

FIGURE 35 Oxidized Surface Of A Cr, 1 Mo, $5^{V}/_{O}Y_2O_3$, .15REA After Air Oxidation At 2000°F/10 Hrs. 15X Mag. Alloy 5YO-1

66072702

FIGURE 36 Oxidized Surface Of Cr, 1 Mo, $5^{V}/_{o}Y_2O_3$, .15REA After Air Exposure At 2000°F/100 Hrs. 15X Mag Alloy 5YO-1

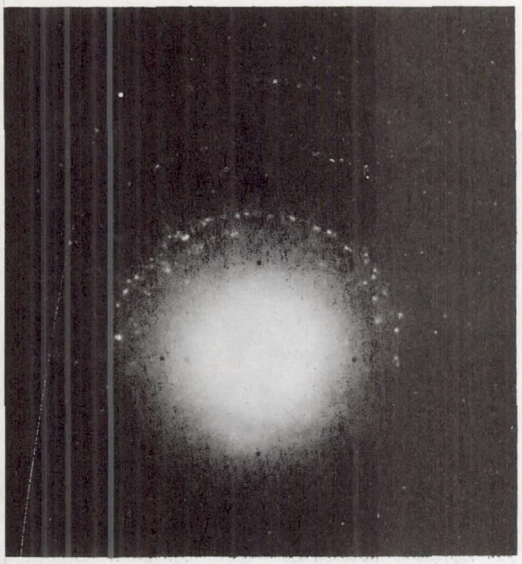

A - HP6-(0^V/oThO$_2$)Hot Rolled + 2200°F/1 hr.

9208

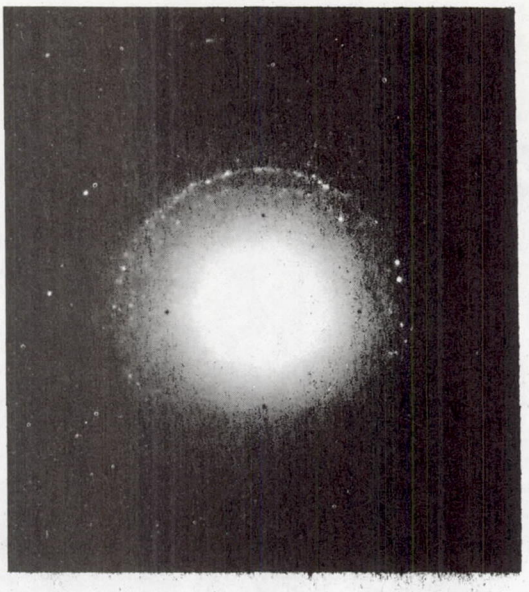

B - HP5-(4^V/oThO$_2$) As-Pressed + 2200°F/1 hr.

9205

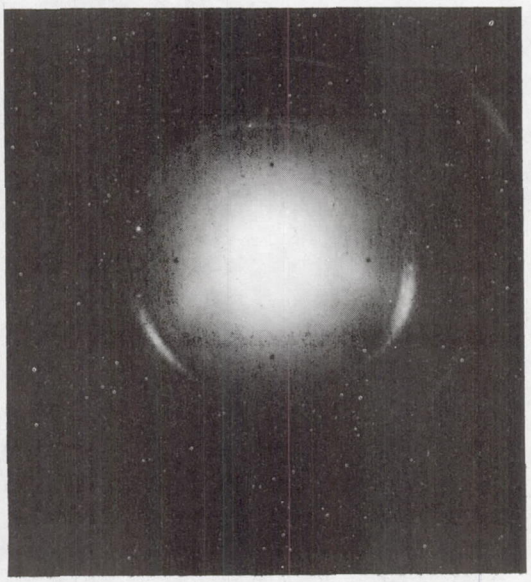

C - HP5-(4^V/oThO$_2$)As Rolled + 2600°F/10 hr.

9200

FIGURE 37 Recrystallization Behavior of Cr-4Mo-.15(La+Y) Alloys Produced from Flake Shaped Powders. A and C were Processed in an Identical Fashion except A has 0^V/oThO$_2$ and C has 4^V/oThO$_2$. The Texture Produced During Rolling (C) Evidently Promotes Resistance to Recrystallization as May be Seen by Comparison of B and C. Mo K_α Radiation.

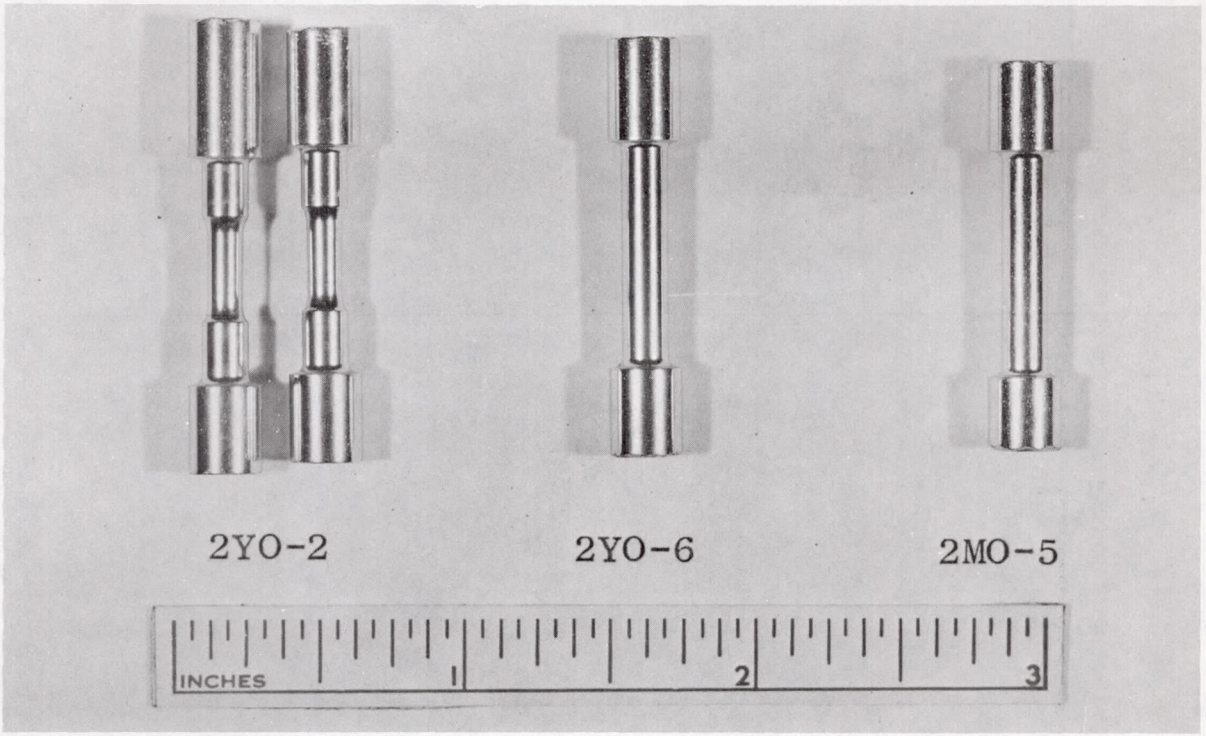

C67022722

FIGUR 38 Button Head Tensile Specimen Used For Mechanical Testing. Double Reduced Specimens Were Used For Ductile To Brittle Transition Testing.

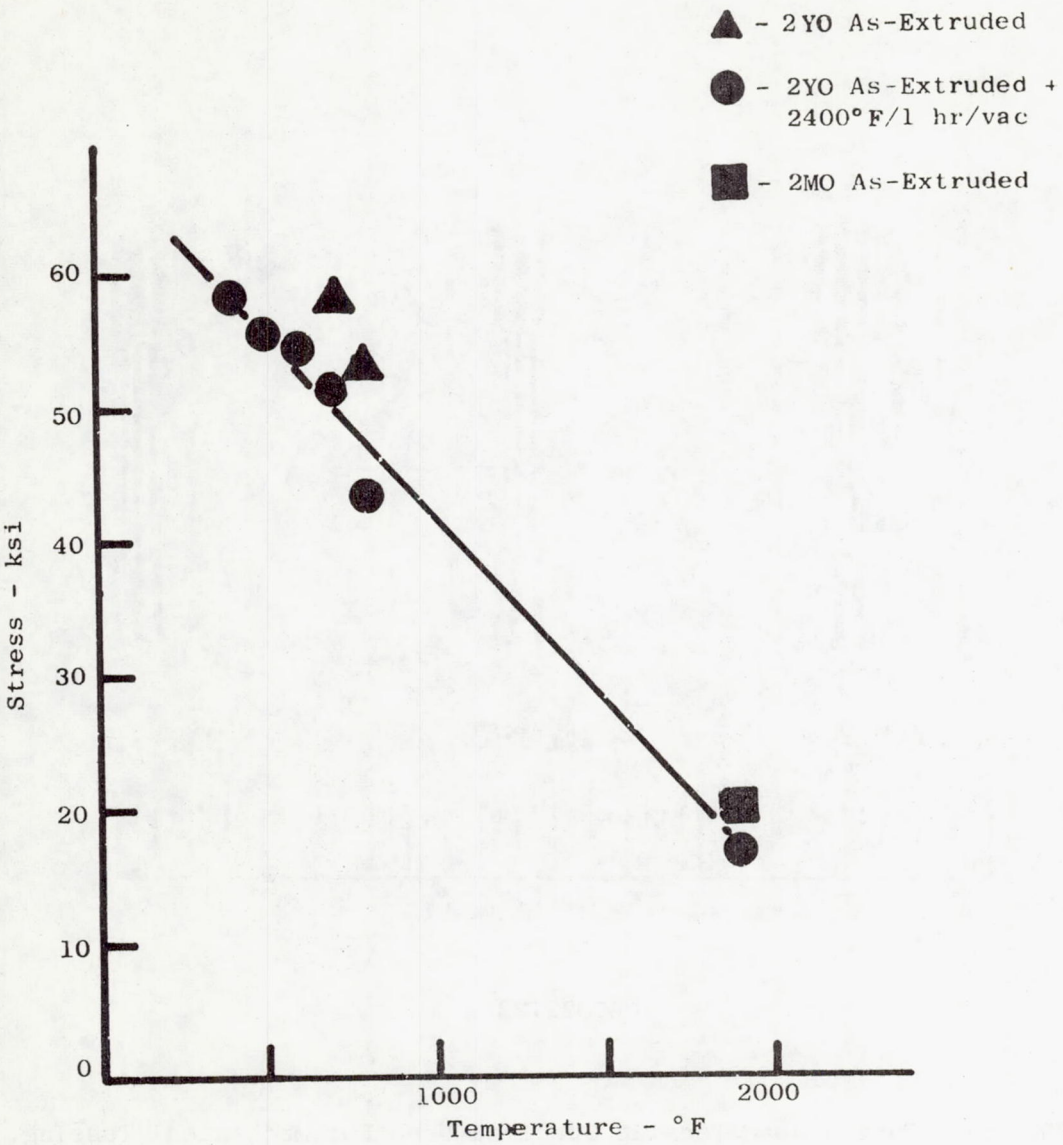

FIGURE 39 Yield Strength of 2YO Alloys as a Function of Temperature.

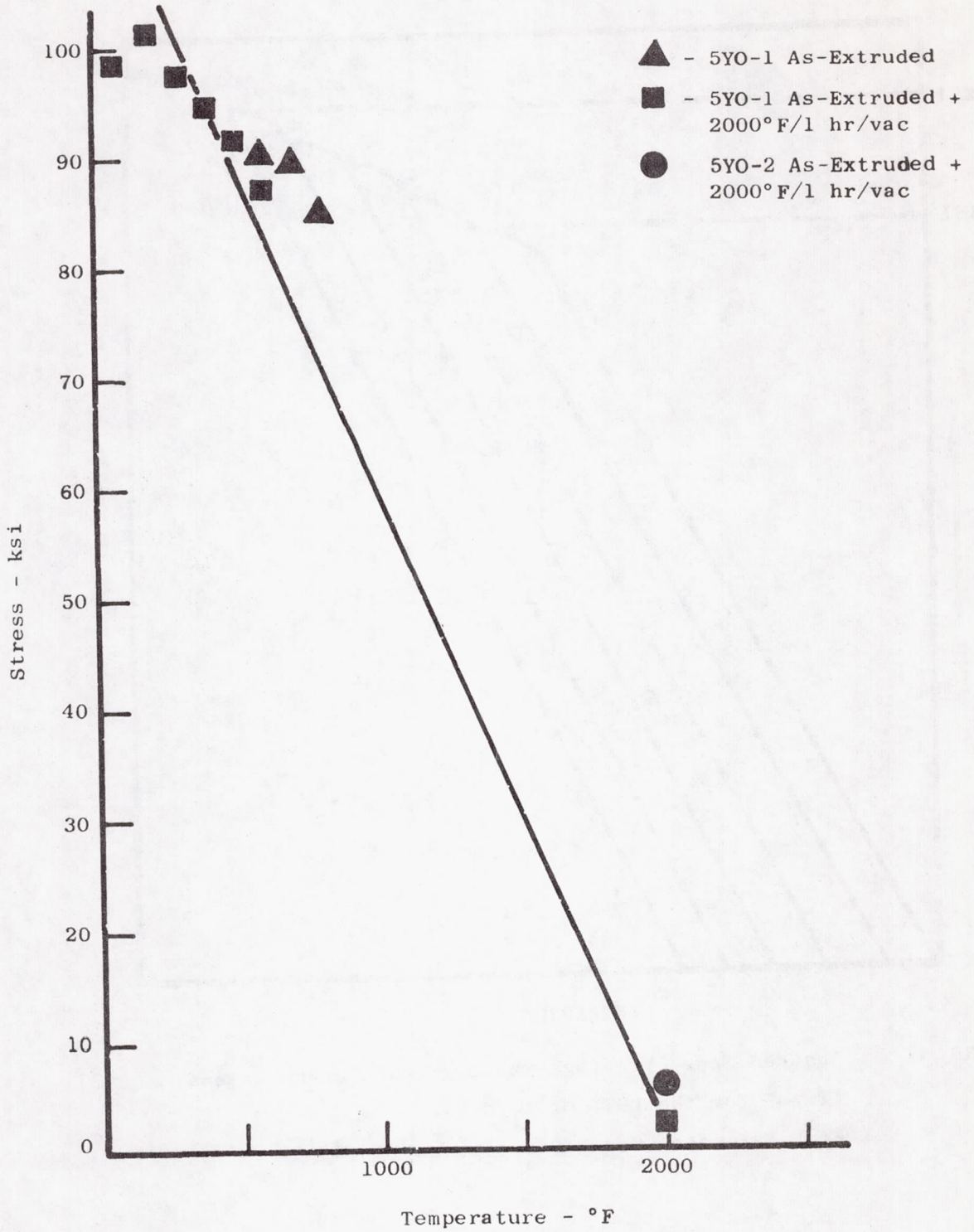

FIGURE 40 Yield Strength of 5YO Alloys as a Function of Temperature.

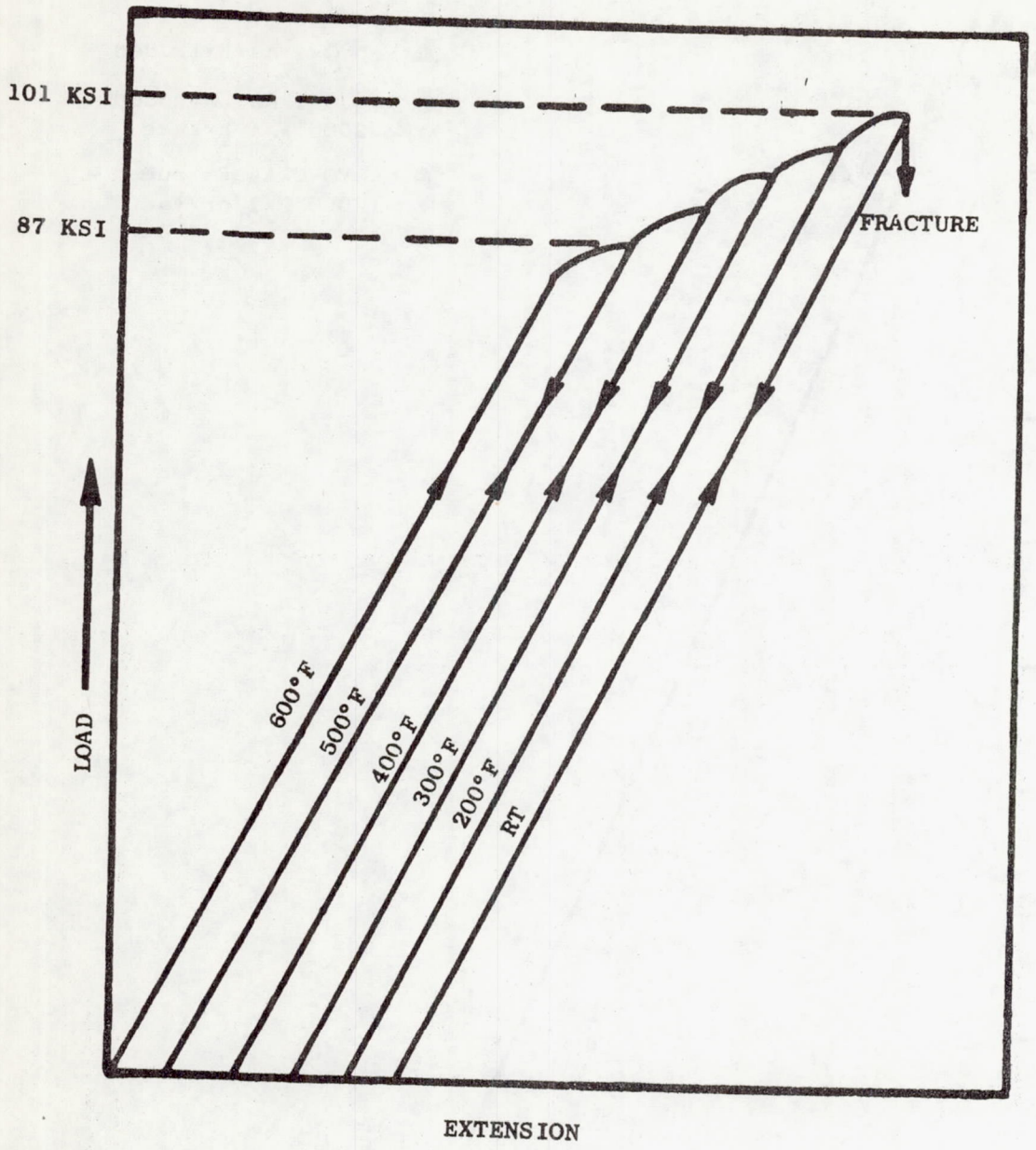

FIGURE 41 Instron Chart Tracings Showing Load Versus Extension (Time) For the DBTT of (5YO-1).
Each Extension Cycle Corresponds to 1% ε.

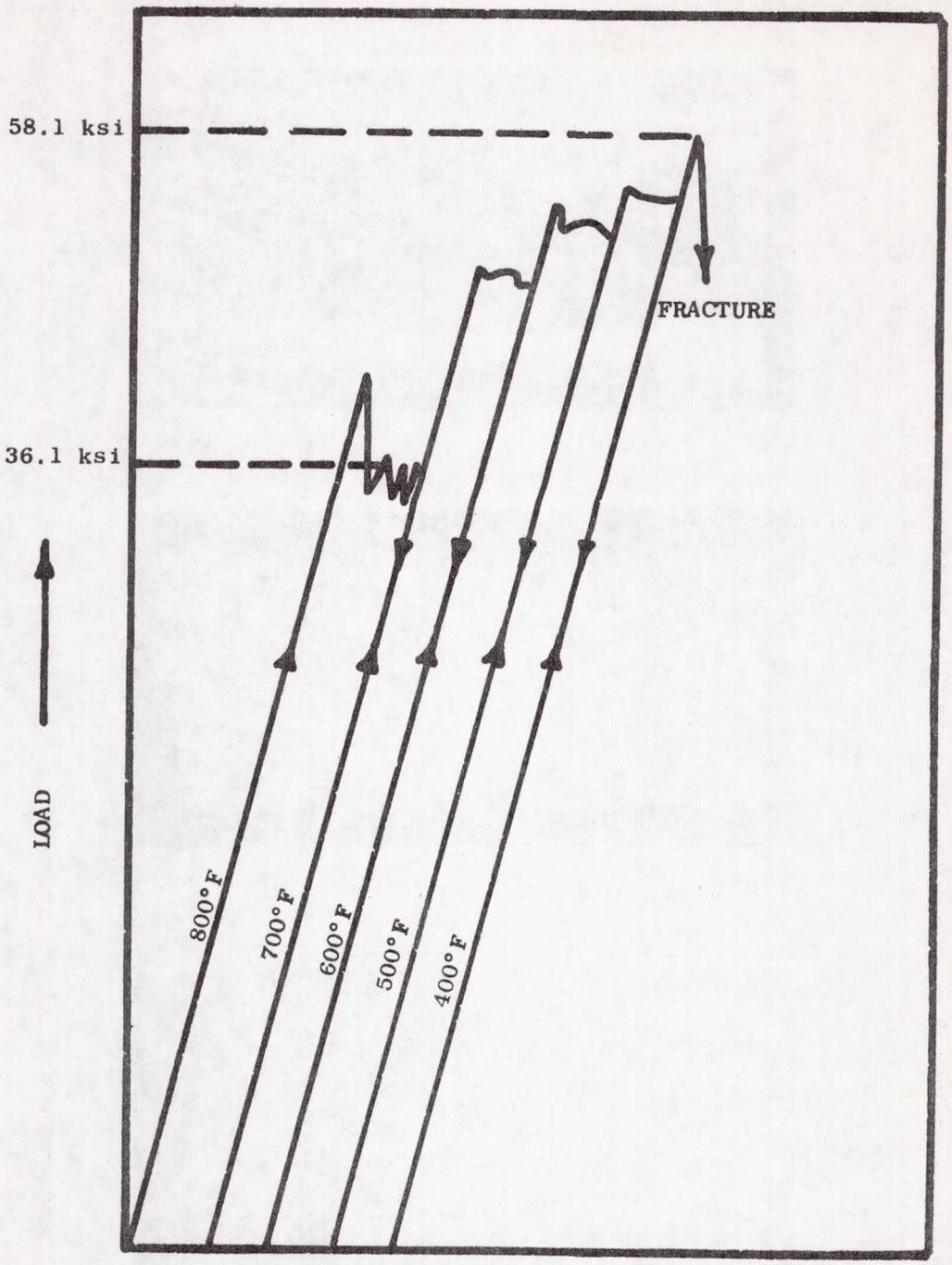

FIGURE 42 Instron Chart Tracings Showing Load Versus Extension (Time) for the DBTT of Alloy 2YO. Each Extension Cycle Corresponds to 1% ϵ.

(a)

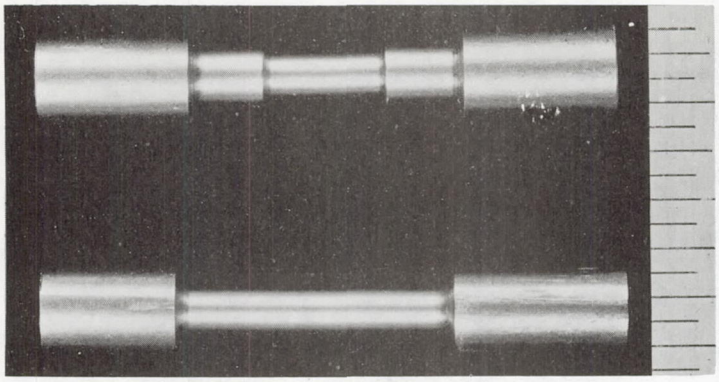

2X C66061601

(b)

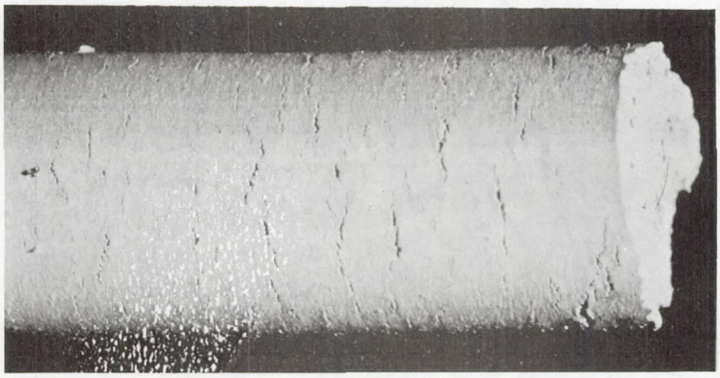

10X C66062802

(c)

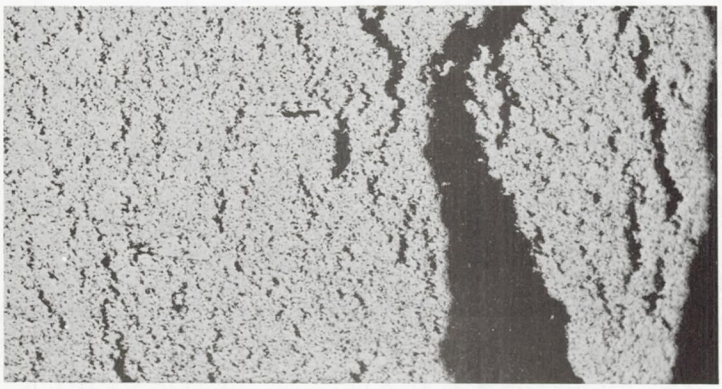

100X M4247

FIGURE 43 Cr-5 $^{V}/_{o}$ Y_2O_3-.9 Mo-.15 REA Tensile Specimen: (a) Original Specimen Configuration for DBTT (top), and Tensile Testing (bottom); (b) Macrophotograph of 2000°F/vac Tensile Fracture; (c) Longitudinal Microstructure of Fracture Gage Length Shown in (b).

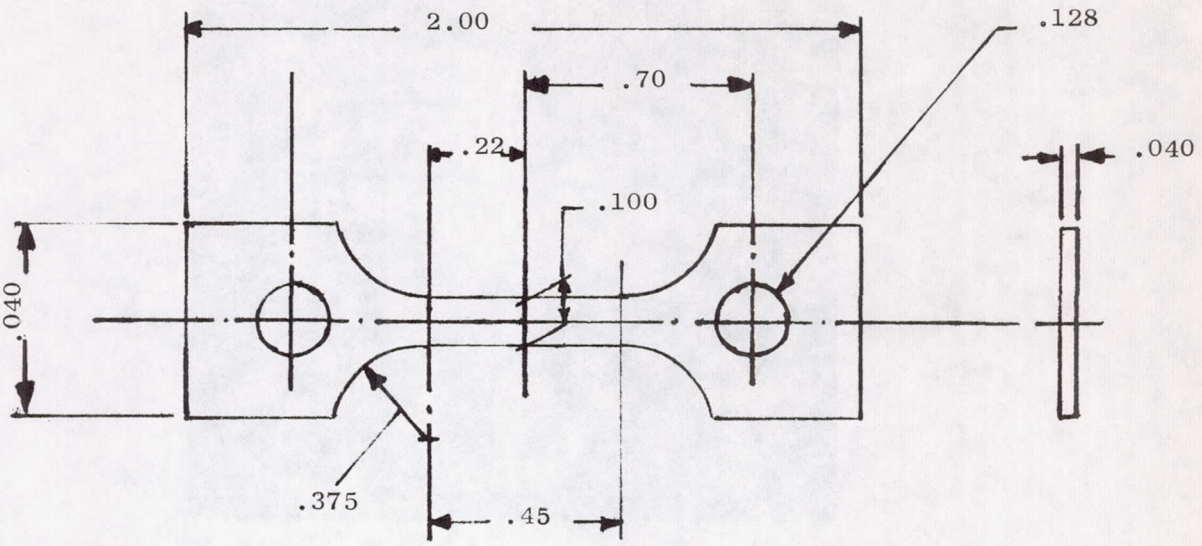

FIGURE 44 Mechanical Test Specimen Used for Tensile, Stress Rupture and DBTT Testing of Oxide Dispersion Strengthened Cr Alloys Processed from Coarse Prealloyed Powder Blends.

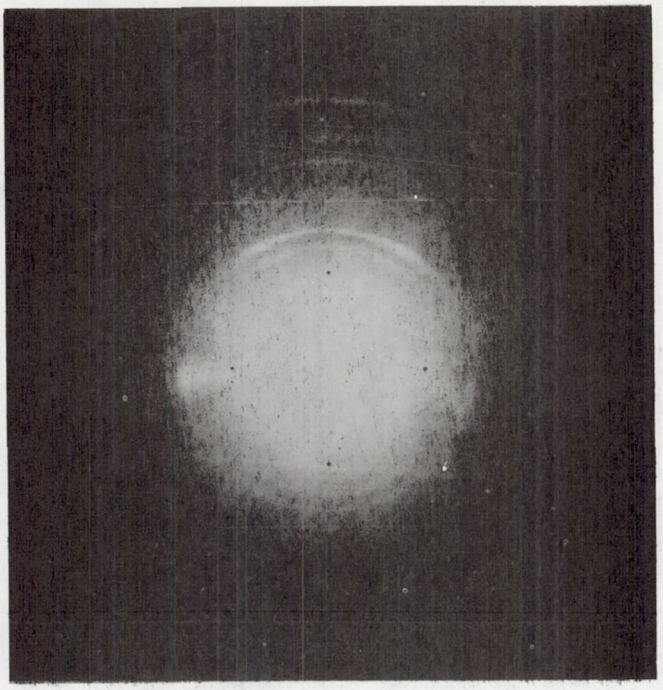

A 9194

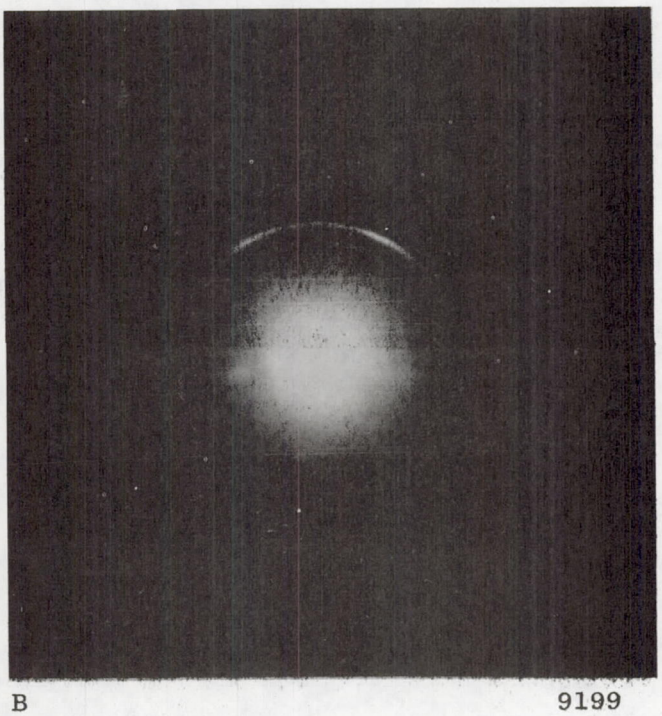

B 9199

FIGURE 45 - Laue Transmission Photos of: (A) 2100°F/81 ksi Tensile Sample; (B) 2100°F/2.5 ksi/.01 hr. Rupture Sample. Taken near the Fracture after Testing. MoKα Radiation.

A

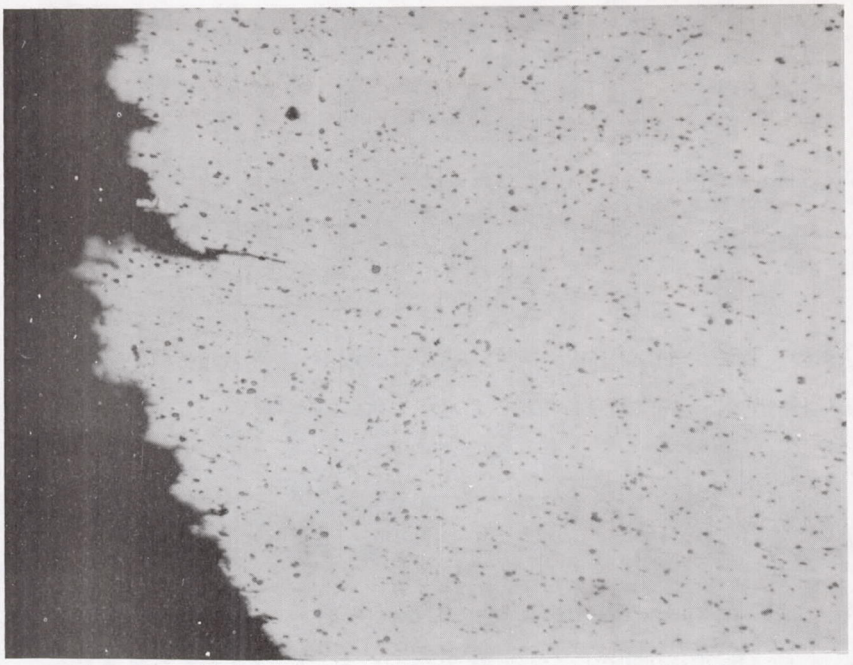

2100°F/81.3 ksi/Tensile

OMJ9580

B

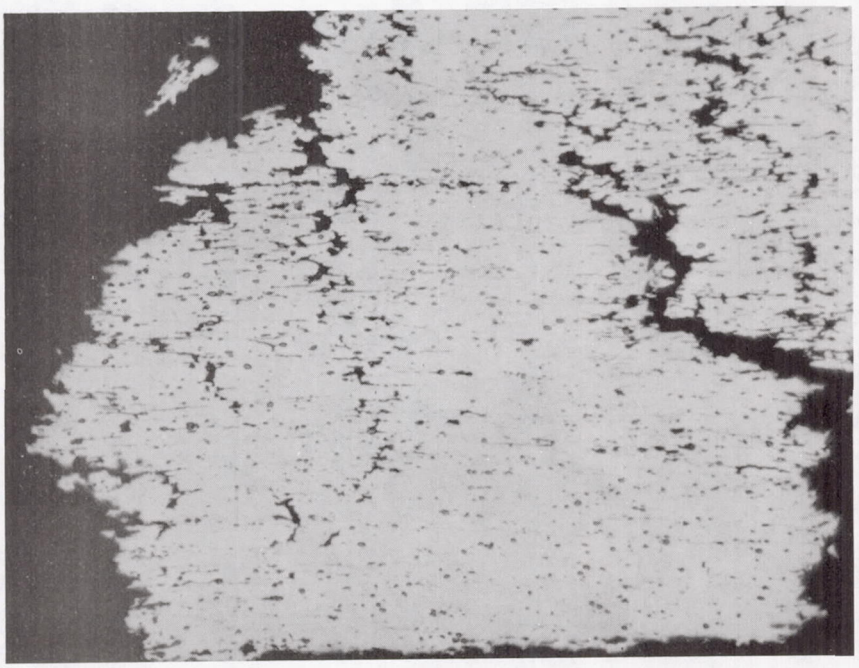

2100°F/2.5 ksi/.01 hr Stress Rupture

OMJ9779

FIGURE 46 Microstructural Appearance of Hot Rolled Cr-4Mo-.15(La+Y)-4V/oThO_2 Fractures. A - 2100°F/81.3 ksi UTS Tensile Fracture; B - 2100°F/2.5 ksi/.01 hr Stress Rupture Specimen. Unetched 500X Mag.

APPENDIX I

CALCULATED CONCENTRATION OF CARBON CONTENT NECESSARY FOR MONOLAYER ADSORPTION OF C ON FLAKE-SHAPED Cr POWDERS.

ASSUMPTIONS:

1. All exposed surfaces are (001)
2. C is adsorbed in the ratio of 1 carbon atom/Cr surface atom

GIVEN:

1. Flake surface area is 9.0 m^2/g Cr
2. Lattice parameter Cr = 2.88 A

CALCULATION: Find weight percent carbon necessary for monolayer adsorption of C on above Cr flakes.

$$\text{No. of adsorption sites} = \frac{\text{Specific Surface Area}}{\text{Area of Adsorption Site}}$$

$$= \frac{9.0}{(2.88 \times 10^{-10})^2} = 1.1 \times 10^{20} \ \frac{\text{sites}}{\text{g Cr}}$$

Weight fraction C

$$= \frac{1.1 \times 10^{20}}{6.02 \times 10^{23}} \times 2 \times 10^{-3} \ \frac{\text{g C}}{\text{g Cr}}$$

An Adsorbed Monolayer = .2 $^{w}/_{o}$ C

APPENDIX II

QUANTITATIVE METALLOGRAPHY

Target dispersoid parameter goals in this program were as follows:

1) As processed material (after consolidation and working)

   Dispersoid Particle Size: 95% of the total number of particles to have a median particle size of less than .05 microns with a maximum size of .1 microns. The remaining 5% of the particles to be less than 0.2 microns.

   Dispersoid IPS: less than 1.5 microns.

2) As worked + 2600°F/10 hours

   Dispersoid Particle Size: 95% of the ThO_2 particles less than .1 microns and no particles greater than .2 microns.

In this report, all IPS values were determined by lineal analysis of plane metallographic sections. In those samples in which severe dispersoid agglomeration was observed, the samples were viewed by electron microscopy but particle size estimates and IPS determinations were conducted at 1000X because of the extremely large oxide sizes. In the alloys which exhibited fine dispersions, all quantitative metallographic analysis was conducted at magnifications of 10,000X or higher.

Interparticle spacing was determined from the following equation:

$$IPS = \frac{1-f}{N_L}$$

(f= volume fraction of oxide and N_L = the number of particles intersected by a randomly place line of unit length).

This relationship is independent of particle shape or size distribution[+]. Further, it is easily measured by lineal analysis. The particle size criterion is more difficult however, because it is stated as a particle size distribution. Size distribution analysis of nonuniform size spheres in a metal matrix cannot be done by lineal analysis of a planar surface. This measurement is most readily handled by size

[+] R. L. Fulman, J. Metals, March, 1953, p 447

measurement of the extracted oxides. Of all the alloys produced, only alloy HP5 was sufficiently fine to warrant the additional effort necessary to determine the particle size distribution analysis on electron extraction replicas such as those in Figures 30 and 31 of the text.

The statistical evaluation of these extracted oxides was done using a Zeiss (Model TG2-3) particle size analyzer. The analyzer is a semi-automatic device in which the eye and judgement of the operator participate in the measuring process. The measurement of the particles by means of the particle size analyzer is relatively simple. Light is projected through the iris diaphragm, which is then imaged on a glass plate. An enlarged electron micrograph is placed on the plate over the illuminated spot. The area of the iris diaphragm is adjusted to coincide with the area of theparticle to be measured. In the case of irregularly shaped particles, the iris is so adjusted that a reasonable estimate of the area of the particle is obtained. Depressing a foot switch activates the appropriate counter thereby recording the particle in its proper size class. Simultaneously a puncher marks the particles as a reminder that the particle has been measured. The data are recorded on the 48 size-class interval counters. The data is then reported as cumulative percent versus particle size. The requirement of 95% less than .05 or .1 microns is thus easily ascertained using this procedure.

As may be seen in Table A, the best dispersion produced in this program (Alloy HP5-8) did not meet the parameter goals. In the as-rolled condition, the median diameter is .07 rather than .05 and the largest particles ($\sim$ 2.5 microns) are an order of magnitude above the designated maximum particle size. The alloy exposed at 2600°F for 10 hours, failed the maximum particle size goal also. The dispersoid was quite stable, however, and median particle size increased only from .07 to .08 microns.

TABLE A

Particle Size Analysis of Cr-4Mo-.15(La+Y)-4^{V}/.ThO_2 (HP5-8) Alloy From Extraction Replicas at 10,000 Mag.

Particle (Diameter) d (Microns)	Percentages of Particles less than d (Cumulative Percent)	
	As Rolled (HP5-8)	As Rolled + 2600°F/10 hours (HP5-8)
.03	.4	.6
.05	19.9	2.6
.07	49.8	37.3
.09	74.8	60.0
.11	88.2	86.3
.13	91.5	93.5
.15	94.2	95.5
.17	95.6	96.8
.19	96.5	
.21	97.4	97.5
.23	98.2	
.25	98.7	98.7
.29	99.3	
.39	99.6	
.49		
.59	99.6	
2.5	100	100